

IMPROVING REMOTELY-SENSED PRECIPITATION ESTIMATES OVER MOUNTAINOUS
REGIONS

A THESIS SUBMITTED TO
THE GRADUATE SCHOOL OF NATURAL AND APPLIED SCIENCES
OF
MIDDLE EAST TECHNICAL UNIVERSITY

BY

MUSTAFA AKÇELİK

IN PARTIAL FULLFILLMENT OF THE REQUIREMENTS
FOR
THE DEGREE OF MASTER OF SCIENCE
IN
CIVIL ENGINEERING

FEBRUARY 2013

Approval of the thesis:

**IMPROVING REMOTELY-SENSED PRECIPITATION ESTIMATES OVER
MOUNTAINOUS REGIONS**

submitted by **MUSTAFA AKÇELİK** in partial fulfillment of the requirements for **the degree of
Master of Science in Civil Engineering Department, Middle East Technical University** by,

Prof. Dr. Canan Özgen
Dean, Graduate School of **Natural and Applied Sciences**

Prof. Dr. Ahmet Cevdet Yalçın
Head of Department, **Civil Engineering**

Assoc. Prof. Dr. İsmail Yücel
Supervisor, **Civil Engineering Dept., METU**

Examining Committee Members:

Assoc. Prof. Dr. Zuhâl Akyürek
Civil Engineering Dept., METU

Assoc. Prof. Dr. İsmail Yücel
Civil Engineering Dept., METU

Assoc. Prof. Dr. Elçin Kentel
Civil Engineering Dept., METU

Assist. Prof. Dr. Koray K. Yılmaz
Geological Engineering Dept., METU

Assist. Prof. Dr. İbrahim Sönmez
Meteorological Engineering Dept., Ondokuz Mayıs University

Date: February 01, 2013

I hereby declare that all information in this document has been obtained and presented in accordance with academic rules and ethical conduct. I also declare that, as required by these rules and conduct, I have fully cited and referenced all material and results that are not original to this work.

Name, Last Name : Mustafa Akçelik

Signature :

ABSTRACT

IMPROVING REMOTELY-SENSED PRECIPITATION ESTIMATES OVER MOUNTAINOUS REGIONS

Akçelik, Mustafa

M.Sc., Department of Civil Engineering

Supervisor: Assoc.Prof.Dr. Ismail Yucel

February 2013, 74 Pages

In support of the National Oceanic and Atmospheric Administration (NOAA) National Weather Service's (NWS) flash flood warning and heavy precipitation forecast efforts, the NOAA National Environmental Satellite Data and Information Service (NESDIS) Center for Satellite Applications and Research (STAR) has been providing satellite based precipitation estimates operationally since 1978. Two of the satellite based rainfall algorithms are the Hydro-Estimator (HE) and the Self-Calibrating Multivariate Precipitation Retrieval (SCaMPR). Satellite based rainfall algorithms need to be adjusted for the orographic events and atmospheric variables for the continued improvement of the estimates. However, unlike the HE algorithm, the SCaMPR does not currently make any adjustments for the effects of complex topography on rainfall estimate. Bias structure of the SCaMPR algorithm suggests that the rainfall algorithm underestimates precipitation in case of upward atmospheric movements and high temperature levels. Also SCaMPR algorithm overestimates rainfall in case of downward atmospheric movements and low temperature levels. A regionally dependent empirical elevation-based bias correction technique and also a temperature based bias correction technique may help to improve the quality of satellite-derived precipitation products. In this study, an orographic correction method and a temperature correction method that will enhance precipitation distribution, improve accuracy and remove topography and temperature dependent bias is developed for the Self-Calibrating Multivariate Precipitation Retrieval (SCaMPR) rainfall algorithm to be used in operational forecasting for meteorological and hydrological applications.

Keywords: Orographic precipitation, updraft, SCaMPR, HE.

ÖZ

DAĞLIK ALANLARDA UZAKTAN ALGILAMA YOLU İLE ELDE EDİLEN YAĞIŞ TAHMİNLERİNİN GELİŞTİRİLMESİ

Akçelik, Mustafa

Yüksek Lisans, İnşaat Mühendisliği Bölümü

Tez Danışmanı: Doç. Dr. İsmail Yücel

Şubat 2013, 74 Sayfa

Ulusal Okyanus ve Atmosfer İdaresi (National Oceanic and Atmospheric Administration - NOAA) Ulusal Hava Durumu Servisi (National Weather Service - NWS) biriminin su baskını uyarı ve şiddetli yağış tahmini çalışmalarına destek kapsamında, NOAA Ulusal Çevre Uydu Veri ve Bilgi Servisi (National Environmental Satellite Data and Information Service - NESDIS) Uydu Uygulama ve Araştırma Merkezi (Center for Satellite Applications and Research - STAR) birimi 1987 yılından beri uydu tabanlı operasyonel yağış tahminleri sağlamaktadır. Uydu tabanlı yağış algoritmalarının iki tanesi Hydro-Estimator (HE) ile Self-Calibrating Multivariate Precipitation Retrieval (SCaMPR)'dir. Uydu tabanlı yağış algoritmaları, tahminlerin devamlı gelişiminin sağlanması için, orografik olaylara ve atmosferik değişkenlere göre uyarlanmalıdır. HE algoritmasının aksine SCaMPR algoritması kompleks topoğrafyanın yağış üzerindeki etkisine yönelik herhangi bir düzeltme yapmamaktadır. Bahsedilen SCaMPR algoritmasında yer alan hata yapısı; yukarı yönlü atmosferik hareket olması ve sıcaklık seviyesinin yüksek olması durumunda algoritma tabanlı yağış tahminlerinde değerinden az gösterme olduğunu göstermiştir. SCaMPR algoritmasının aşağı yönlü atmosferik hareket olması ve sıcaklık seviyesinin düşük olması durumunda algoritma tabanlı yağış tahminlerinde ise değerinden fazla gösterme olduğu görülmüştür. Bölgesel tabanlı deneysel yüksekliğe dayalı bir hata düzeltme tekniği ve ayrıca sıcaklığa dayalı bir hata düzeltme tekniği uydu tabanlı yağış ürünlerinin kalitesini arttırmaya yardım edebilecektir. Bu çalışmada, Self-Calibrating Multivariate Precipitation Retrieval (SCaMPR) yağış algoritması için yağış dağılımını geliştirecek, tahmin doğruluğu iyileştirecek ve topoğrafya ve sıcaklı tabanlı hatayı giderecek orografik düzeltme metodu ve sıcaklık düzeltme metodu, meteorolojik ve hidrolojik uygulamalardaki operasyonel tahminler için geliştirilmiştir.

Anahtar kelimeler: Orografik yağış, yukarı yönlü hava akımı, SCaMPR, HE.

To my family,

ACKNOWLEDGMENTS

It would not have been possible to write this master thesis without the help and support of the kind people around me, to only some of whom it is possible to give particular mention here.

First of all, I would like to thank to my dear supervisor, Assoc. Prof. Dr. İsmail YÜCEL for her never ending support, continuous understanding, invaluable patience, and guidance throughout this study. Her guidance made me clarify and realize my goals which I will remember forever.

Then, I would like to thank profoundly my family. This thesis study would not have been possible without their endless love and faithful support.

I also want to present my special thanks to my supervisor, Board of Inspection president Mr. Selçuk BAKKALOĞLU for his precious care and support.

I owe thanks to my friends Mehmet Akın ÇETİNKAYA and Birand ADAL for their amazing helps and supports throughout my studies. Big thanks also should be given to my precious colleagues in Ministry of Environment And Urbanization, especially Berk UZUN and Yasin GÖVEN for their care, and constant support.

TABLE OF CONTENTS

ABSTRACT	v
ÖZ	vi
ACKNOWLEDGMENTS.....	viii
LIST OF TABLES	xi
LIST OF FIGURES.....	xii
LIST OF SYMBOLS	xv
LIST OF ABBREVIATIONS	xvi
CHAPTER 1	1
1. INTRODUCTION.....	1
1.1. Statement of the Problem	1
1.2. Objective of the Study.....	1
1.4. Description of the Thesis.....	2
CHAPTER 2	3
2. LITERATURE REVIEW.....	3
2.1. Satellite Rainfall Algorithms.....	3
2.1.1. Satellites	3
2.2. Definition of Orographic Precipitation.....	4
2.3. Orographic Correction.....	5
2.3.1. Resultant Wind Speed	6
2.3.2. Fetch Length.....	6
2.3.3. Slope.....	6
2.3. Correction Algorithm	7
CHAPTER 3	9
3. SATELLITE RAINFALL ALGORITHMS AND STUDY AREA	9
3.1. Satellite Rainfall Algorithms.....	9
3.1.1. The Hydro Estimator, HE.....	9
3.1.2. The Self-Calibrating Multivariate Precipitation Retrieval, SCaMPR.....	9
3.2. Study Area.....	11
CHAPTER 4	15
4. METHODOLOGY AND ANALYSIS	15
4.1. Introduction.....	15
4.2. Preparation of Required Data and Information	16
4.2.1. Gauge Measurements	16
4.2.2. SCaMPR and HE Estimates	16
4.2.3. North American Mesoscale Forecast System (NAM) model data.....	17

4.2.4. Digital Topography	17
4.2.5 Representativeness of SCaMPR Estimates and NAM data for Gauge Stations	18
4.2.6. Statistics of Gauge vs. SCaMPR data	20
4.2.7. Statistics of Gauge vs. HE data	33
4.3. Sensitivity Analysis to Develop Updrafts	34
4.4. Updraft vs. Multiplicative Error Analysis	36
4.4.1. Winter Period	37
4.4.2. Summer Period.....	49
4.5. Stability Analysis for Correction Method	54
4.6. Developing Final Correction Algorithm	65
4.6.1. Winter Period	65
4.6.2. Summer Period.....	65
CHAPTER 5	67
5. RESULTS	67
5.1. Winter Period	67
5.2. Summer Period.....	68
CHAPTER 6	71
6. DISCUSSION AND CONCLUSIONS.....	71
REFERENCES	73

LIST OF TABLES

Table 3.1: The elevation breakdown of the gauge stations over a) 250 m and b) 500 m terrain elevation bands.....	13
Table 4.1: Availability of gauge stations over study duration.....	16
Table 4.2: Comparison of radiosonde and 700 hPa NWP data wind vector components at 4th July 2004 00 UTC	19
Table 4.3: A sample contingency table used on defining the capability of satellite rainfall algorithm to detect rain events	20
Table 4.4: The capability of SCaMPR algorithm to detect rain events in summer period for (a) 1 hour temporal resolution and (b) 6 hour temporal resolution.....	21
Table 4.5: The capability of SCaMPR algorithm to detect rain events in winter period for (a) 1 hour temporal resolution and (b) 6 hour temporal resolution.....	21
Table 4.6: All data statistics of SCaMPR estimates over gauge measurements during 2002, 2003, and 2004 summer periods and summation of these three periods (Named as summer in table) for 1 hour temporal resolution (a) and for 6 hour temporal resolution (b).....	22
Table 4.7: All data statistics of SCaMPR estimates over gauge measurements during 2002 – 2003 and 2003 - 2004 winter periods and summation of these two periods (Named as winter in table) for 1 hour temporal resolution (a) and for 6 hour temporal resolution (b).....	23
Table 4.8: Hit pixel data statistics of SCaMPR estimates over gauge measurements during 2002, 2003, and 2004 summer periods and summation of these three periods (Named as summer in table) for 1 hour temporal resolution (a) and for 6 hour temporal resolution (b).....	23
Table 4.9: Hit pixel data statistics of SCaMPR estimates over gauge measurements during 2002 – 2003 and 2003 - 2004 winter periods and summation of these two periods (Named as winter in table) for 1 hour temporal resolution (a) and for 6 hour temporal resolution (b).....	24
Table 4.10: The capability of HE algorithm to detect rain events in summer periods of 2002 – 2003 years for (a) 1 hour temporal resolution and (b) 6 hour temporal resolution	33
Table 4.11: All data statistics of HE estimates over gauge measurements during 2002, and 2003 summer periods for 1 hour temporal resolution (a) and for 6 hour temporal resolution (b).....	33
Table 4.12: Hit pixel data statistics of HE estimates over gauge measurements during 2002, and 2003 summer periods for 1 hour temporal resolution (a) and for 6 hour temporal resolution (b)....	34
Table 4.13: Trendline and resulting normalized correction equations with precipitation limit values for winter period measured for different fetch values	47
Table 4.14: Results of application of correction equations achieved using winter data, statistics of the all data series (a) and hit pixels (b) before and after orographic correction.....	48
Table 4.15: Trendline and resulting normalized correction equations for downwind (a) and upwind (b) values with precipitation limit values for winter period measured for different fetch values	52
Table 4.16: Results of application of correction equations achieved using summer data, statistics of the all data series (a) and hit pixels (b) before and after orographic correction	53
Table 5.1: Results of application of correction factors to 1 hour temporal resolution for all data (a) and for hit pixels (b) in winter periods of 2002 – 2004 years	67
Table 5.2: Results of application of correction factors to 6 hour temporal resolution for all data (a) and for hit pixels (b) in winter periods of 2002 – 2004 years	67
Table 5.3: Results of application of correction factors to 1 hour temporal resolution for all data (a) and for hit pixels (b) in summer periods of 2002 – 2004 years	68
Table 5.4: Results of application of correction factors to 6 hour temporal resolution for all data (a) and for hit pixels (b) in summer periods of 2002 – 2004 years	69

LIST OF FIGURES

Figure 2.1: Visible/Infrared data (Cloud top temperature) rain estimation algorithm.....	4
Figure 2.2: Orographic precipitation formation and participating elements	5
Figure 3.1: 24-hour HE rainfall estimation over continental Europe and North Atlantic ending 12.01.2003 12:00 UTC.....	10
Figure 3.2: SCaMPR rain rate estimation algorithm.....	11
Figure 3.3: Digital topography of the study area with gauge locations and elevations overlaid as circles (left), satellite image of the same location (right).....	12
Figure 3.4: The latitudinal locations over west to east transect and elevation breakdown of gauge stations.....	13
Figure 4.1: Flowchart of the methodology used in the orographic correction analysis.....	15
Figure 4.2: Digital topographic map of the study area.....	18
Figure 4.3: 700 hPa NAM wind fields for u component (top) and v component (bottom) in m/s at 4th July 2003 00 UTC	19
Figure 4.4 (a): Seasonal total precipitation measurement, total SCaMPR estimation and multiplicative bias ratio for 2002 summer period	25
Figure 4.4 (b): Seasonal total precipitation measurement, total SCaMPR estimation and multiplicative bias ratio for 2003 summer period	25
Figure 4.4 (c): Seasonal total precipitation measurement, total SCaMPR estimation and multiplicative bias ratio for 2004 summer period	26
Figure 4.5 (a): Seasonal total precipitation measurement, total SCaMPR estimation and multiplicative bias ratio for 2002 - 2003 winter period.....	27
Figure 4.5 (b): Seasonal total precipitation measurement, total SCaMPR estimation and multiplicative bias ratio for 2003 - 2004 winter period.....	27
Figure 4.6: Gauge transect selected to investigate elevation vs. precipitation characteristics and SCaMPR algorithm performance	28
Figure 4.7: Seasonal total precipitation measurement, total SCaMPR estimation and multiplicative bias ratio for the selected gauge transect for 2002 (a), 2003 (b) and 2004 (c) summer periods.....	29
Figure 4.8: Seasonal total precipitation measurement, total SCaMPR estimation and multiplicative bias ratio for the selected gauge transect for 2002 - 2003 (a) and 2003 - 2004 (b) winter periods.....	30
Figure 4.9: Scatter plots of gauge measurements vs. SCaMPR estimations for 1 hour temporal resolution in 2002 (a), 2003 (c) and 2004 (e) and for 6 hour temporal resolution in 2002 (b), 2003 (d) and 2004 (f) summer periods	31
Figure 4.10: Scatter plots of gauge measurements vs. SCaMPR estimations for 1 hour temporal resolution in 2002 - 2003 (a) and 2003 - 2004 (c) and for 6 hour temporal resolution in 2002 - 2003 (b) and 2003 - 2004 (d) winter periods	32
Figure 4.11: Slope values corresponding to 5 km and 10 km fetch lengths over a rough terrain.....	35
Figure 4.12: Orographic adjustment factors based on updraft values calculated with Vicente et al. (2002) formulation	36
Figure 4.13: Total gauge / total SCaMPR accumulation as a function of w using all data points from the winters of 2002-2003 and 2003-2004. Threshold precipitation and estimation limits are 0.1 mm, fetch length is 10 km.....	37

Figure 4.14: Total gauge / SCaMPR accumulations corresponding to vertical velocity bins using data from winter periods of 2002-2003 and 2003-2004. Threshold precipitation and estimation limits are 150 mm for 0.100 m/s updraft bin (a) and 450 mm for 0.500 m/s updraft bin (b). Fetch length is 10 km.	39
Figure 4.15: Total gauge / SCaMPR accumulations corresponding to vertical velocity bins using data from winter periods of 2002-2003 and 2003-2004. Threshold precipitation and estimation limits are 200 mm for 0.100 m/s updraft bin (a) and 475 mm for 0.500 m/s updraft bin (b). Fetch length is 15 km.	40
Figure 4.16: Total gauge / SCaMPR accumulations corresponding to vertical velocity bins using data from winter periods of 2002-2003 and 2003-2004. Threshold precipitation and estimation limits are 175 mm for 0.100 m/s updraft bin (a) and 450 mm for 0.500 m/s updraft bin (b). Fetch length is 20 km.	41
Figure 4.17: Total gauge / SCaMPR accumulations corresponding to vertical velocity bins using data from winter periods of 2002-2003 and 2003-2004. Threshold precipitation and estimation limits are 150 mm for 0.100 m/s updraft bin (a) and 400 mm for 0.500 m/s updraft bin (b). Fetch length is 7.5 minute wind duration.	42
Figure 4.18: Total gauge / SCaMPR accumulations corresponding to vertical velocity bins using data from winter periods of 2002-2003 and 2003-2004. Threshold precipitation and estimation limits are 175 mm for 0.100 m/s updraft bin (a) and 400 mm for 0.500 m/s updraft bin (b). Fetch length is 10 minute wind duration.	43
Figure 4.19: Total gauge / SCaMPR accumulations corresponding to vertical velocity bins using data from winter periods of 2002-2003 and 2003-2004. Threshold precipitation and estimation limits are 150 mm for 0.100 m/s updraft bin (a) and 450 mm for 0.500 m/s updraft bin (b). Fetch length is 14 minute wind duration.	44
Figure 4.20: Total gauge / SCaMPR accumulations corresponding to vertical velocity bins using data from winter periods of 2002-2003 and 2003-2004. Threshold precipitation and estimation limits are 150 mm for 0.100 m/s updraft bin (a) and 450 mm for 0.500 m/s updraft bin (b). Fetch length is 15 minute wind duration.	45
Figure 4.21: Total gauge / SCaMPR accumulations corresponding to vertical velocity bins using data from winter periods of 2002-2003 and 2003-2004. Threshold precipitation and estimation limits are 175 mm for 0.100 m/s updraft bin (a) and 600 mm for 0.500 m/s updraft bin (b). Fetch length is 20 minute wind duration.	46
Figure 4.22: Correction equations achieved using winter data plotted against updraft.....	48
Figure 4.23: Total gauge / SCaMPR accumulations corresponding to 0.500 m/s vertical velocity bins using data from summer periods of 2002-2004. Threshold precipitation and estimation limits are 100 mm, fetch length is 10 km.	49
Figure 4.24: Total gauge / SCaMPR accumulations corresponding to 0.500 m/s vertical velocity bins using data from summer periods of 2002-2004. Threshold precipitation and estimation limits are 100 mm, fetch length is 10 minute wind duration.	50
Figure 4.25: Total gauge / SCaMPR accumulations corresponding to 0.500 m/s vertical velocity bins using data from summer periods of 2002-2004. Threshold precipitation and estimation limits are 700 mm, fetch length is 14 minute wind duration.	51
Figure 4.26: Total gauge / SCaMPR accumulations corresponding to 0.500 m/s vertical velocity bins using data from summer periods of 2002-2004. Threshold precipitation and estimation limits are 500 mm, fetch length is 15 minute wind duration.	51
Figure 4.27: Correction equations achieved using summer data plotted against updraft	53
Figure 4.28: Variation of Temperature between summer and winter periods defined as the cumulative distribution of hit pixels vs. temperature	55
Figure 4.29: Total gauge / SCaMPR accumulations corresponding to point temperature values (a) and accumulations corresponding to 0.4 °K temperature bins (b) using data from winter periods of 2002-2003 and 2003-2004	56

Figure 4.30: Total gauge / SCaMPR accumulations corresponding to point temperature values (a) and accumulations corresponding to 0.4 °K temperature bins (b) using data from summer periods of 2002-2004.	58
Figure 4.31: Variation of specific humidity between summer and winter periods defined as the cumulative distribution of hit pixels vs. specific humidity	59
Figure 4.32: Total gauge / SCaMPR accumulations corresponding to point specific humidity values for winter periods of 2002-2003 and 2003-2004 (a) and summer periods of 2002-2004.	60
Figure 4.33: Variation of equivalent potential temperature between summer and winter periods defined as the cumulative distribution of hit pixels vs. dthe	61
Figure 4.34: Total gauge / SCaMPR accumulations corresponding to point equivalent potential temperature values for winter periods of 2002-2003 and 2003-2004 (a) and summer periods of 2002-2004	62
Figure 4.35: Variation of integrated moisture convergence between summer and winter periods defined as the cumulative distribution of hit pixels vs. iqcn	63
Figure 4.36: Total gauge / SCaMPR accumulations corresponding to point integrated moisture convergence values for winter periods of 2002-2003 and 2003-2004 (a) and summer periods of 2002-2004	64
Figure 5.1: Scatter plots of gauge measurements vs. SCaMPR estimations for 6 hour temporal resolution in winter periods (a) and in summer periods (b) after application of orographic correction	70

LIST OF SYMBOLS

ELR	: Environmental lapse rate
T_b	: Cloud top temperature
T_d	: Dew point temperature
V	: Resultant wind speed
S	: Terrain net slope
∇h	: Terrain height gradient in the direction of resultant wind
u	: Meridian component of resultant wind
v	: Latitudinal component of resultant wind
n	: Fetch length
w	: Topographically driven vertical air movement, either updraft or downdraft
T	: Temperature at 700 hPa level
RR _S	: Satellite based rain rate estimation
RR _C	: Corrected rain rate estimation

LIST OF ABBREVIATIONS

SCaMPR	: Self-Calibrating Multivariate Precipitation Retrieval
HE	: Hydro-Estimator
NAM	: North American Mesoscale Forecast System
NAME	: North American Monsoon Experiment
NOAA	: National Oceanic and Atmospheric Administration
NESDIS	: National Environmental Satellite Data and Information Service
NWS	: National Weather Service
STAR	: Center for Satellite Applications and Research

CHAPTER 1

INTRODUCTION

1.1. Statement of the Problem

Over mountainous regions, estimation as well as measurement of precipitation still remains challenging. As a conventional approach, these estimates and measurements are made with usage of rain gages which provide real time data. But topography has a big impact on the rain amount that catchment receives particularly over areas where moist air currents meet mountainous blocks. Therefore point gauges generally do not well represent the catchments, located over a rough topography.

In order to obtain correct distribution of rainfall over a rough topography with usage of aforementioned gages, the spatial density of these gages must be high, which may be achieved by only a network of gauges. But even in case of an existing rain gage network, the spatial density may be too coarse to capture variability of rainfall at small scales. Also operation and maintenance of these gages raises the question of access. Moreover, over mountainous regions, estimation of flash flood events also raise as a problem as they change greatly in short distance and time.

The problem of having an inadequate gage network system may be overcome with the usage of rainfall estimates. Now-casting rainfall estimates over a catchment area along with a surface runoff model may estimate flash flood events. Such rain estimates are generally made by use of radar and satellite based rainfall algorithms. Radar provides an indirect measurement of rainfall, but mountainous regions often lack good radar coverage due to blockage of the beam by mountain blocks. Satellite rainfall algorithms provide a less accurate estimation of rainfall, but provide high spatial and temporal resolutions and complete coverage of the area. Also over mountainous regions, radar is generally not in operation and rain gage data are very rare or non-existent. Therefore, satellite based rainfall algorithms are promising alternatives to fulfill such need. For this purpose, the National Oceanic and Atmospheric Administration (NOAA) National Environmental Satellite Data and Information Service (NESDIS) Center for Satellite Applications and Research (STAR) has been providing satellite based precipitation estimates operationally since 1978. Two operational satellite based rainfall algorithms are the Hydro Estimator (HE) (Scofield and Kuligowski, 2003) and the Self-Calibrating Multivariate Precipitation Retrieval (SCaMPR) (Kuligowski, 2002).

Satellite based rainfall algorithms need to be adjusted for the orographic events and atmospheric variables for the continued improvement of the estimates. However, unlike the operational HE algorithm, SCaMPR currently does not contain any adjustments for complex topography or any atmospheric variable in rainfall estimation. In this study, an orographic adjustment method and a temperature adjustment method that will enhance precipitation distribution, improve accuracy and remove topography and temperature dependent bias will be developed for the Self-Calibrating Multivariate Precipitation Retrieval (SCaMPR) rainfall algorithm to be used in operational forecasting for meteorological and hydrological applications.

Also nowadays, in hydraulic and hydrological applications over mountainous regions, obtaining surface runoff data raises as a problem. In such models, lacking flow data is generally obtained by using the drainage area ratio method (Korleski and Strickland, 2009). However, rainfall estimates over a catchment area along with a surface runoff model may also provide lacking flow data for these models.

1.2. Objective of the Study

The first objective of this work will be to provide a comprehensive comparison of SCaMPR rain rates with respect to rain gage transects. Then, an orographic adjustment will be developed with reference to multiplicative error analysis. The satellite-derived SCaMPR quantitative precipitation estimates to the gage precipitation measurement ratios will be compared to pertinent parameters such as slope,

relative wind direction and relative wind speed, as well as atmospheric stability indicators, such as temperature and specific humidity. The relationships that are obtained during this analysis will be used to create a more accurate terrain adjustment for SCaMPR products.

The aim of this study is to introduce an orographic correction and a temperature correction which is expected to improve the accuracy of the SCaMPR algorithm and to provide real-time high-resolution quantitative precipitation estimates over complex terrains using NOAA Geostationary Operational Environmental Satellites (GOES) data. The correction study will cover the summer and winter periods separately and performance of the SCaMPR algorithm will be analyzed for both of these seasons.

1.4. Description of the Thesis

This thesis comprises six chapters. Chapter 1 is the Introduction. It highlights current need for the orographic correction for satellite rainfall algorithms with effect of the complex topography on the rainfall, and states the objectives of the study. Chapter 2 provides background information on the satellite rainfall algorithms with orographic precipitation topic, studies done on this topic and possible methods for reflecting the effect of the orography on the satellite rainfall algorithms. Furthermore, Satellite rainfall algorithms the Hydro Estimator (HE) and the Self-Calibrating Multivariate Precipitation Retrieval (SCaMPR) and the study area are explained in detail in Chapter 3. The proposed methodology and its variables are explained and analyzed in Chapter 4. In addition, both stability of the atmosphere and upwind or downwind motion of the air block over the terrain are analyzed in this chapter. Chapter 5 covers the results of the application of orographic correction. Finally, the results are discussed in Chapter 6 and recommendations for future research are identified.

CHAPTER 2

LITERATURE REVIEW

2.1. Satellite Rainfall Algorithms

Satellite rainfall algorithms rely on data extracted from two types of satellites: geostationary satellites (geosynchronous satellites) and polar orbiting satellites. The methodology of the algorithms is based on from which satellite type the data is coming from. Generally satellite data from visible/infrared and microwave part of the spectrum is used in the algorithms.

Geostationary and polar orbiting satellites provide different spatial coverage feature over the terrain, but from the perspective of more accurate estimates, spatial coverage is not the only factor. The more important factor is the resolution of satellite data, in terms of temporal and spatial extents. Temporal resolution (TR) refers to the frequency of a measurement with respect to time. It may be described as the average time span between two measurements of satellite for the same spot. Spatial resolution (SR) on the other hand, is described as the ability to distinguish small details of an object over an image. It is the on-ground dimensions of an image pixel. The higher resolution of an image will result in more accurate and detailed rainfall estimation. Fine resolution; both temporal and spatial, is crucial in forecasting flash flood events in complex terrain as weather conditions can vary greatly over short distances and time which may cause significant weather related hazards. Satellite based rainfall estimates can provide critical rainfall information in regions where data from other sources are unavailable or unreliable, such as over oceans or sparsely populated regions.

2.1.1. Satellites

A geosynchronous satellite is a satellite in geosynchronous orbit, with an orbital period the same as the Earth's rotation period. A special case of geosynchronous satellite is the geostationary satellite, which has geosynchronous orbit directly above the Earth's equator. Geosynchronous satellites remain permanently in the same area of the sky, as viewed from a particular ground station.

The geostationary satellites provide data from the visible/infrared part of the spectrum. They are available at relatively higher spatial resolution (3-4 km) at sub-satellite point and higher temporal resolution (15 min) compared to the polar satellites. The visible/infrared data provides cloud top properties in case of a cloud presence. With the usage of visible/infrared data, the main method used for rainfall estimation is relating cloud top temperature (T_b) to the rainfall amount measured on the ground. All atmospheric events occur in the lowest principal layer of the atmosphere called, Troposphere. Within this layer, temperature decreases with the increasing altitude. This decrease is named as lapse rate. The environmental lapse rate (ELR), is defined as the rate of decrease of temperature with altitude in the stationary atmosphere at a given time and location. On average, it is defined as:

$$\text{ELR} = 6.49 \text{ }^\circ\text{K (}^\circ\text{C)} / 1000 \text{ m} \quad (2.1)$$

As the cloud top temperature (T_b) can be obtained from the visible/infrared image, cloud top height can also be retrieved. The cloud top is the highest altitude of the visible portion of the cloud. At this level, dew point can also be calculated. The dew point is the temperature below which the water vapor in a volume of humid air at a constant pressure will start to condense into liquid water. In other words, cloud base is the lowest elevation where temperature and dew point temperature (T_d) of the parcel are equal. Dew point is a function of air temperature and relative humidity.

Once both cloud top and cloud base is determined, the cloud height can be estimated easily. As a basic understanding, larger cloud heights refer to larger precipitation amounts specifically for the cumuliform precipitation types. From this point, rainfall estimate may be expressed as a linear, exponential or logarithmic function of cloud top temperature (T_b). This methodology is summarized in Figure 2.1.

A polar orbiting satellite passes above or nearly above both poles of the Earth on each revolution. It therefore has an inclination of (or very close to) 90 degrees to the equator.

In addition to the visible/infrared data, polar orbiting satellites provide data from the microwave part of the spectrum as well. Microwave data are available at relatively lower spatial resolution (5-15 km) at sub-satellite point and lower temporal resolution (~twice a day) compared to the geostationary satellites. Microwave data provides information from the cloud interior, such as liquid-water content and ice. Via Microwave data, cloud water and ice content are related to rainfall rate. As microwave data penetrates into the cloud through emission, the estimations based on these data are more accurate. On the other hand, polar orbiting satellites have a coarse temporal resolution. They are available with a temporal resolution of twice a day; therefore an estimation based solely on microwave data may be more accurate but will not reflect the changes precipitation within the estimation period. As a result, microwave data is only used for the calibration of the available rainfall estimation from visible/infrared data which is available at a higher temporal resolution, up to 15 minutes.

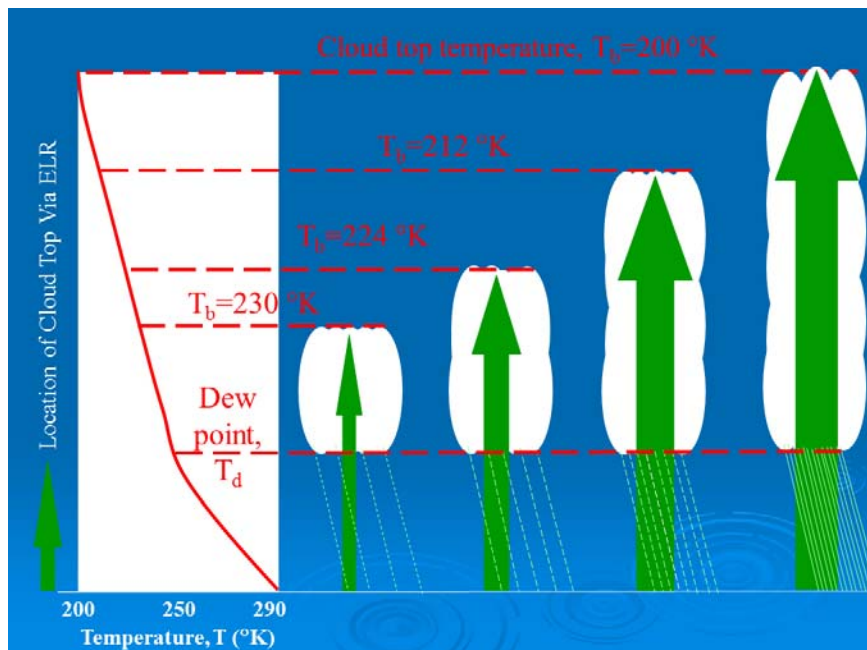


Figure 2.1: Visible/Infrared data (Cloud top temperature) rain estimation algorithm

2.2. Definition of Orographic Precipitation

Orographic precipitation is defined as the precipitation that has been generated or modified by vertical atmospheric motions induced by topography and wind. Formation of orographic precipitation is driven by topography: when air block, with the effect of resultant wind, hits a hill, it is forced to rise parallel to the slope of hill surface, causing moisture to condense and eventually forming precipitation (Smith, 2006).

The effect of the topography on the precipitation has always been evident. It has been shown that, in an event of storm, small hills may get as twice precipitation as surrounding terrain (Bergeron, 1961). Rainfall amounts over a terrain depend on the air flow over the mountains and the disturbances created by the mountains, resulting with the cooling and condensation of the ascending moist air block with upwind force, thus forming precipitation. The influence of mountains upon rainfall is often profound, causing some place to receive more rainfall, for example, Cherrapunji in India is the wettest place on earth, where monsoon flow encounters the southern Himalayas, or Eastern black sea region is the wettest place in Türkiye, where moist wind over black sea encounters Kaçkar Mountains, and causing some places to be drier, for example, the central valleys of the Atacama desert is the driest place on earth, shielded by surrounding mountains.

Orographic precipitation is described as a mountain range whose axis lies perpendicular to the resultant wind direction, thus windward side of the mountain receives much of the precipitation and

lee side receives less. As a result rain shadow is formed, creating a sharp transition in climate, flora and fauna between two sides of the mountain range (Roe, 2005). The Tibetan Plateau is the unique example for the effects of orography on the precipitation and resultant climatic transition, the rain shadow. Moist weather originating from Indian Ocean does not make it past the Himalayas and lead to an arid climate on the lee side.

From the interrelation of weather, namely resultant wind and changing terrain topography, a vertical motion will be formed. An updraft or downdraft is the vertical movement of air as a result of this relation. Upwind motion of the air block with the effect of the resultant wind is defined as updraft while opposite movement is defined as downdraft. Total movement of the air mass upward as a result of the orography is called orographic lifting.

Updrafts are generally seen on the windward side of the mountain where resultant wind encounters with the terrain, where downdrafts are seen at the lee side of the mountain. The wind portions of the orographic lifting can be seen in Figure 2.2.

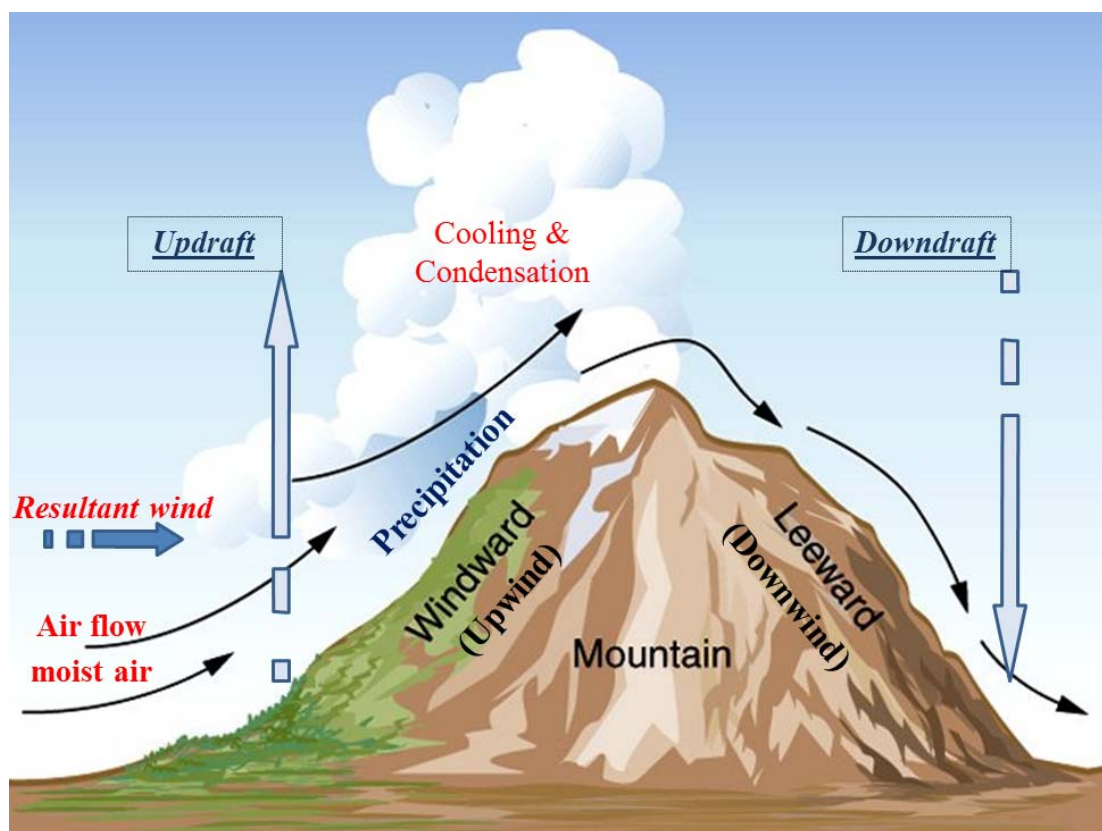


Figure 2.2: Orographic precipitation formation and participating elements

Updraft is defined as the dot product of the net terrain slope with the resultant wind speed.

2.3. Orographic Correction

Orographic precipitation is induced by three main factors, thus orographic correction techniques use the interaction among these parameters: the resultant wind vector V determined at a specific atmospheric pressure level, the fetch length n over which terrain effects will be taken into account and the local terrain height gradient (slope) ∇h in the direction of the resultant wind vector, V . In the past studies, the length of hill is taken as a factor to define the effect of orography (Carruthers and Choularton, 1983), but in the latter studies this is added to into slope calculation as fetch length to include effect of changing hill surface to the slope (Vicente et al., 2002, Kwon et al., 2008).

2.3.1. Resultant Wind Speed

The wind field data as meridian (u) and latitudinal (v) components are taken from a numerical weather prediction model called the North American Mesoscale Forecast System (NAM) that is run operationally over North America. NAM wind fields are provided for different pressure levels, although surface wind field was present, it was not used as the interaction between surface and wind vectors will result in the disturbance of the wind field. Since undisturbed wind vector is needed to represent the correct relation between wind and surface, the wind field at 700 hPa pressure level is taken into account. This wind field is analyzed carefully to reflect the topography-wind relation properly.

2.3.2. Fetch Length

The fetch, often called the fetch length, is the scale length over which terrain effects will be taken into consideration for the resultant wind. Fetch length along with the wind speed (or strength) determines the magnitude of upwind force that causes orographic precipitation. According to Urbanski (1982), the optimum fetch length for terrain effects is 10 km. Nevertheless, it is shown that a variable fetch length based on wind speed is found to be more effective, thus a 15-minute fetch length is analyzed limiting fetch to vary from 4 km to 24 km depending upon wind speed (Vicente et al., 2002). Also another orographic correction method was developed by optimizing the fetch length by using constant distance values, 9, 12, 15, and 18 km respectively (Kwon et al., 2008).

In the analysis, fetch length is selected both as a constant horizontal scale and as a function of wind speed and time. In the latter alternative, fetch length is defined as;

$$n = V \left[t / (1000 \text{ m/pixel}) \right] \quad (2.1)$$

where; n is the fetch length converted into pixels, V is the resultant wind speed in m/s, t is the duration assigned for assessment of fetch length in second. Each pixel in the model has a width of 1000 m, which is added to the equation as a conversion factor.

2.3.3. Slope

Both Vicente et al. (2002) and Kwon et al. (2008) used the same approach for slope definition. The same slope calculation methodology is adopted in this analysis as this approach takes into account both windward and leeward region, namely upwind and downwind direction. The topographical effect is examined by relating the wind vector (V) to the gradient of the local terrain height in the wind direction. It is assumed that the atmospheric vertical motion, either updraft or downdraft is forced by resultant wind V blowing over a terrain area whose net slope is S. At a given location X, the net slope S is determined by a type of an averaged terrain height within the horizontal length scale of (2n + 1) pixels centered at X. In this method, the average slope with n pixels upwind and downwind region of location is analyzed. In this methodology, the slope is calculated as follows:

(2n + 1) grid points are considered with centering the station location X. The points at the upwind direction of point X (n points) along with station point X (a total of n + 1 points) are assigned as point A. For any A point, terrain slope (S_{AB}) values between the point A (varying from X - n to X) and a total of n downwind points named B (varying from A + 1 to A + n for a given A) is defined by;

$$S_{AB}^{1..n} = \frac{Z_B - Z_A}{x(B) - x(A)} \quad (2.2)$$

where Z_B and Z_A are the elevations of the points B and A respectively, while $x(B)$ and $x(A)$ are the pixel locations of the two points, thus giving the horizontal distance between two points by $x(B)$ and $x(A)$. As the B points locates downwind of point A, varying from point (A + 1) to point (A + n), the corresponding slopes [i.e., $S_{AB}^{(1)}$, $S_{AB}^{(2)}$, ..., $S_{AB}^{(n)}$] are calculated for each A points. The point slope values of each A points (i.e., $S_A^{(i)}$) are then denoted as a maximum slope out of n values of S_{AB} values giving a total of n + 1 point slopes; that is,

$$S_A^{1..n+1} = \text{Max} \left[S_{AB}^{(1)}, S_{AB}^{(2)}, \dots, S_{AB}^{(n)} \right] \quad (2.3)$$

As the point A varies from a point X - n to a point X, totaling n + 1 points, the average point slopes of these n + 1 points are taken to get a net slope S for a given location X; that is,

$$S = \frac{\left(\sum_{A=1}^{A=n+1} S_A \right)}{(n+1)} \quad (2.4)$$

where point ($A = 1$) is the ($X - n$) point while point ($A = n + 1$) is the (X) station point. Using this method, weighted average of the maximum slopes within the $(2n + 1)$ pixels which centers the station point X are taken. After the slope S is determined, the movement of the air block over the surface of the mountain, updraft or downdraft can be calculated by the inner product of the resultant wind velocity vector, V and S is the net slope of the station location, that is,

$$w = (V \bullet S) \quad (2.5)$$

where w is the magnitude of the vertical atmospheric movement, either updraft or downdraft.

2.3. Correction Algorithm

The rainfall rates are observed to increase significantly over the surface of hills than the surrounding flat areas. To define this phenomenon the first mechanism is proposed by Bergeron (1965). Smith (1973) defined the upslope model, which enhance precipitation proportional to the slope, product of resultant wind to the elevation gradient and integrated moisture. Smith (2003) and Smith and Barstad (2004) developed this model by integrating microphysics and linear wave dynamics to the model. Various models were improved to include effect of complex topography on rain estimates, in terms of both distribution and intensity (Collier, 1975; Bell, 1978; Sinclair, 1994; Misumi et al., 2001; Roe, 2005). Vicente et al. (2002) defined a completely different approach to include effect of complex topography on rain estimates: by developing a topographic correction technique which will be used to calibrate visible/infrared based precipitation estimates. Kwon et al. (2008) provided an application example based on the slope definition developed by Vicente et al. (2002). In this study, it is aimed to develop the topographic correction technique first defined by Vicente et al. (2002) by incorporating microwave based rain rates.

Vicente et al. (2002) defined an orographic adjustment factor, M that will adjoin the effect of the topographic effects to the satellite rainfall estimations. If there is no topographically driven vertical movement on the air block of interest, then there will be no adjustment for orography. For multiplicative orographic formulation, this adjustment value will be unit, quantitatively 1.0 as multiplication of rain estimation with 1.0 will result with the original estimation. As this factor should have no effect on the rainfall estimations on a flat terrain, this adjustment factor is defined as:

$$M = 1 + VS \quad (2.6)$$

This adjustment factor is applied to the rainfall estimations as a multiplication factor based on the updraft value of rainfall estimation in question. As a result, new estimation value will be:

$$RR_C = RR_S \times (1 + VS) = RR_S \times M \quad (2.7)$$

where RR_C is the rain rate estimation corrected for topographic effects and RR_S is the satellite based rain rate estimation.

It is shown that although M may take negative values from the equation, it will not represent a meaningful physical value as it will end up with negative rainfall estimation. Based on Urbanski (1982) relating orographic lifting effects and multiplicative error values of rainfall estimations, Vicente et al. (2002) limited M value to be between 0.2 and 3.5.

Vicente et al. (2002) showed that orographic correction enhances satellite based precipitation estimates that are without correction. However, a validation of this correction algorithm could not be carried out due to the lack of a dense network of surface rainfall measurements.

Although Vicente et al. (2002) developed a multiplicative adjustment formulation; Kwon et al. (2008) proposed an additive methodology for adjustment. First, satellite rainfall estimation algorithm is defined as,

$$RR_S (\text{mm/h}) = 0.0157(SI)^{1.734} + 1.7 \quad (2.9)$$

where RR_S is the simulated rain rate, and SI is the scattering index. To define the orographic effects, Kwon et al. (2008) first derived additive error values between the model-produced rain rates and

simulated rain rates; and then related to the topographically forced upslope motion. This relation shows a positive correlation at the upstream region, thus showing that in the presence of topographically forced vertical motion, the scattering-based satellite rainfall algorithm underestimate rain rate.

In the analysis, Kwon et al. (2008) also added two parameters to the correction equation: the water vapor mixing ratio (q) and low level moisture convergence (Q_{con}). On the other hand the analyses are done for only upstream region over the mountain area as correlation coefficients in the downstream region appear to be less meaningful. As a result correction algorithm based on updraft values are formed as follows:

$$RR_1(\text{mm/h}) = 0.0157(SI)^{1.734} + 7.586 V \times S + 0.8 \quad (2.10)$$

As the simulated rain estimation algorithm is defined in the equation (2.8), the resulting orographic adjustment factor developed by Kwon et al. (2008) is found to be:

$$M = 7.586 V \times S - 0.9 \quad (2.11)$$

When the other two parameters are added to the correction algorithm, final algorithms are obtained as,

$$RR_2(\text{mm/h}) = 0.0157(SI)^{1.734} + 1.296(q - 4.162) V \times S + 0.8 \quad (2.12)$$

$$RR_3(\text{mm/h}) = 0.0157(SI)^{1.734} + 1.353(Q_{con} + 4.497) V \times S + 0.8 \quad (2.13)$$

Vicente et al. (2002) provided a theoretical approach to reflect topographic effects to satellite based rain rate estimations. Kwon et al. (2008) provided another approach to the same issue, also provided an application example. Defined correction algorithms are applied to the simulated rain rates and results are compared to the model-produced rain rates.

CHAPTER 3

SATELLITE RAINFALL ALGORITHMS AND STUDY AREA

3.1. Satellite Rainfall Algorithms

To support short-term rainfall estimations for flash flood warning and heavy precipitation forecast, the NOAA/ NESDIS STAR provides operational satellite based precipitation estimates both in image and data formats. These products are intended to be used for short-term estimates of rainfall at high spatial and temporal resolution. Two operational satellite based rainfall estimate models are the HE (Scofield and Kuligowski 2003) and the SCaMPR (Kuligowski 2002).

3.1.1. The Hydro Estimator, HE

The Hydro Estimator (HE) uses infrared (IR) data from NOAA's Geostationary Operational Environmental Satellites (GOES) to estimate rainfall rates. It has been an operational satellite rainfall algorithm at NESDIS since 2002.

The Hydro Estimator (HE) uses a single-channel (10.7 μm) brightness temperature to derive raining areas and rain rates. Raining areas are derived according to rain/no rain discrimination via brightness temperature of the pixel relative to nearby pixels. If the brightness temperature of the pixel is colder than average of the surrounding, then the pixel is denoted as active rain area whereas for warmer condition, the pixel is denoted as inactive cold cloud with no rainfall. HE provides instantaneous rain rates at every 15 minutes. The algorithm also automates corrections using numerical weather prediction model data, including;

- Precipitable water, which enhances rainfall in moist regions,
- Relative humidity, which reduce rainfall in arid regions with significant sub-cloud evaporation of raindrops
- Orography, which both increase and decrease rainfall data based on wind field - digital topography interaction.

The adjustment for orography detailed in Vicente et al. (2002) is incorporated into the HE algorithm. The orography adjustment uses wind fields at 850 hPa level and topography from a digital elevation model at 4-km resolution to derive the vertical component of wind.

The image data output of the HE 24-hour rainfall rate estimation ending at 01.12.2013 12:00 UTC for areas covered by the satellite Meteosat-9, the regions of Europa, North Atlantic, North Africa, is shown on Figure 3.1.

Yucel et al. (2009) evaluated the HE algorithm with and without orographic correction method over a mountainous region to evaluate the performance of satellite derived rainfall estimates for terrain induced precipitation events. In the study of Vicente et al. (2002) a comprehensive validation of correction was not carried out due to the lack of a dense network of surface rainfall measurements. With the installation of a new event based surface raingage network (NERN) over a complex topography of northern Mexico, a performance analysis of the algorithm became possible. Yucel et al. (2009) showed that satellite based rainfall algorithm, HE, derives precipitation with less frequent but more intense than observed on the ground, with overestimation that is more evident with high rainfall amounts. Also, it is stated that the current orographic correction method in the HE algorithm does show some positive impact on accuracy, but its magnitude is not sufficient to substantially remove elevation-dependent bias structure.

3.1.2. The Self-Calibrating Multivariate Precipitation Retrieval, SCaMPR

The Self-Calibrating Multivariate Precipitation Retrieval (SCaMPR) algorithm aims to combine the relative strengths of infrared (IR) and microwave (MW) based precipitation estimates. Infrared data are available at high spatial and temporal resolution, but in the infrared range, raining clouds are opaque, the infrared radiation cannot penetrate into clouds rather they are reflected from top of the clouds. Thus precipitation information must be inferred from cloud-top properties such as temperature

and texture. In contrast, raining clouds are semitransparent at MW frequencies. Therefore MW radiances can provide cloud interior properties such as liquid water content and ice, thus resulting in a more robust relationship with precipitation rates. However, MW data are available only from polar orbit platforms, and thus are available at low temporal (~twice a day) and spatial resolution.

SCaMPR uses GOES infrared data as a source of predictor information, thus optimizing the temporal and spatial resolution of the estimates. The MW data from polar orbit platforms are used as target information to optimize the accuracy of the estimations. The selection of predictors and calibration are performed in two steps by SCaMPR: rain/no rain discrimination using discriminant analysis as in HE algorithm, and precipitation rate calibration using multiple regressions. The resulting calibration coefficients are applied to independent GOES data to obtain SCaMPR rain rate estimations.

The SCaMPR algorithm does not feature any correction for terrain effects through orographic adjustment on rainfall estimation.

The details about the SCaMPR rain rate estimation algorithm are summarized by Kuligowski (2002) and basic steps are visualized in Figure 3.2.

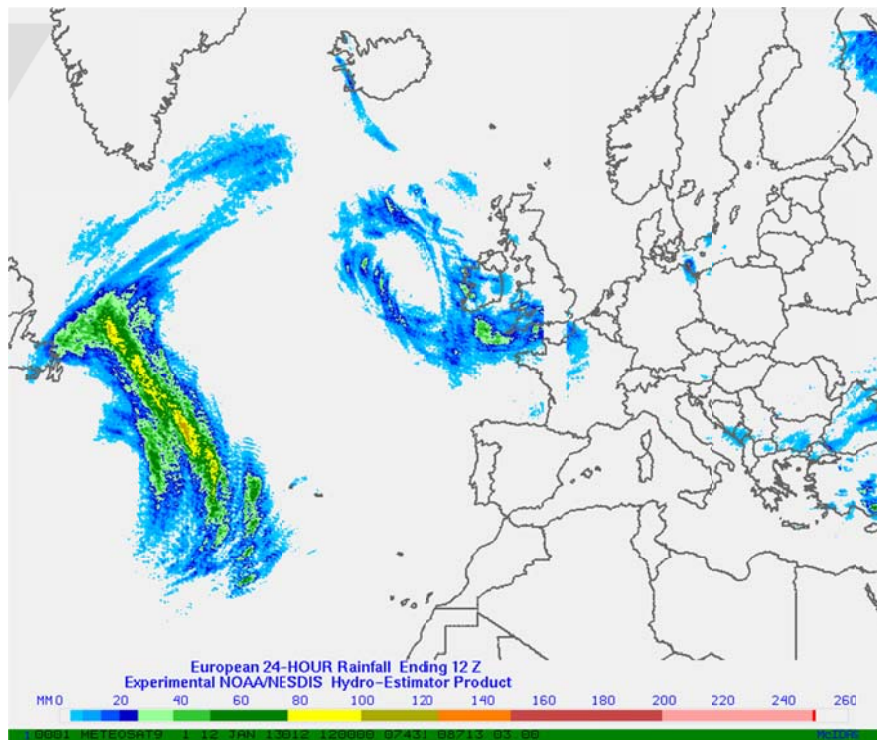


Figure 3.1: 24-hour HE rainfall estimation over continental Europe and North Atlantic ending 12.01.2003 12:00 UTC

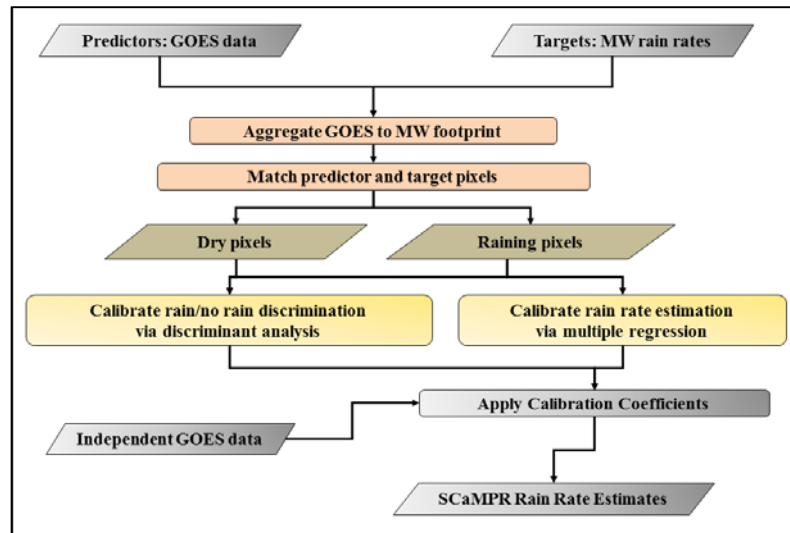


Figure 3.2: SCaMPR rain rate estimation algorithm (Kuligowski, (2002))

3.2. Study Area

The study area is located in the semi-arid climate region of north-western Mexico, between the Gulf of California and Sierra Madre Occidental mountain range (Figure 3.3). The selection of the study area is made because of the existence of a unique rain gage network located over Sierra Madre Occidental mountain range. This network is installed as a part of North American Monsoon Experiment (NAME) program and has the capability to sample the temporal and spatial patterns of rainfall across regional topographic gradients. Gochis et al. (2007) demonstrated the ability of the network to capture diurnal and regional based precipitation characteristics. Such a rain gage network with the same capability is not existent in Türkiye, thus this study could not be conducted for Türkiye.

The study area is located between latitudes 23° and 31° North and longitudes 104° and 112° West as shown in Figure 3.3. The target area is approximately 180,000 km². The study area receives majority of its rainfall from convective and tropical storms during the summer monsoon season and from frontal storms during winter (Yücel et al., 2009). Spring season generally passes dry. Monsoon rains come to the Sierra Madre in June, as the high pressure area moves north, leading to wet summer seasons. These summer rains typically continue until mid to late September when a drier regime is re-established over the fall season. The spring and fall seasons are separated out by a weaker wet season in the winter. Most of the study area experiences a rainy season from June to mid-October and significantly less rain during the remainder of the year. For instance, long term precipitation average of years from 1981 to 2010 for winter period (Lasting from start of December to end of March) is 128.8 mm and for summer period (Lasting from start of July to end of September) is 554.6 mm for the station located at 26.43° North and 108.22° West coordinates (Servicio Meteorológico Nacional – National Meteorology Service, 2013). In addition to changing rainfall distribution over seasons, rainfall also increases in the higher elevations of the mountain range. Temperature of the study area is fairly constant over the seasons and varies solely as a function of elevation. During the monsoon period in summer, temperatures remain high, whereas during winter temperatures stay at cool level. For instance, long term temperature average of years from 1981 to 2010 for winter period (Lasting from start of December to end of March) is 18.5°C and for summer period (Lasting from start of July to end of September) is 29.0°C for the station located at 26.43° North and 108.22° West coordinates (Servicio Meteorológico Nacional – National Meteorology Service, 2013).

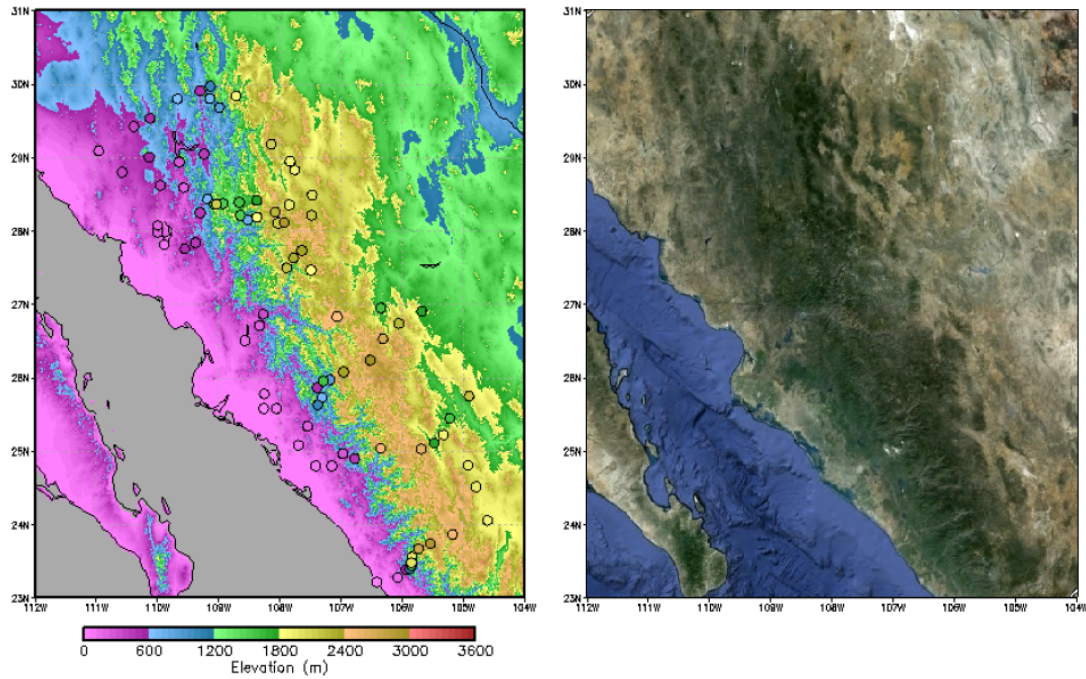


Figure 3.3: Digital topography of the study area with gauge locations and elevations overlaid as circles (left), satellite image of the same location (right)

As seen in Figure 3.3, a gauge network exist over west–east transects through the Sierra Madre Occidental mountains, which lays over northwest – southeast axis. The gauge network, which consists of 85 point gauge stations, provides high spatial resolution to represent precipitation distribution over terrain elevation. The elevation breakdown and longitudinal locations of the gauge network is provided in Figure 3.4. Also the elevation is partitioned in Table 3.1 into 250 and 500 m terrain elevation bands to show the variation of gauge distribution over elevation. It is clear in Figure 3.4 that the elevations of the gauge stations get higher moving from west to east, as the network advances through the mountain range. The gauge stations are well distributed over the study area. The closest distances between two adjacent gauge stations in the network are 4.7, 4.8 and 9.2 km respectively.

Gauge network over the Sierra Madre Occidental mountain range is a unique network designed for the purpose of hydrological and meteorological model developments, thus enables a research of terrain effects on rainfall possible.

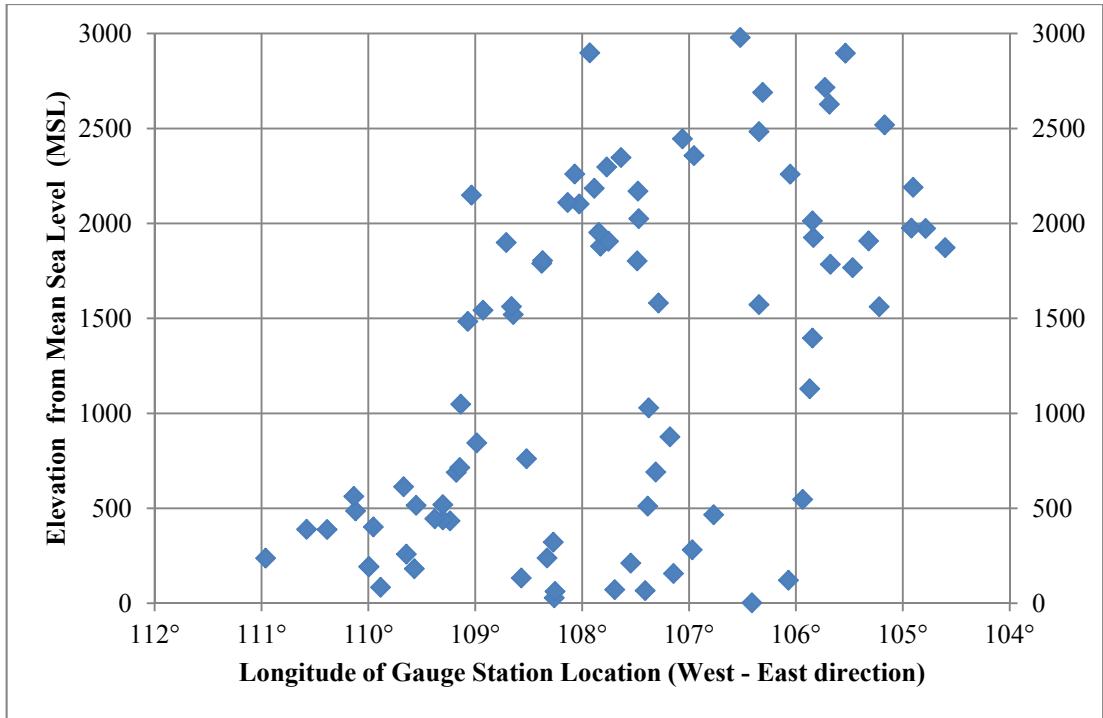


Figure 3.4: The latitudinal locations over west to east transect and elevation breakdown of gauge stations

Table 3.1: The elevation breakdown of the gauge stations over a) 250 m and b) 500 m terrain elevation bands

a)	Elevation Band (m)	MSL (0) - 250	250 - 500	500 - 750	750 - 1000	1000 - 1250	1250 - 1500
	# of stations	15	11	9	3	3	2
	Elevation Band (m)	1500 - 1750	1750 - 2000	2000 - 2250	2250 - 2500	2500 - 2750	2750 - 3000
	# of stations	6	14	8	7	4	3

b)	Elevation Band (m)	MSL (0) - 500	500 - 1000	1000 - 1500	1500 - 2000	2000 - 2500	2500 - 3000
	# of stations	26	12	5	20	15	7

CHAPTER 4

METHODOLOGY AND ANALYSIS

4.1. Introduction

The methodology used in this study in order to achieve the orographic correction algorithm is summarized in Figure 4.1.

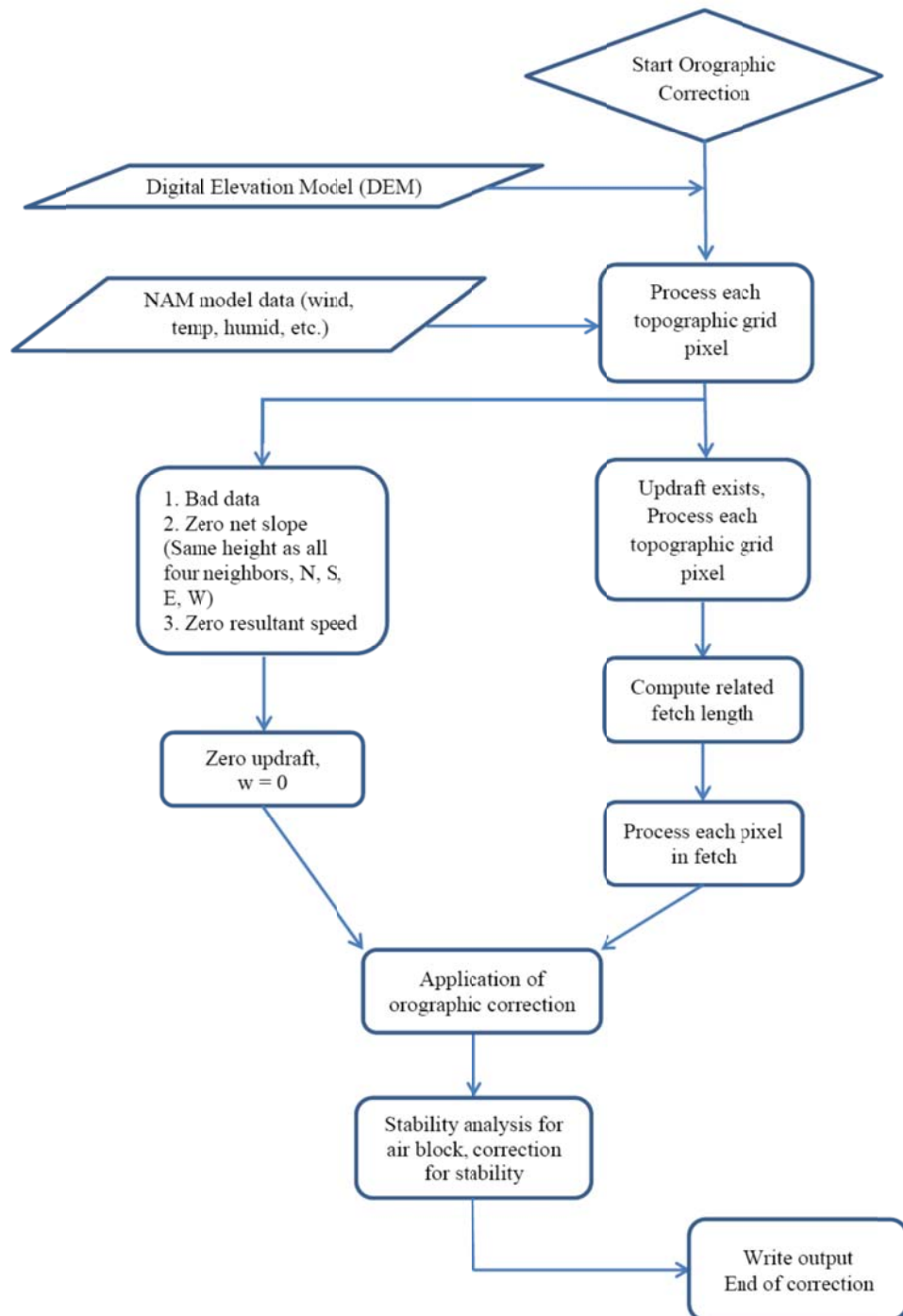


Figure 4.1: Flowchart of the methodology used in the orographic correction analysis

4.2. Preparation of Required Data and Information

Three sets of data are used for this study, gauge measurements, SCaMPR estimates and the NAM environmental model outputs. At the end of the analysis, the improved correction equation is tested over the study basin using the gauge measurements, SCaMPR estimates and corrected SCaMPR estimates. The analyses are done for both winter (2002 – 2003 and 2003 – 2004 years) and summer (2002, 2003 and 2004 years) season data separately using gauge measurements as the ground truth data. Furthermore, achieved results are compared with the orographic correction performance of HE algorithm for summer season (2002 and 2003 years). Winter period is defined to be starting from the beginning of December to the end of March, while summer period is defined to be from start of July to the end of September. The determination of the summer and winter periods are formed on the basis of the monsoon period and extraction of dry periods.

4.2.1. Gauge Measurements

The gauges are part of an event-based rainfall observation network located in north-west Mexico, established as part of the North American Monsoon Experiment (NAME); (North American Monsoon Experiment, 2013) provides gauge-based precipitation measurements with sufficient temporal and spatial sampling resolution to examine the climatological structure of diurnal convective activity over north-west Mexico. The measurements are point measurements of cumulative rainfall amount with 1 hour temporal resolution.

Spatial and temporal patterns of NAME event gauge network during 2002 – 2004 periods are analyzed and preliminary diagnostics were provided by Gochis et al. (2003, 2004, 2007); it has shown that the spatial patterns of the observed precipitation follows the regional hydroclimatology.

A total of 85 gauge stations, installed during the study period of 2002 – 2004, are overlaid on complex topography in Figure 3.3. Therefore not all gauges are available during the study period of this study. The availability of gauge stations is presented in Table 4.1.

Table 4.1: Availability of gauge stations over study duration

Winter Period			Summer Period		
Year	# of installed gauges	# of reporting gauges	Year	# of installed gauges	# of reporting gauges
2002 - 2003 winter	45	41	2002 summer	48	48
2003 - 2004 winter	66	66	2003 summer	78	75
			2004 summer	85	85

4.2.2. SCaMPR and HE Estimates

SCaMPR instantaneous rain rates are provided with 15 minutes interval but they are converted to hourly cumulative intervals for the temporal match with hourly gauge measurements. Gauge measurements are point-wise measurements while SCaMPR estimates are pixel-wise with 4 km spatial resolution. After matching the 4-km SCaMPR pixel with each of the station locations, time series of SCaMPR estimates are prepared for each of the stations for the whole study period. SCaMPR data are provided as hourly grid image with grid sizes 1116 columns and 908 rows. The grid location is specified as starting from 9.903333 degrees North and 120.033611 degrees West with meridional (N/S) resolution of 0.044319184 degrees in latitude and zonal (E/W) resolution of 0.035931241 degrees in longitude.

HE rain rates are provided with the same temporal (1hr) and spatial (4km) resolution as SCaMPR rates. As in SCaMPR estimates, the actual HE estimates are available in 15 minutes time steps so they are aggregated into 1 hour durations for the same purpose. Time series of HE pixels coinciding with the gauge measurements over the study area are used. HE data with and without orographic correction method is available to be used in comparison with SCaMPR estimates. Orographic correction technique used in the HE algorithm is an operational correction technique; therefore, the performance of this correction technique may be addressed as a criterion for the proposed orographic correction methodology that will be defined in this study.

4.2.3. North American Mesoscale Forecast System (NAM) model data

The temporal resolution of NAM modeling system is 6 hours so that it is run four times a day (at 00z, 06z, 12z and 18z) and provides atmospheric variables at 10km spatial resolution. Wind fields in m/s (both in u (longitudinal) and v (meridional) direction, in separate files), temperature in °K and specific humidity in kg/m³ for both 700 hPa level and at a constant height above the terrain, which is no more than 50 hPa from surface, are provided. Also equivalent potential temperature difference in °K between 700 hPa and surface with integrated moisture convergence kg/m²/s between 700 hPa and surface are provided. (North American Mesoscale Forecast System, 2013)

NAM model data are provided as grid images, with 250 rows and 450 columns, as 1 image for every 6 hour model output. The grid location is specified as starting at 35 degrees North and 125 degrees West with grid spacing of 0.1 degrees in each direction. As being performed with SCaMPR estimates, time series of these atmospheric variables at each rainfall gauge location are obtained for whole study period.

In the analysis, in order to define biases related with the atmospheric indices, index values for the 700 hPa level is taken although surface level values were present. In the updraft analysis, the undisturbed wind field, which is proposed wind vector in case of missing surface wind interaction, is required to define the correct relation between wind and surface. This wind field is provided at the 700 hPa level. Also surface temperature values may lead to erroneous relations as the heating of the surface is not equal, especially over the rough surfaces.

4.2.4. Digital Topography

Digital topography (STAR, 2013) of the study region is provided at 1 km resolution to calculate slopes for a given fetch length for orographic correction. The grid image is in size of 3000 x 3000 pixel, starting at 37.4856 degrees North and 119.9858 degrees West, proceeding along row and column increments of 0.008333 degrees. Values are height values defined in meters above the sea level. Digital topography is provided in Figure 4.2.

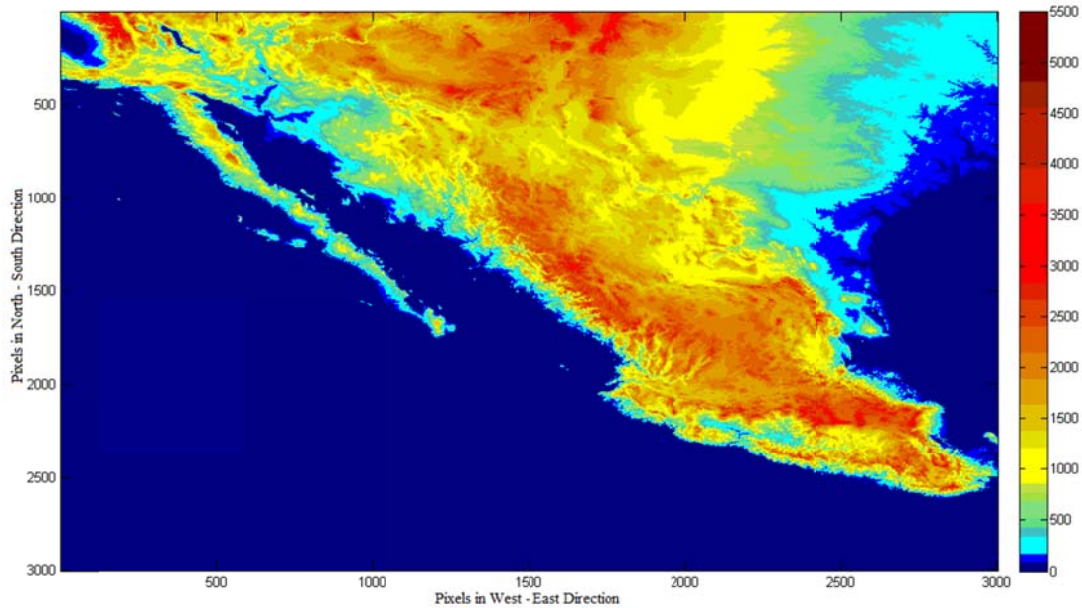


Figure 4.2: Digital topographic map of the study area

4.2.5 Representativeness of SCaMPR Estimates and NAM data for Gauge Stations

The topography of the terrain is defined by a 3000x3000 pixels digitized map, formed of 1km by 1km pixels whereas satellite rainfall estimates are provided with 4km by 4km pixels and gauge measurements are obtained at point-wise observations.

In order to control representativeness of NAM data pixels for the station points they are overlaying, the NAM data are compared to the atmospheric soundings obtained from the website of University of Wyoming (Wyoming University, 2013) Atmospheric wind variable is checked for five radiosonde stations located in the study area, and they are compared with the 700 hPa wind field derived from NAM. First the 700 hPa NAM wind field is displayed for 4th July 2003 at 00 UTC in Figure 4.3.

For the validation purposes, these wind fields are compared with the radiosonde data from five locations for the same time period obtained from University of Wyoming web page and results are presented in Table 4.2.

It is found out that radiosonde data and NAM data features an average of 1.85 m/s difference in the u direction and an average of 0.11 m/s difference in the v direction. Therefore these findings suggest that the NAM data may represent the atmospheric indices over the terrain, and thus they can be appropriate to use in correction.

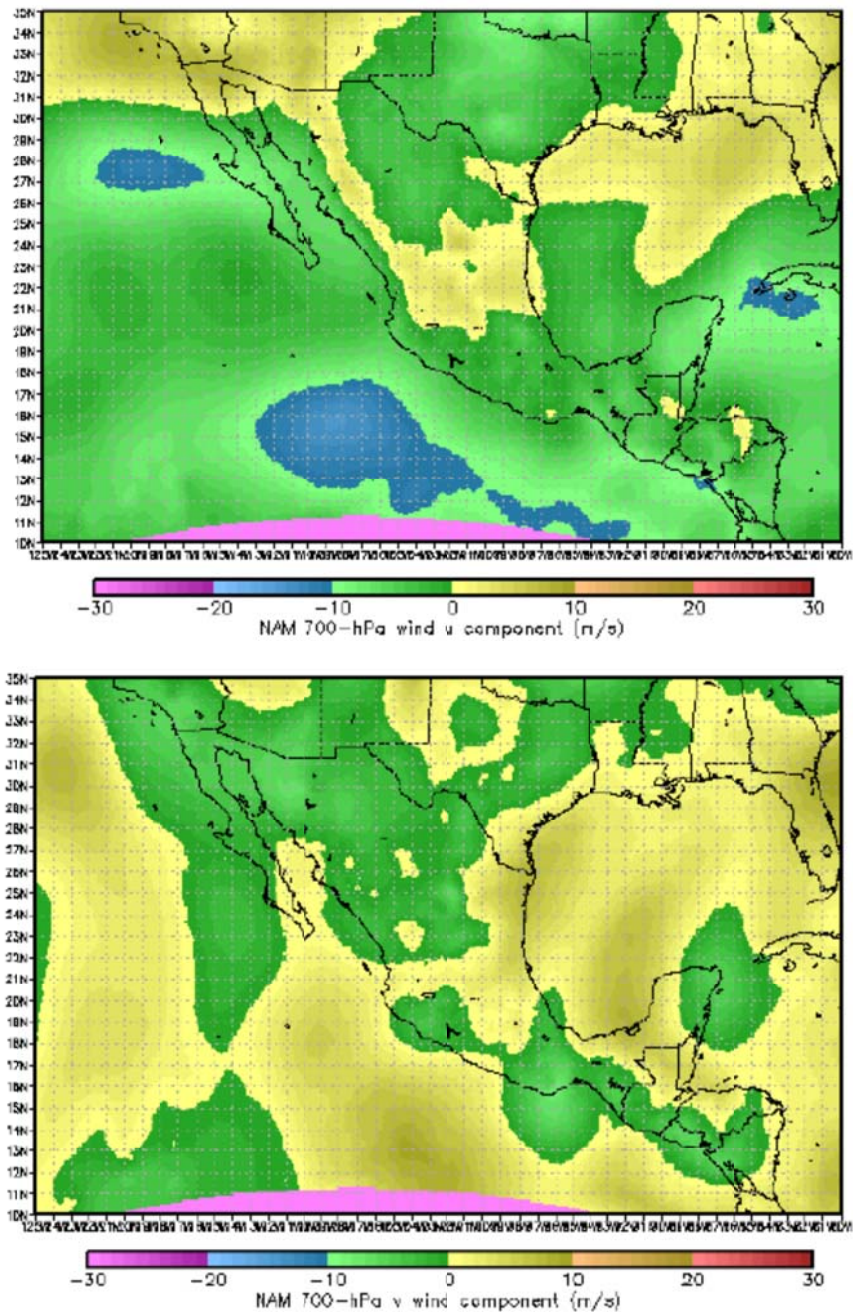


Figure 4.3: 700 hPa NAM wind fields for u component (top) and v component (bottom) in m/s at 4th July 2003 00 UTC

Table 4.2: Comparison of radiosonde and 700 hPa NWP data wind vector components at 4th July 2004 00 UTC

Station name	Latitude	Longitude	Radiosonde Data					NAM Data	
			Wind direction	Wind Speed (knots)	Wind Speed (m/s)	u (m/s)	v (m/s)	u (m/s)	v (m/s)
NKX	32.85	-117.11	300	25.00	12.86	11.14	-6.43	7.23	-5.35
TUS	32.23	-110.96	310	8.00	4.12	3.15	-2.65	4.57	-4.42
EPZ	31.86	-106.70	105	4.00	2.06	-1.99	0.53	-1.33	-1.23
BRO	25.91	-97.41	165	10.00	5.14	-1.33	4.97	0.35	7.31
76679	19.43	-99.13	115	1.00	0.51	-0.47	0.22	-2.35	0.88

Although the gauge stations are evenly distributed over the terrain area and terrain height, it is found out that some stations are closer over the network. Nevertheless none of the 4 km x 4 km SCaMPR pixels cover more than one gauge stations. Therefore in this study, it is assumed that uncertainty raised by the spatial representativeness between point gauge measurements and 4km averaged rainfall estimates is negligible. Even though it may raise a potential issue while it leads to more erroneous results over mountainous regions where spatial distribution of precipitation is uneven, the use of high resolution SCaMPR estimates may minimize this issue. To reduce uncertainties related to temporal scale during development of orographic correction, hourly rainfall estimates are aggregated to 6 hour interval as NAM data are available at 6 hour resolution.

4.2.6. Statistics of Gauge vs. SCaMPR data

Following statistics are used to validate satellite based rain rate estimations and gauge measurements.

Correlation, also named as Pearson Correlation Coefficient, is expressed as the covariance of the observations and estimates divided by the product of their respective standard deviations. It is defined as:

$$C = \frac{\sigma_{oe}}{\sigma_o \sigma_e} = \frac{\sum_{i=1}^n (o_i - \bar{o})(e_i - \bar{e})}{\sqrt{\sum_{i=1}^n (o_i - \bar{o})^2} \sqrt{\sum_{i=1}^n (e_i - \bar{e})^2}} \quad (4.1)$$

Where o_i and e_i are the observation and estimation respectively while \bar{o} and \bar{e} are mean values of observation and estimation data series.

Root Mean Square Error, RMSE, is computed for n number of estimates (e) and observations (o), considering error components due to bias and due to the lack of correspondence between the estimates and observations. It is defined as:

$$RMSE = \sqrt{\frac{1}{n} \sum_{i=1}^n (e_i - o_i)^2} \quad (4.2)$$

Bias in a data series of n values is defined in two methods, first the average of differences between observations and estimations, and second the ratio of total estimations to the total measurements.

$$Bias(Difference) = \frac{1}{n} (e_i - o_i) \quad (4.3)$$

$$Bias(Ratio) = \frac{\sum_{i=1}^n (e_i)}{\sum_{i=1}^n (o_i)} \quad (4.4)$$

In order to define the capability of satellite rainfall algorithm to detect rain events, contingency table is constructed between the satellite product and the rain gauge data. A sample contingency table is presented in table 4.3 to analyze two variables with defined sub-categories.

Table 4.3: A sample contingency table used on defining the capability of satellite rainfall algorithm to detect rain events

	Zero Estimate	Nonzero Estimate
Zero Observation	A	B
Nonzero Observation	C	D

Based on the elements of the contingency table, the following categorical statistics are considered for the analysis.

Probability of detection (POD) is the fraction of non-zero observations that are correctly detected by the estimate:

$$POD = \frac{D}{C + D} \quad (4.5)$$

False Alarm Rate (FAR), is the fraction of non-zero estimates that were matched with zero observations:

$$FAR = \frac{B}{B + D} \quad (4.6)$$

Heidke Skill Score (HSS) is a skill measure for discrimination. A value of 1 indicates perfectly correct discrimination; a value of 0 indicates no better skill than chance; a negative value indicates less skill than chance:

$$HSS = \frac{2(AD - BC)}{(A + B)(B + D) + (C + D)(A + C)} \quad (4.7)$$

The statistics are computed for two cases: all data and hit pixel data. Also the statistics are computed for the summer and winter seasons separately. All statistics are provided for two temporal resolutions of 1 hour and 6 hour. Hit pixel data denotes for time pixel when both gauge measurement and SCaMPR estimates have values greater than 0.1.

The capability of satellite rainfall algorithm to detect rain events in summer period is provided for 1 hour temporal resolution in Table 4.4 (a), and for 6 hours temporal resolution in Table 4.4 (b). For winter period, the result is provided for 1 hour temporal resolution in Table 4.5 (a), and for 6 hours temporal resolution in Table 4.5 (b).

Table 4.4: The capability of SCaMPR algorithm to detect rain events in summer period for (a) 1 hour temporal resolution and (b) 6 hour temporal resolution (Note that summer line in the table is the summation of three summer periods)

a)	POD	FAR	HSS	b)	POD	FAR	HSS
2002	0.6052	0.6537	0.3836	2002	0.6863	0.4359	0.4933
2003	0.5974	0.6742	0.3551	2003	0.6937	0.4658	0.4606
2004	0.6115	0.6318	0.3897	2004	0.7028	0.4331	0.4800
Summer	0.6052	0.6519	0.3759	Summer	0.6963	0.4462	0.4755

Table 4.5: The capability of SCaMPR algorithm to detect rain events in winter period for (a) 1 hour temporal resolution and (b) 6 hour temporal resolution (Note that winter line in the table is the summation of two winter periods)

a)	POD	FAR	HSS	b)	POD	FAR	HSS
2002 - 2003	0.3571	0.7192	0.2892	2002 - 2003	0.4247	0.6431	0.3324
2003 - 2004	0.3955	0.6382	0.3572	2003 - 2004	0.4807	0.5287	0.4351
Winter	0.3810	0.6719	0.3301	Winter	0.4588	0.5777	0.3935

When the hourly estimation and measurements are aggregated into 6 hour temporal resolution, the probability of SCaMPR algorithm to detect rain events, POD ratio, is increased by 15% for summer and 18% for winter estimations. Also it lead to 33% decrease in false alarms in summer estimations and 15% decrease in false alarms in winter estimates. Heidke Skill Score is increased by 27% and 18% for summer and winter estimations respectively. Therefore, the findings suggest that the representativeness issue of gauge data by SCaMPR estimations may be solved by aggregating the data in larger intervals. On the other hand, the data could not be further aggregated, for instance in 24 hour interval, as the in-between missing data were high, especially in gauge data.

The statistical performance of SCaMPR algorithm to accurately represent gauge data is analyzed with the aforementioned statistical indices. For summer period, all data statistics are provided for 1 hour temporal resolution in Table 4.6 (a) and for 6 hours temporal resolution in Table 4.6 (b). For winter period, all data statistics are provided for 1 hour temporal resolution in Table 4.7 (a) and for 6 hours temporal resolution in Table 4.7 (b). For summer period, hit pixel data statistics are provided for 1 hour temporal resolution in Table 4.8 (a) and for 6 hours temporal resolution in Table 4.8 (b). For winter period, hit pixel data statistics are provided for 1 hour temporal resolution in Table 4.9 (a) and for 6 hours temporal resolution in Table 4.9 (b).

Table 4.6: All data statistics of SCaMPR estimates over gauge measurements during 2002, 2003, and 2004 summer periods and summation of these three periods (Named as summer in table) for 1 hour temporal resolution (a) and for 6 hour temporal resolution (b)

a)	Data length	Real data length	Correlation	Bias (Difference)	Bias (Ratio)	RMSE
2002	106896	79004	0.2668	0.1752	2.0413	1.5747
2003	173706	150774	0.2768	0.1869	2.0245	1.6313
2004	189295	165174	0.2821	0.1936	1.8568	1.8969
Summer	469897	394952	0.2780	0.1874	1.9472	1.7369

b)	Data length	Real data length	Correlation	Bias (Difference)	Bias (Ratio)	RMSE
2002	17856	11507	0.4108	1.1504	2.0334	5.6387
2003	29016	22224	0.4111	1.1670	2.0100	5.6869
2004	31620	23890	0.4263	1.2530	1.8693	6.5919
Summer	78492	57621	0.4190	1.1994	1.9477	6.0695

Table 4.7: All data statistics of SCaMPR estimates over gauge measurements during 2002 – 2003 and 2003 - 2004 winter periods and summation of these two periods (Named as winter in table) for 1 hour temporal resolution (a) and for 6 hour temporal resolution (b)

a)

	Data length	Real data length	Correlation	Bias (Difference)	Bias (Ratio)	RMSE
2002 - 2003	130725	110260	0.3386	-0.0102	0.7550	0.3643
2003 - 2004	193314	184588	0.2744	0.0049	1.1109	0.4987
Winter	324039	294848	0.2803	-0.0007	0.9827	0.4532

b)

	Data length	Real data length	Correlation	Bias (Difference)	Bias (Ratio)	RMSE
2002 - 2003	21825	16951	0.5224	-0.0773	0.7090	1.4652
2003 - 2004	32010	28200	0.4110	0.0341	1.1293	1.9313
Winter	53835	45151	0.4185	-0.0077	0.9708	1.7707

Table 4.8: Hit pixel data statistics of SCaMPR estimates over gauge measurements during 2002, 2003, and 2004 summer periods and summation of these three periods (Named as summer in table) for 1 hour temporal resolution (a) and for 6 hour temporal resolution (b)

a)

	Real data length	Hit pixels data length	Correlation	Bias (Difference)	Bias (Ratio)	RMSE
2002	79004	3470	0.1314	0.4708	1.1627	5.5833
2003	150774	7176	0.1909	0.0540	1.0179	5.6831
2004	165174	9278	0.1947	0.3087	1.0999	6.0758
Summer	394952	19924	0.1834	0.2452	1.0810	5.8525

b)

	Real data length	Hit pixels data length	Correlation	Bias (Difference)	Bias (Ratio)	RMSE
2002	11507	1787	0.2128	3.9721	1.6293	12.0153
2003	22224	3617	0.2485	3.1822	1.5008	11.6152
2004	23890	4304	0.2720	3.5124	1.4956	12.9743
Summer	57621	9708	0.2554	3.4740	1.5207	12.3073

Table 4.9: Hit pixel data statistics of SCaMPR estimates over gauge measurements during 2002 – 2003 and 2003 - 2004 winter periods and summation of these two periods (Named as winter in table) for 1 hour temporal resolution (a) and for 6 hour temporal resolution (b)

a)	Real data length	Hit pixels data length	Correlation	Bias (Difference)	Bias (Ratio)	RMSE
2002 - 2003	110260	1203	0.2608	-0.8660	0.5559	2.2691
2003 - 2004	184588	2156	0.0970	0.2698	1.1488	2.8576
Winter	294848	3359	0.1079	-0.1370	0.9264	2.6618

b)	Real data length	Hit pixels data length	Correlation	Bias (Difference)	Bias (Ratio)	RMSE
2002 - 2003	16951	547	0.4599	-2.4024	0.5734	6.5275
2003 - 2004	28200	950	0.1872	1.2747	1.2500	8.5098
Winter	45151	1497	0.2126	-0.0689	0.9870	7.8438

The first point to be noted is that SCaMPR produces much higher bias values during summer period, for 1 hour accumulations bias difference is 0.1874 in summer periods while the algorithm feature nearly zero bias difference in winter periods. The performance of the SCaMPR algorithm is also lower in summer period, for 1 hour accumulations, SCaMPR and gauges diverges with a RMSE value of 1.7369 for summer periods while it is only 0.4532 for winter periods. SCaMPR tends to estimate higher rainfall amount during the summer period, and lower rainfall amount in winter, which may explain the high difference of POD, FAR, and HSS indices between summer and winter data.

A closer analysis of the individual station data reveals that the bias of SCaMPR is not consistent at all. Seasonal total precipitation measurement and corresponding SCaMPR estimation amounts along with multiplicative bias ratios for available stations in 2002, 2003 and 2004 summer periods are plotted with respect to station elevation in Figure 4.4. When the precipitation amounts of summer period, precipitation characteristics with changing elevation and performance of SCaMPR algorithm to reflect this precipitation are investigated, the first thing to be noted is that 2002 summer period where total precipitation amounts stays below 400 mm level, passes much drier than 2003 and 2004 summer periods, where total summer precipitation amounts come out to be as high as 800 mm. Also, increasing station elevation does not reflect any clue about the precipitation characteristics; two stations at 500 m elevation level and four stations at 1900 m level receives 30% to 50% less rainfall when compared to close elevation levels, but the other stations shows nearly same rainfall regime within each other with a few exceptions. On the other hand, during summer period, average bias ratios between gauge measurements and SCaMPR estimates show the effect of orography at high elevation levels; depending on seasonal precipitation amounts and average bias ratios, it is clear that SCaMPR algorithm fails to reflect the increasing precipitation amounts at high elevation levels, especially over 1900 m level, where increasing precipitation by topographic effect is not captured, resulting a decrease in bias ratio. Moreover, the effect of orography on precipitation is much clear during winter period, where bias ratio decreases steadily over the gauge transect. The SCaMPR algorithm shows an average bias ratio of 2.0 for all three of the summer period, even there are some stations with bias ratio as high as 3.5 especially in 2004 summer. Nonetheless, increasing station elevation neither forms a distinct precipitation characteristic nor shows an effect on the performance of SCaMPR algorithm in summer periods.

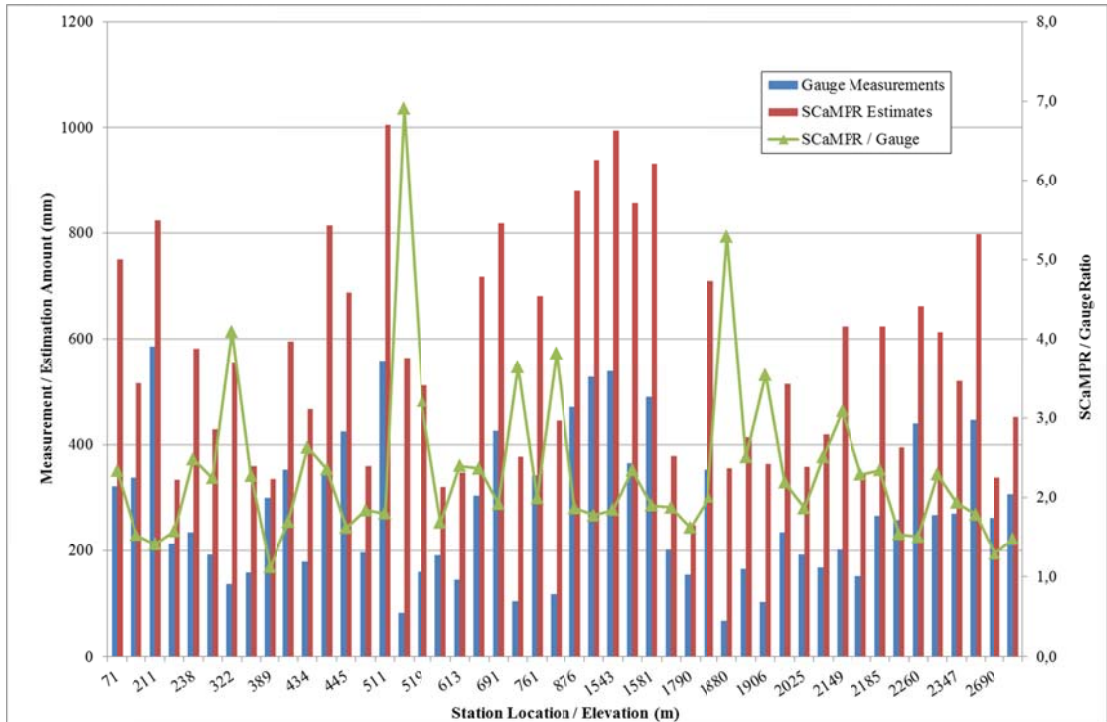


Figure 4.4 (a): Seasonal total precipitation measurement, total SCaMPR estimation and multiplicative bias ratio for 2002 summer period

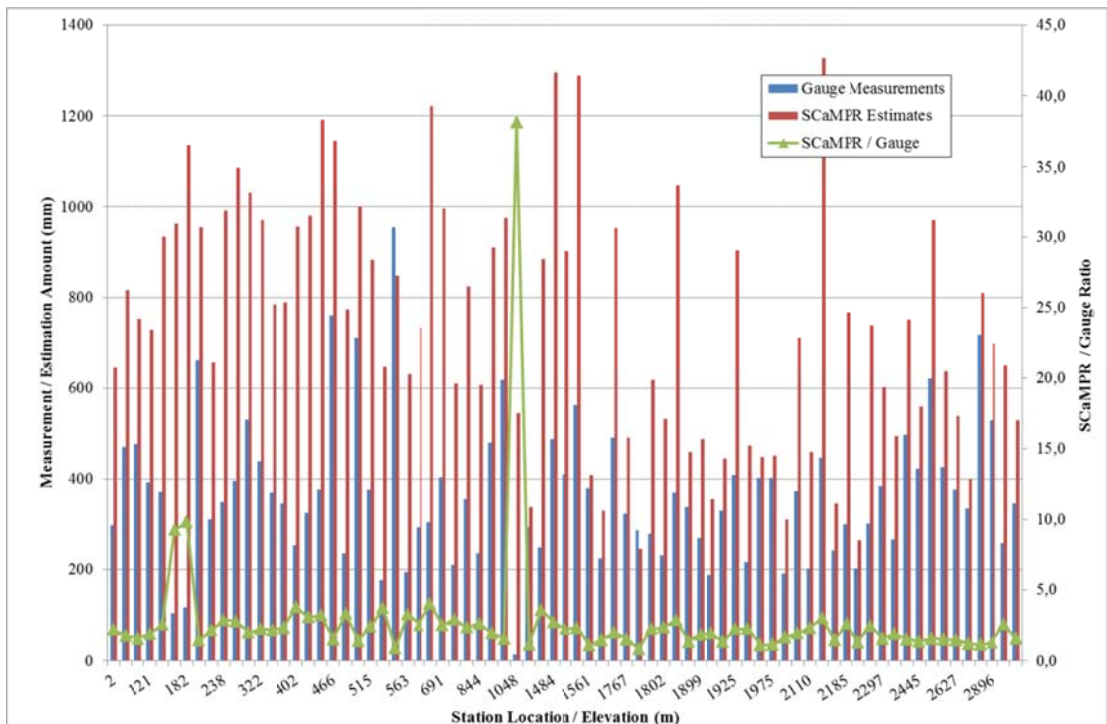


Figure 4.4 (b): Seasonal total precipitation measurement, total SCaMPR estimation and multiplicative bias ratio for 2003 summer period

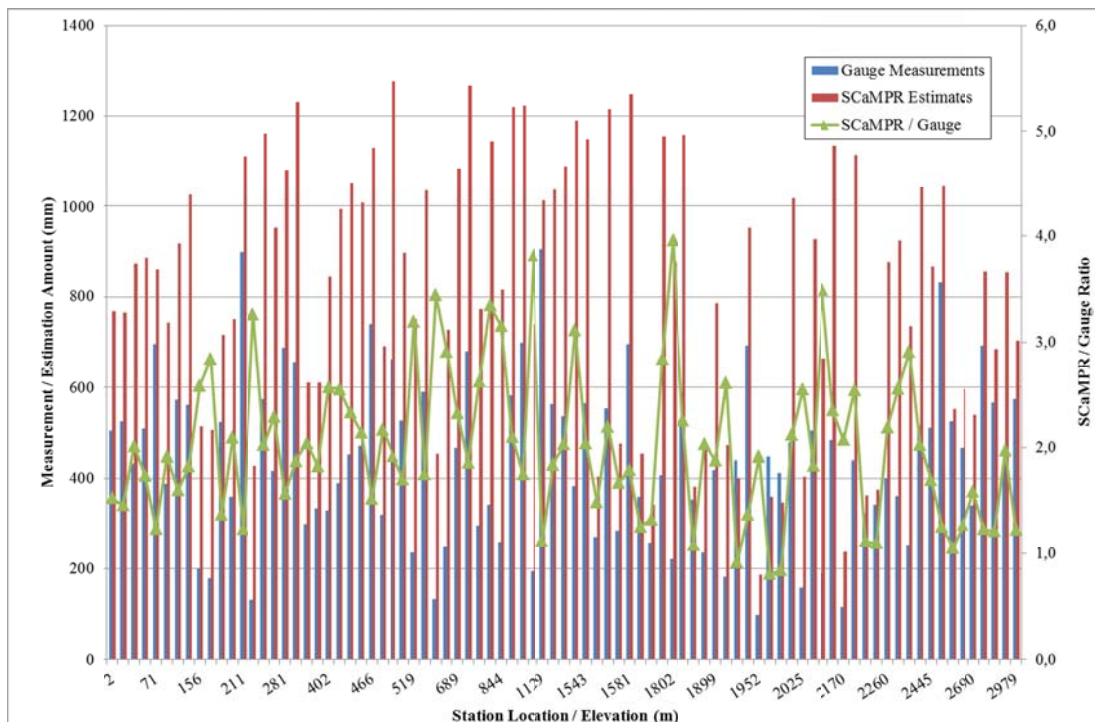


Figure 4.4 (c): Seasonal total precipitation measurement, total SCaMPR estimation and multiplicative bias ratio for 2004 summer period

Seasonal total precipitation measurement and corresponding SCaMPR estimation amounts along with multiplicative bias ratios for available stations in 2002 – 2003 and 2003 – 2004 winter periods are plotted with respect to station elevation in Figure 4.5. When the precipitation characteristics with changing elevation and performance of SCaMPR algorithm to reflect this precipitation are investigated, the first thing to be noted is that the total precipitation amounts are found out to be much less than those seen in summer period, experiencing 25% to 40% of average summer precipitation during winter. Precipitation amounts are doubled in stations located over 1500 m during 2002 – 2003 winter period, but in 2003 – 2004 winter period, this increase is not distinct over the same level. Also during 2002 – 2003 winter period, SCaMPR algorithm produces much less rainfall, giving out bias ratio averaging at 0.5 level. SCaMPR estimates are improved during 2003 – 2004 winter period, but still at much of the stations, bias ratio stays below 1.0 level. Again, increasing station elevation neither forms a distinct precipitation characteristic nor shows an effect on the performance of SCaMPR algorithm in winter periods.

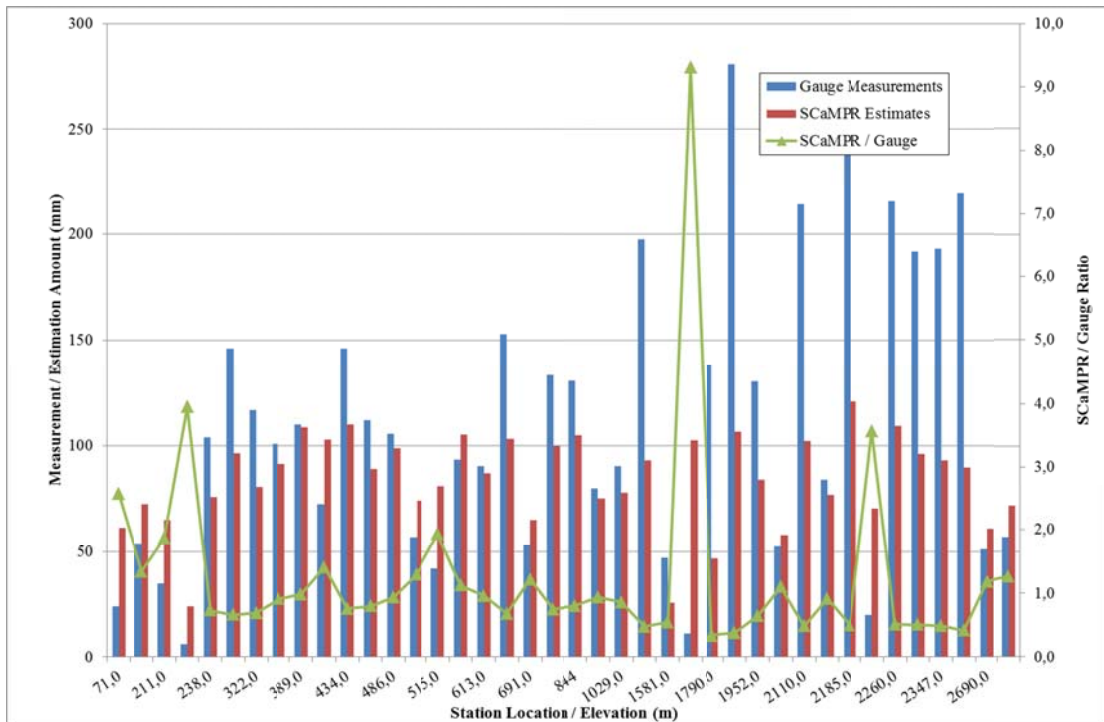


Figure 4.5 (a): Seasonal total precipitation measurement, total SCaMPR estimation and multiplicative bias ratio for 2002 - 2003 winter period

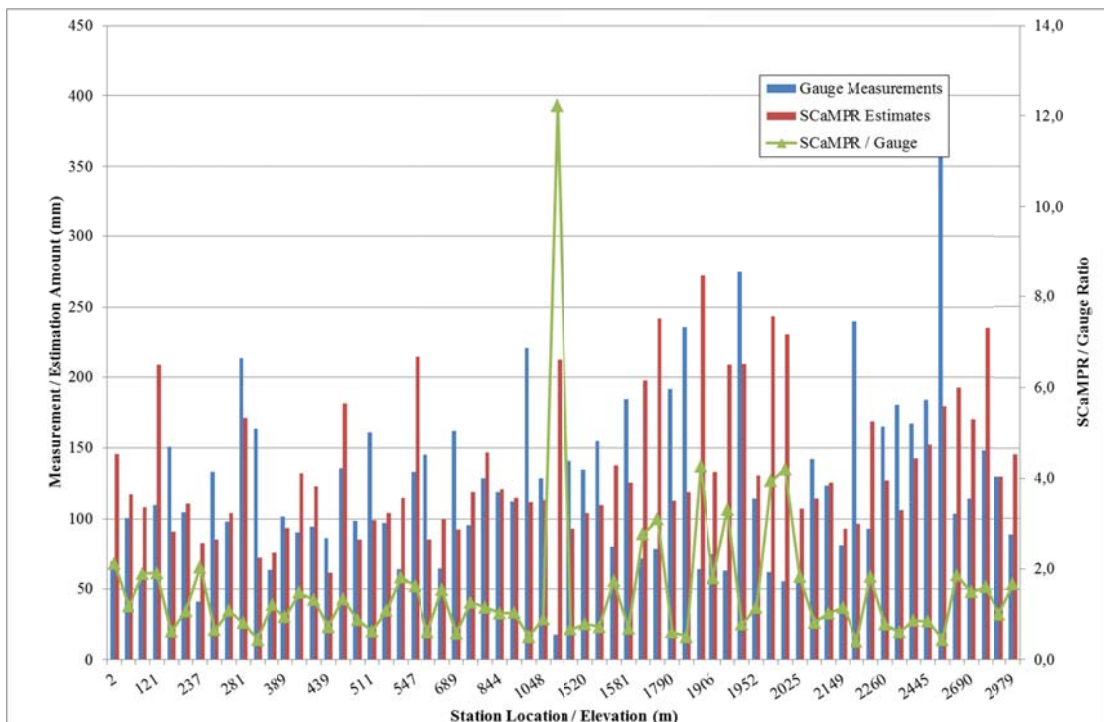


Figure 4.5 (b): Seasonal total precipitation measurement, total SCaMPR estimation and multiplicative bias ratio for 2003 - 2004 winter period

In order to further investigate precipitation characteristics with changing elevation and performance of SCaMPR algorithm to reflect this precipitation, a transect of 10 gauge stations are selected as shown in Figure 4.6, and seasonal total precipitation measurement and corresponding SCaMPR estimation amounts along with multiplicative bias ratios for these stations in 2002, 2003 and 2004 summer periods are plotted with respect to station elevation in Figure 4.7 and also for these stations in 2002 – 2003 and 2003 – 2004 winter periods are plotted with respect to station elevation in Figure 4.8.

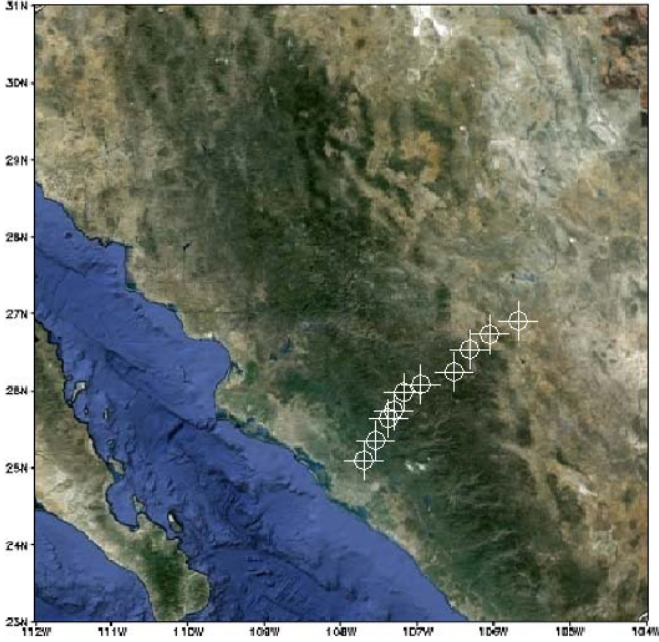
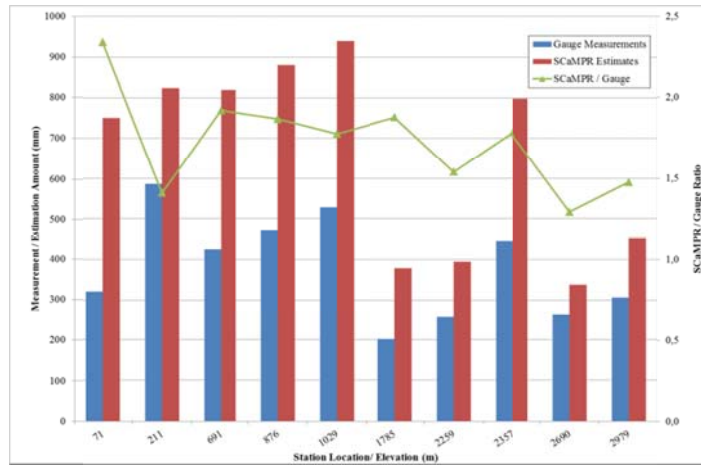
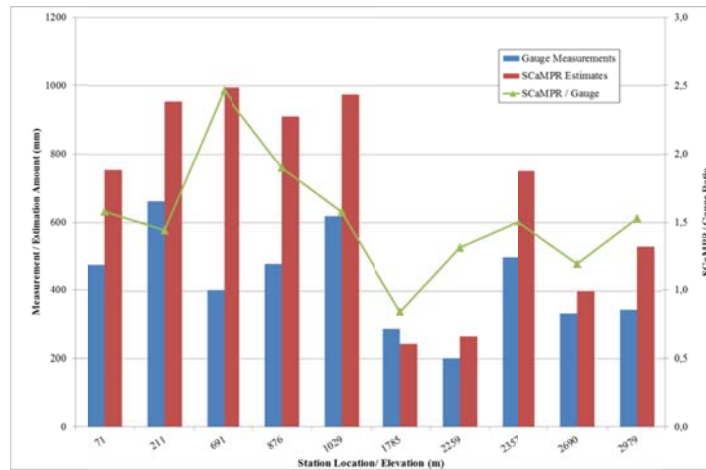


Figure 4.6: Gauge transect selected to investigate elevation vs. precipitation characteristics and SCaMPR algorithm performance

a)



b)



c)

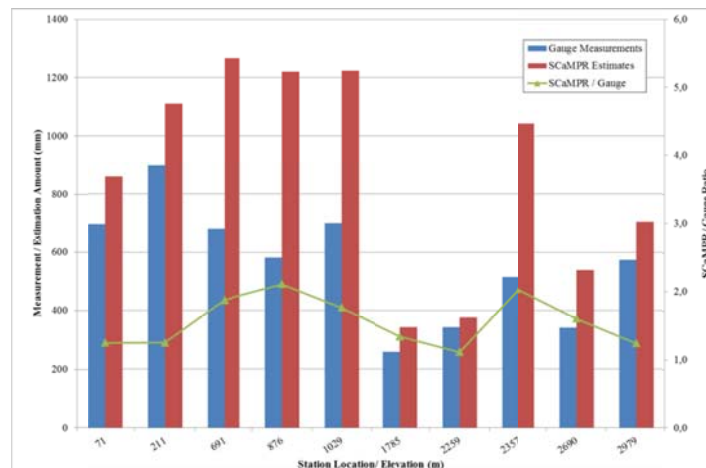
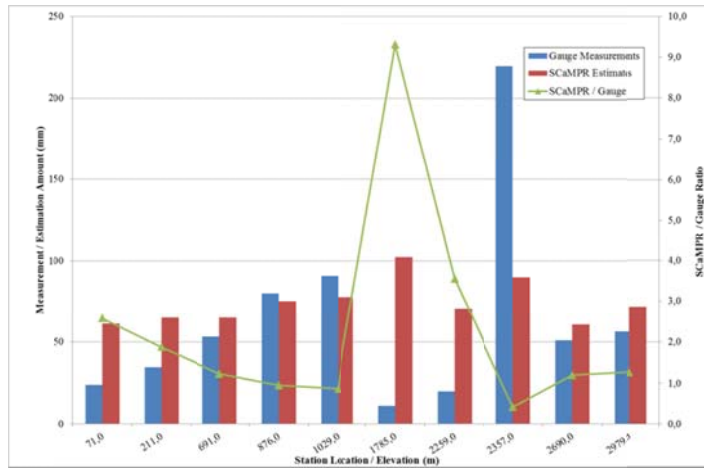


Figure 4.7: Seasonal total precipitation measurement, total ScaMPR estimation and multiplicative bias ratio for the selected gauge transect for 2002 (a), 2003 (b) and 2004 (c) summer periods

a)



b)

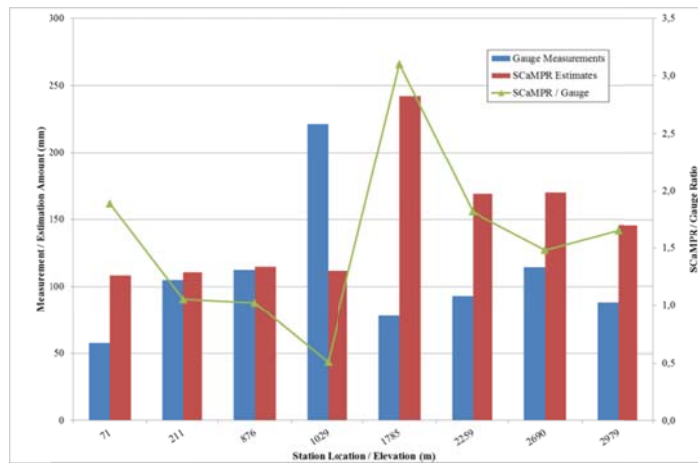


Figure 4.8: Seasonal total precipitation measurement, total SCaMPR estimation and multiplicative bias ratio for the selected gauge transect for 2002 - 2003 (a) and 2003 - 2004 (b) winter periods

The selected gauge transect shows no direct relation between rainfall and elevation. Also performance of the SCaMPR algorithm with the increasing elevation is found out to have the similar pattern observed over the whole gauge network; bias ratio between gauge measurements and SCaMPR estimates decreases with increasing elevation. Also, to further define the existence of any orography dependent bias on the SCaMPR estimations, gauge measurements and SCaMPR estimations are plotted on scatter graphs for both summer periods (Figure 4.9) and winter periods (Figure 4.10).

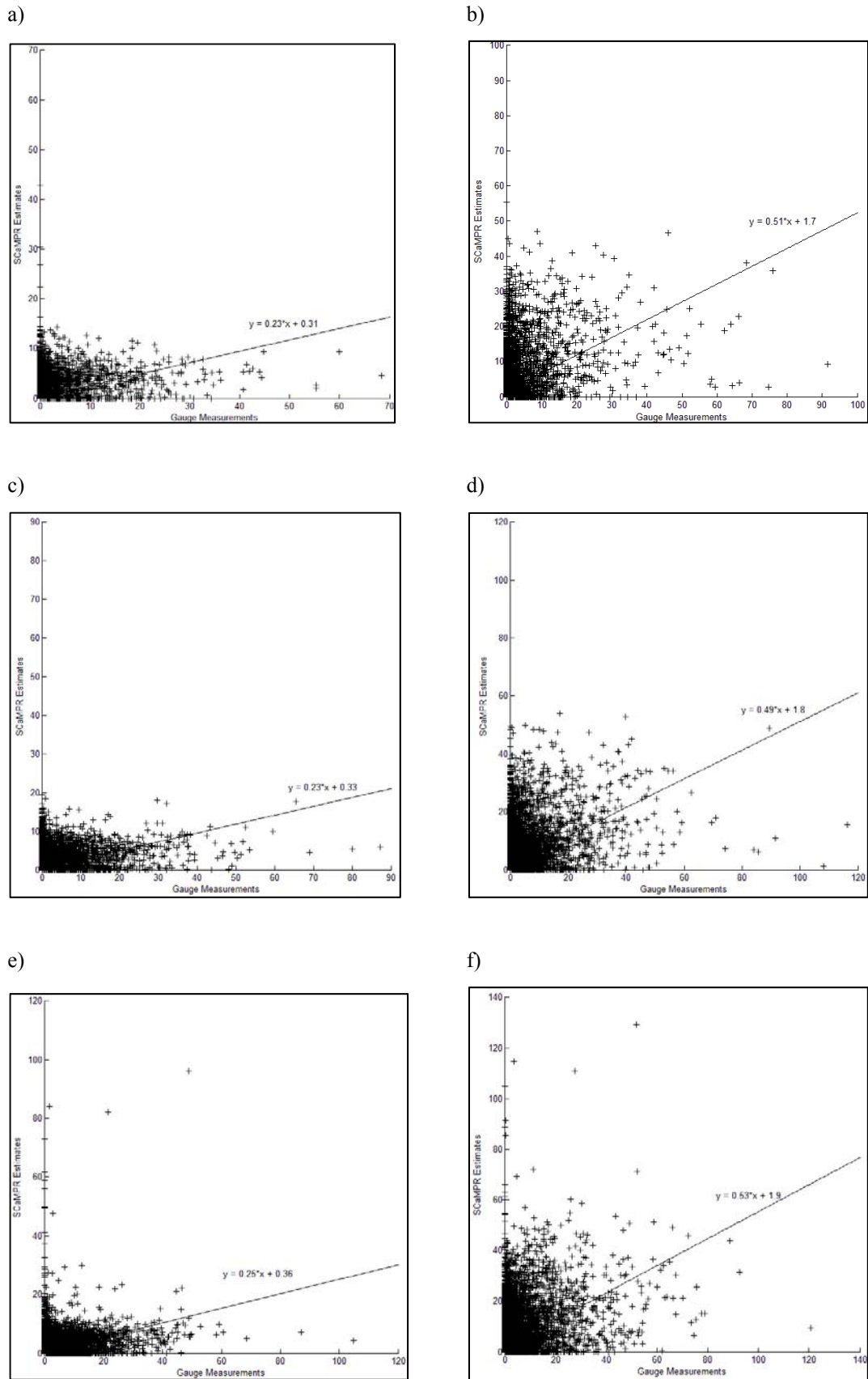


Figure 4.9: Scatter plots of gauge measurements vs. SCaMPR estimations for 1 hour temporal resolution in 2002 (a), 2003 (c) and 2004 (e) and for 6 hour temporal resolution in 2002 (b), 2003 (d) and 2004 (f) summer periods

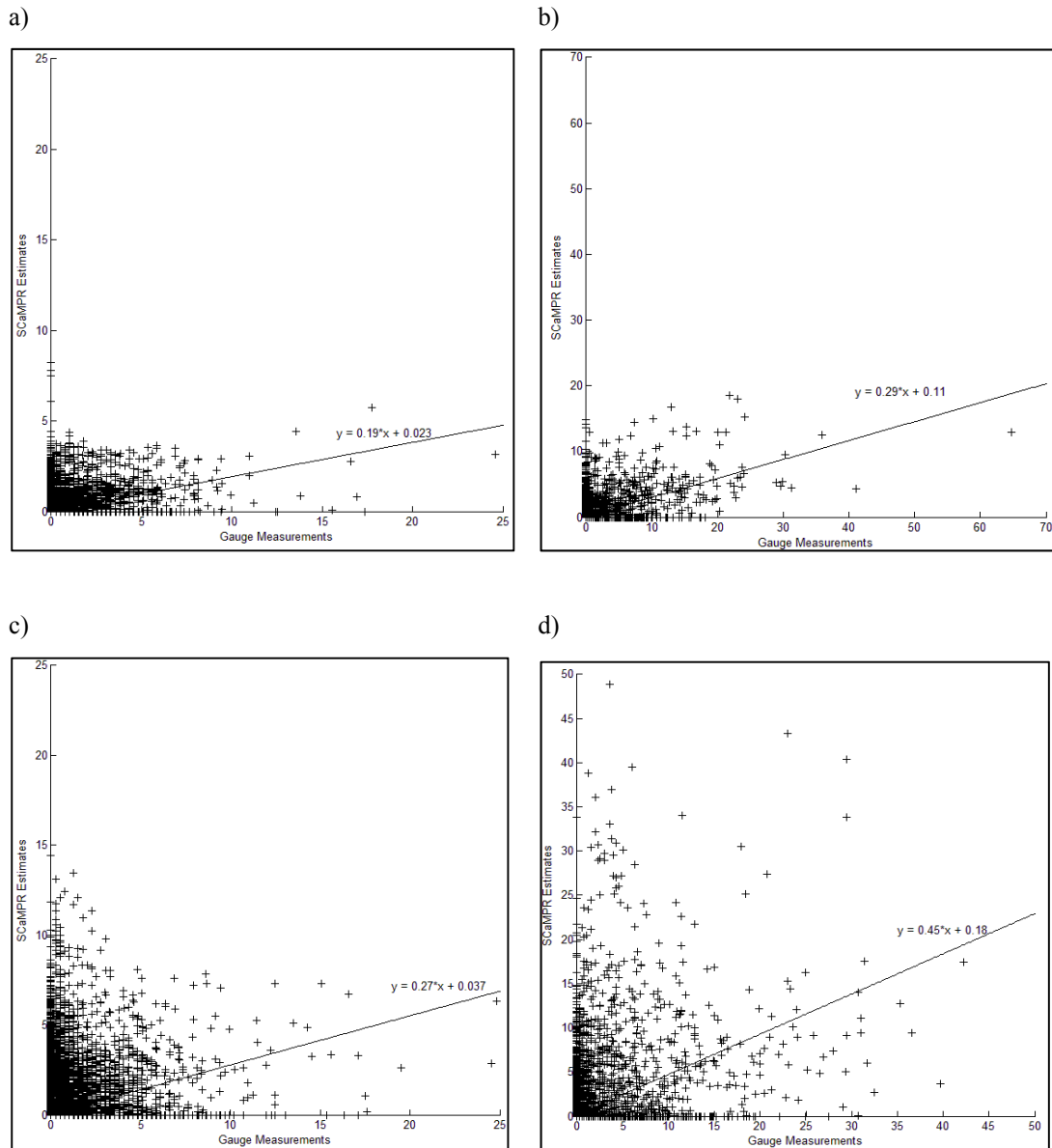


Figure 4.10: Scatter plots of gauge measurements vs. SCaMPR estimations for 1 hour temporal resolution in 2002 - 2003 (a) and 2003 - 2004 (c) and for 6 hour temporal resolution in 2002 - 2003 (b) and 2003 - 2004 (d) winter periods

As orographic precipitation is triggered by the slope of the terrain and resultant wind speed blows over the terrain, no relation may be obtained with investigating rainfall profile with respect to increasing elevation. A closer analysis of the individual time data reveals that the bias of SCaMPR is also not consistent at all. There are some instances where SCaMPR misses or fails to capture a heavy rain event at the gauges, even at the summer periods, where average bias ratio stays over 2.0, but more significantly there are numerous instances where SCaMPR indicates a heavier rain event that is not indicated by the gauges, even when there is no rain at all. This is supported by the statistics; even though winter statistics shows nearly zero bias difference and unit bias ratio, the RMSE and POD, FAR and HSS indices show bad representation of gauge data through SCaMPR estimates. As the mountainous region over study area forms a block to the airflows over the terrain, which results with high amounts of surface air movements, both upwind and downwind; false alarms, bad representations and missing rainfalls in the SCaMPR estimations may be explained with the orography induced effects.

4.2.7. Statistics of Gauge vs. HE data

HE estimates are obtained as two different series: one with orographic correction included and the other without orographic correction. HE data was obtained for summer periods of 2002 and 2003 years only. The capability of HE satellite rainfall algorithm to detect rain events in summer period is provided for 1 hour temporal resolution in Table 4.10 (a), and for 6 hours temporal resolution in Table 4.10 (b). The statistical performance of HE data for summer periods is also analyzed. All data statistics are provided for 1 hour temporal resolution in Table 4.11 (a) and for 6 hours temporal resolution in Table 4.11 (b). Hit pixel data statistics are provided for 1 hour temporal resolution in Table 4.12 (a) and for 6 hours temporal resolution in Table 4.12 (b).

Table 4.10: The capability of HE algorithm to detect rain events in summer periods of 2002 – 2003 years for (a) 1 hour temporal resolution and (b) 6 hour temporal resolution

a)	POD	FAR	HSS	b)	POD	FAR	HSS
HE without orographic correction	0.3529	0.5641	0.3427	HE without orographic correction	0.4754	0.3497	0.4308
HE with orographic correction	0.3558	0.5669	0.3430	HE with orographic correction	0.4751	0.3493	0.4308

Table 4.11: All data statistics of HE estimates over gauge measurements during 2002, and 2003 summer periods for 1 hour temporal resolution (a) and for 6 hour temporal resolution (b)

a)	Data length	Real data length	Correlation	Bias (Difference)	Bias (Ratio)	RMSE
HE without orographic correction	273928	150820	0.2157	0.2310	2.2361	2.6199
HE with orographic correction	273928	150820	0.2237	0.2519	2.3478	2.6803

b)	Data length	Real data length	Correlation	Bias (Difference)	Bias (Ratio)	RMSE
HE without orographic correction	45763	13192	0.3776	1.7303	2.4120	10.2247
HE with orographic correction	45763	13192	0.3863	1.7962	2.4658	10.2823

Table 4.12: Hit pixel data statistics of HE estimates over gauge measurements during 2002, and 2003 summer periods for 1 hour temporal resolution (a) and for 6 hour temporal resolution (b)

a)	Real data length	Hit pixels data length	Correlation	Bias (Difference)	Bias (Ratio)	RMSE
HE without orographic correction	150820	4114	0.0998	4.5488	2.3477	10.7445
HE with orographic correction	150820	4170	0.1156	4.8133	2.4278	10.8997

b)	Real data length	Hit pixels data length	Correlation	Bias (Difference)	Bias (Ratio)	RMSE
HE without orographic correction	13192	1515	0.2115	12.6136	2.7164	26.0224
HE with orographic correction	13192	1519	0.2243	13.0260	2.7760	26.0887

The capability of HE algorithm to detect rainfall events come out to be lower than SCaMPR algorithm. For 1 hour temporal resolution, SCaMPR detects rain events with a 0.6052 POD ratio, while HE algorithm achieves nearly half of this score, with 0.3529. For 6 hour temporal resolution, results are the same with POD ratios 0.6993 and 0.4754 for SCaMPR and HE respectively.

Also performance of the HE algorithm is much worse than SCaMPR. While SCaMPR features bias differences of 0.1874 for 1 hour temporal resolution and 1.1994 for 6 hour temporal resolution; HE features 0.2310 and 1.7303 bias differences respectively. Even after orographic correction, bias values stays at the same level. Moreover, HE shows RMSE values of 2.6199 for 1 hour temporal resolution and 10.2247 for 6 hour temporal resolution; SCaMPR gives 1.7369 and 6.0695 RMSE values respectively.

Application of orographic correction leads to 3.7% increase for 1 hour temporal resolution and 2.3% increase for 6 hour temporal resolution in the correlation between HE estimates and gauge measurements. On the other hand, the performance of the algorithm gets worse. Bias difference between HE estimates and gauge measurement increase with 3.8% for 1 hour temporal resolution and 5.8% for 6 hour temporal resolution. Multiplicative bias ratio and RMSE values get worsened after application of orographic correction. These results are more evident over hit pixel statistics. However, it is better to keep in mind that HE analysis only covers 2002-2003 period while SCaMPR covers 2002-2004 period. Also it should be noted that even though statistical performance of the HE algorithms over the gauge network decreases with the application of orographic correction, the orography-related errors are eliminated.

4.3. Sensitivity Analysis to Develop Updrafts

In order to develop the updrafts from the inter-relation of the obtained NAM wind fields and digital topography, the same slope definition defined by Vicente et al. (2002) is used. To test the efficiency of proposed slope definition, sensitivity analysis over a discrete/artificial topography is performed. The reason of using artificial topography is that it helps whether the proposed method is functioning properly or not under number of experimental cases. Instead of the real map and wind data, the following cases are analyzed using artificial topography:

Case 1: positive and constant u wind ($u > 0$), zero v wind ($v = 0$), topography slopes upward to the east with no N-S slope.

Case 2: v wind and topography is same as case 1, but with varying (positive) values of u.

Case 3: positive and constant u wind ($u > 0$), zero v wind ($v = 0$), sinusoidal varying topography in the east-west direction (no N-S slope).

Case 4: v wind and topography is same as case 3, but with varying (positive) values of u.

Case 5: positive and constant u wind ($u > 0$), zero v wind ($v = 0$), sinusoidal varying topography in both east-west and north-south direction.

Case 6: v wind and topography is same as case 5, but with varying (positive) values of u.

Case 7: topography is same as case 5, positive and constant u wind ($u > 0$) and v wind ($v > 0$).

Case 8: topography is same as case 5, varying u wind ($u > 0$) and v wind ($v > 0$).

Although the slope values are successfully obtained via the slope formulation suggested by Vicente et al. (2002), the fetch length still remains as an issue. The findings suggested that the terrain effects can only be defined by application of an ideal fetch length that will reflect this effect via aforementioned slope calculation. Urbanski (1982) suggested 10-km fetch length to address the terrain effects, whereas Vicente et al. (2002) recommended 15-minute fetch length. In this thesis, both constant fetch length and fetch length as a function of duration is taken into account to select the best option to reflect terrain effects. The effect of fetch length on slope calculation can be seen in Figure 4.11, where 5 km and 10 km fetch lengths are compared over a rough terrain.

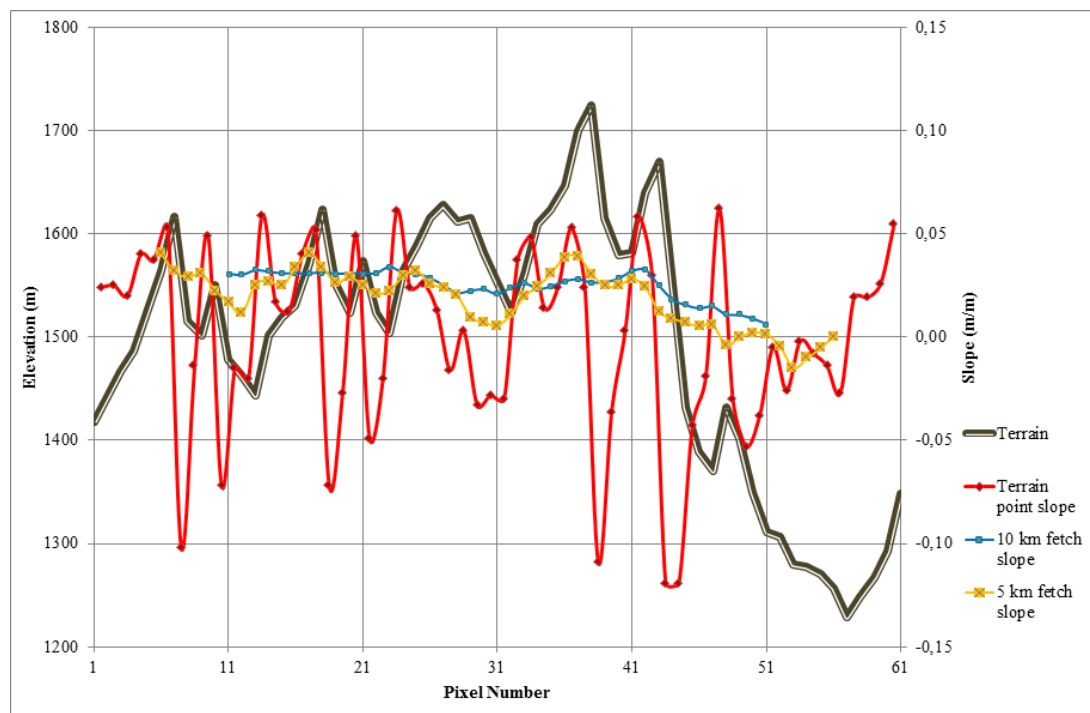


Figure 4.11: Slope values corresponding to 5 km and 10 km fetch lengths over a rough terrain

As can be noted from Figure 4.11, a smaller fetch length reflects sharp valleys over the terrain much better. For instance, a lower fetch length, 5 km in the figure, reflects the changes of slope resulting from the sharp valley located around 30th pixel and sharp crest located around 37th pixel, while a longer fetch length, 10 km in the figure, does not take these into account. Therefore the selection of

the fetch length must be made based on the effects of these terrain changes on real precipitation data. Once the optimum fetch length is found, effects of orography on rainfall may be defined.

4.4. Updraft vs. Multiplicative Error Analysis

The aforementioned orographic correction methods defined by Vicente et al. (2002) and Kwon et al. (2008) point out two different approaches. Vicente et al. (2002) defined a multiplicative correction formulation based on vertical movement of air block, where the correction formulation is given in Equation 2.7. Resulting orographic adjustment factor based on this correction formulation is illustrated in Figure 4.12.

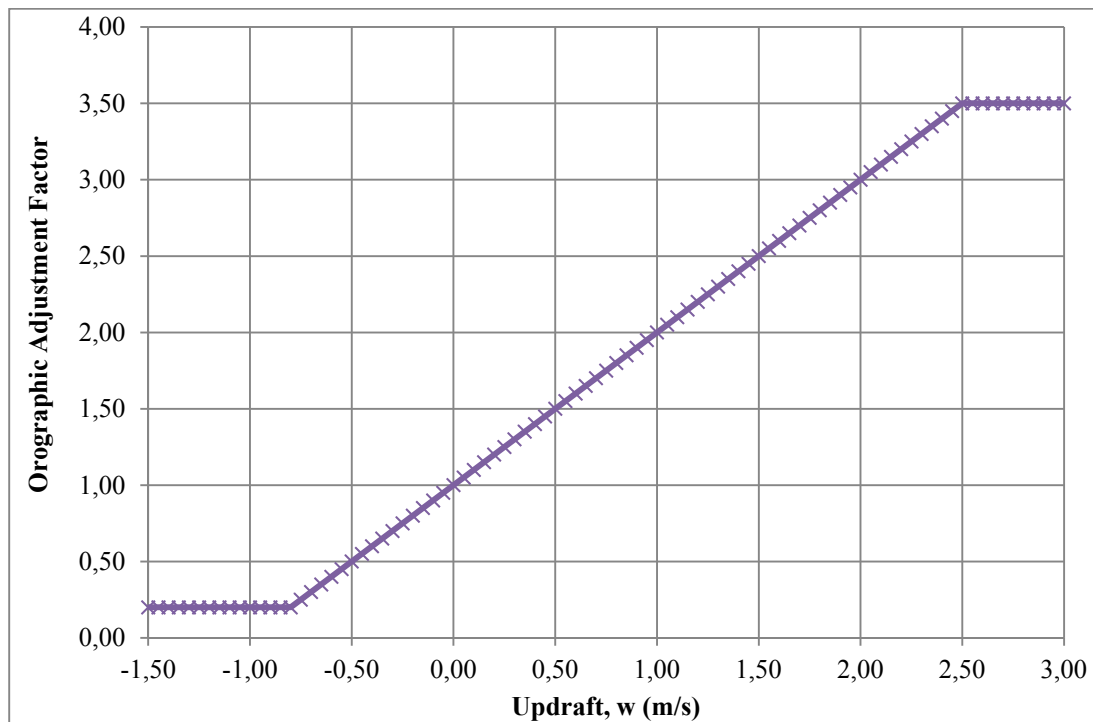


Figure 4.12: Orographic adjustment factors based on updraft values calculated with Vicente et al. (2002) formulation

Kwon et al. (2008) proposed an additive methodology for the orographic correction. This methodology is not adopted in the analysis due to the following reasons: First the methodology does not put forward a correction for the downdraft movement of air, only updraft is considered. The defined correction equation (Equation 2.11) offers decrease in the rain estimate up to 0.10 m/s updraft, which is not supported by theoretical background. Additive approach also disturbs the rain/no rain discrimination defined by the satellite based rainfall algorithm. Finally this formulation was developed according to model rain data, instead of gauge measurements; suspicious accuracy of the model rain estimation may compromise the applicability to the independent gauge data. Nevertheless, multiplicative error analysis yields better relationship with respect to updraft than additive error analysis.

It is aimed to develop a multiplicative correction algorithm, therefore updrafts are analyzed with respect to multiplicative error values of gauge measurements and SCaMPR estimates. In order to stick by the rain/no rain discrimination of the satellite based rainfall algorithm, only hit pixels are used in this analysis. Using hit pixels, the need for orographic adjustment in SCaMPR is better isolated and this way, the orographic impact is more enhanced over rough terrain. Also 6 hour gauge and SCaMPR data are used to eliminate any representativeness issue.

4.4.1. Winter Period

The total gauge measurements and SCaMPR estimations are obtained as a function of orographically driven vertical velocity, calculated based on 10 km fetch length. The results are plotted in Figure 4.13, with only points with at least 0.1 mm rain accumulation in both gauge measurements and SCaMPR estimates in order to avoid false alarms and unreasonable ratio values.

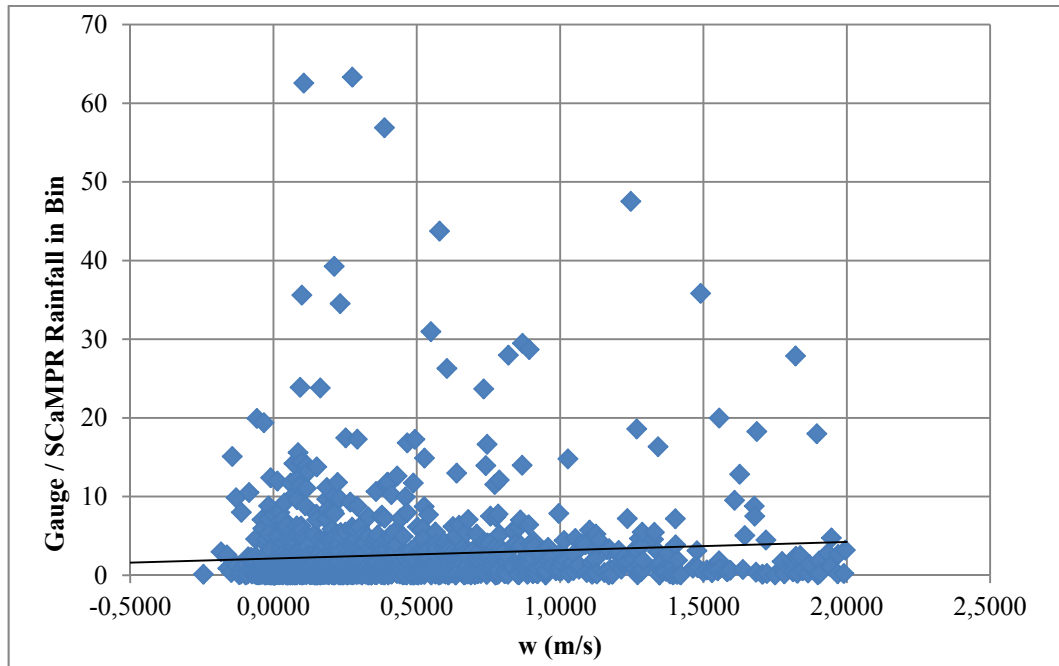


Figure 4.13: Total gauge / total SCaMPR accumulation as a function of w using all data points from the winters of 2002-2003 and 2003-2004. Threshold precipitation and estimation limits are 0.1 mm, fetch length is 10 km.

As expected, the adjustments are upward, reflecting presumably the underestimation by SCaMPR at strong upwind movements and overestimation by SCaMPR at downwind movements. However, the accumulations of the data points stay at low values, which results with unreasonable ratio values as high as 65. These unreasonable values may be omitted with application of a higher threshold value for rain accumulations for both gauge measurements and SCaMPR estimates, which will result in a decrease of data amount, and raise the question of representativeness of used data volume to the study area. Therefore this approach is not adopted. The small accumulations in many of the w intervals in the raw data suggest that the point w intervals are too small to address the orography. To figure out this, the data from adjoining intervals were added together, and again the values were plotted only if the accumulation exceeded a specified threshold value assigned based on the width of the updraft bin selected. Aggregations were done into intervals ranging from 0.100 m/s to 0.500 m/s. This aggregation will also help elimination of representativeness issue. Along with aggregating 1 hour gauge and SCaMPR data into 6 hours' time, aggregating the gauge and SCaMPR in bins of vertical velocity values will contribute to spatial representativeness, as longer time periods can produce significant reduction in representativeness errors.

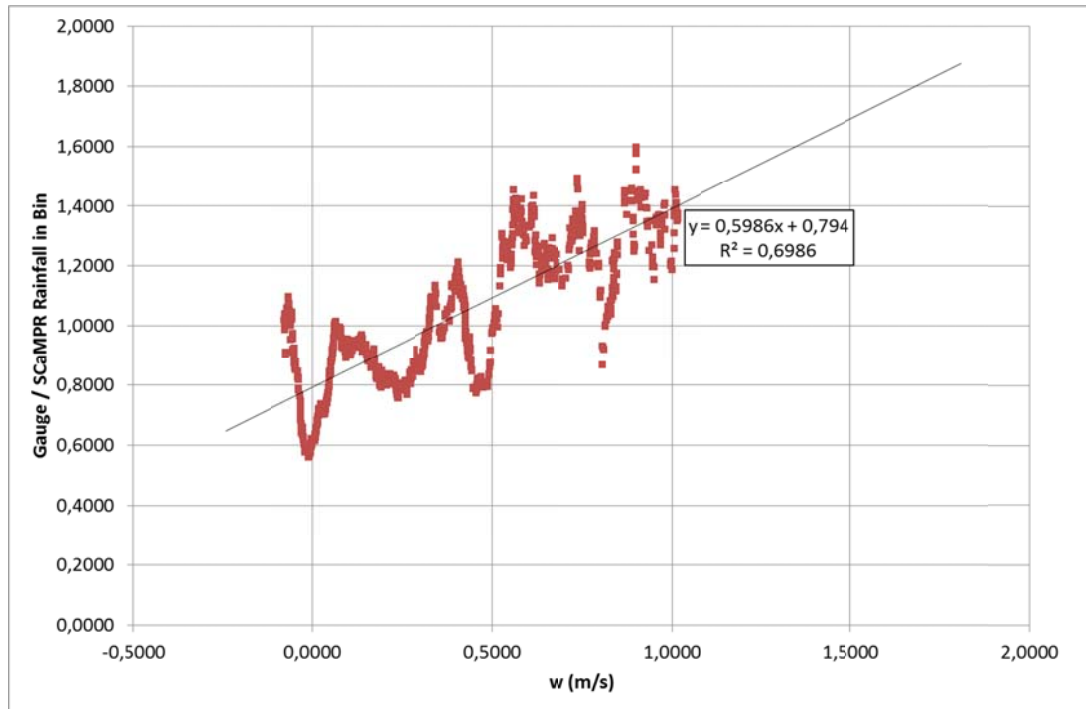
Gauge/SCaMPR rainfall accumulations corresponding to 0.100 m/s and 0.500 m/s vertical velocity bins are plotted in Figure 4.14.

Figure 4.14 shows a scatter diagram of gauge / SCaMPR accumulations vs. orographically driven vertical velocity and a trendline fitted to define the in-between relation of aforementioned variables. The positive slopes of the fit lines clearly suggest that satellite based SCaMPR algorithm underestimates rain rate in the presence of topographically forced upward motion, as well as

overestimates the rain rate in the presence of topographically forced downward motion. The resulting adjustment formulation also conforms to the correction equation suggested by Vicente et al. (2002)

The same analysis are performed for 15 km (Figure 4.15), 20 km (Figure 4.16), 7.5 minute duration (Figure 4.17), 10 minute duration (Figure 4.18), 14 minute duration (Figure 4.19), 15 minute duration (Figure 4.20) and 20 minute duration (Figure 4.21) fetch lengths and the results are plotted respectively.

a)



b)

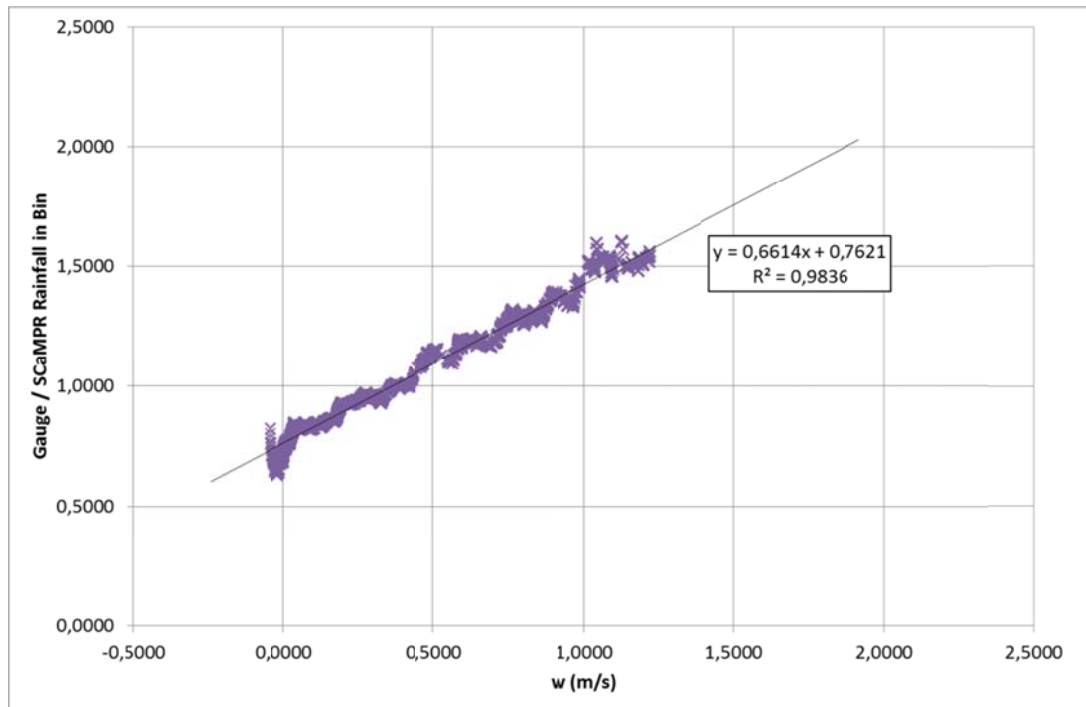
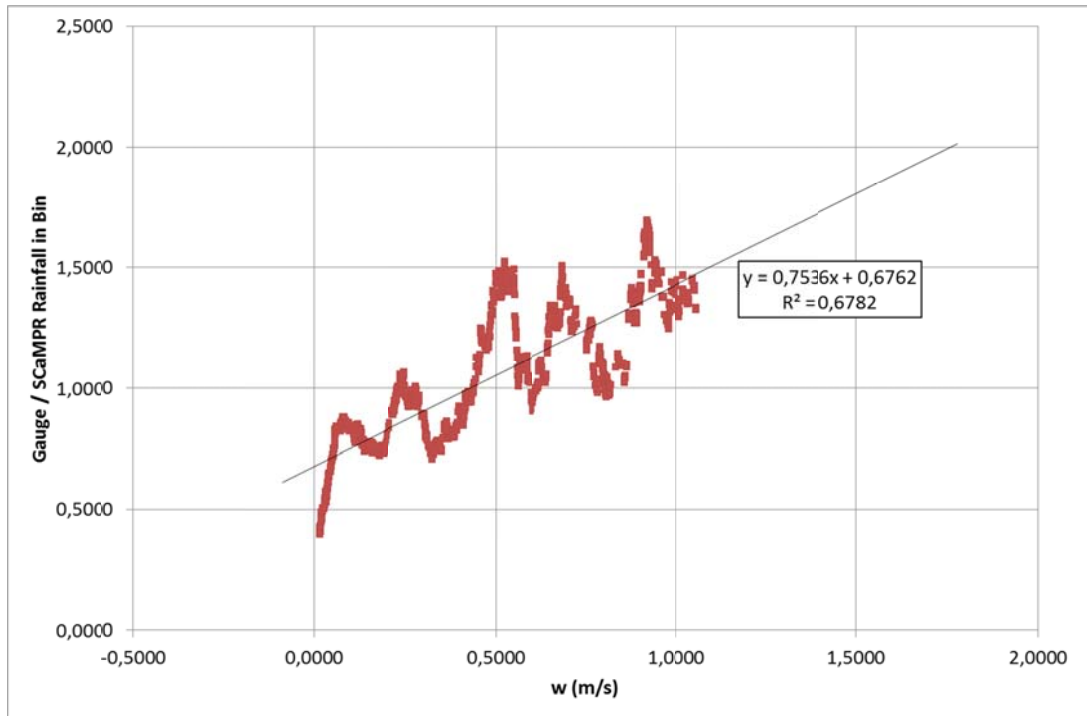


Figure 4.14: Total gauge / ScaMPR accumulations corresponding to vertical velocity bins using data from winter periods of 2002-2003 and 2003-2004. Threshold precipitation and estimation limits are 150 mm for 0.100 m/s updraft bin (a) and 450 mm for 0.500 m/s updraft bin (b). Fetch length is 10 km.

a)



b)

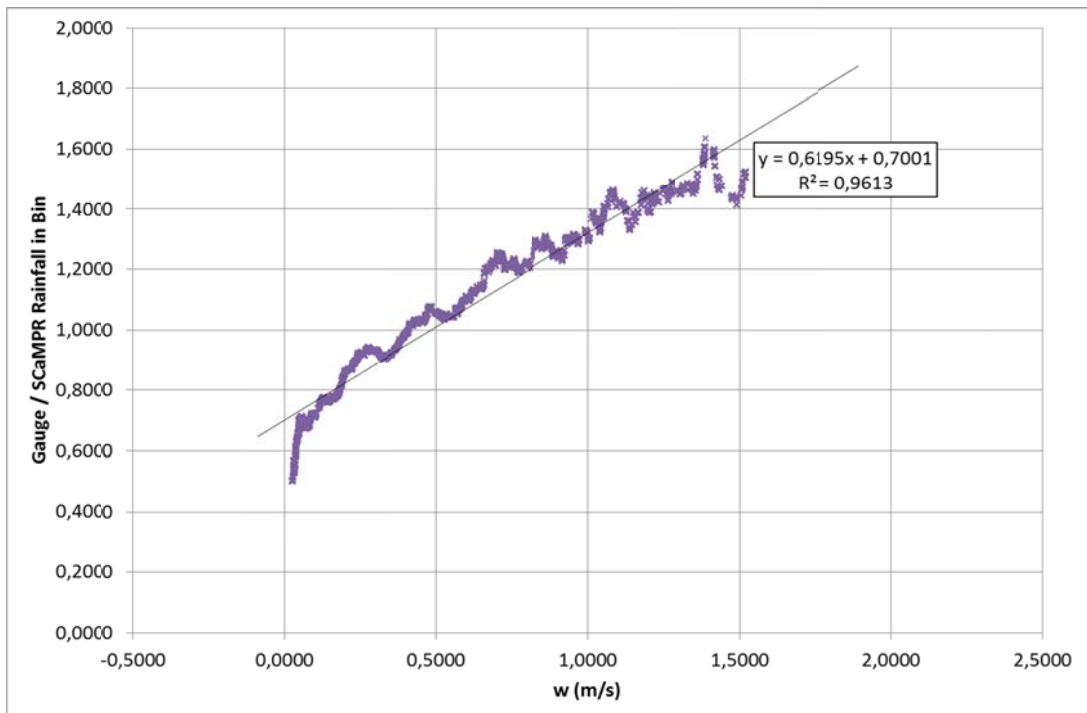
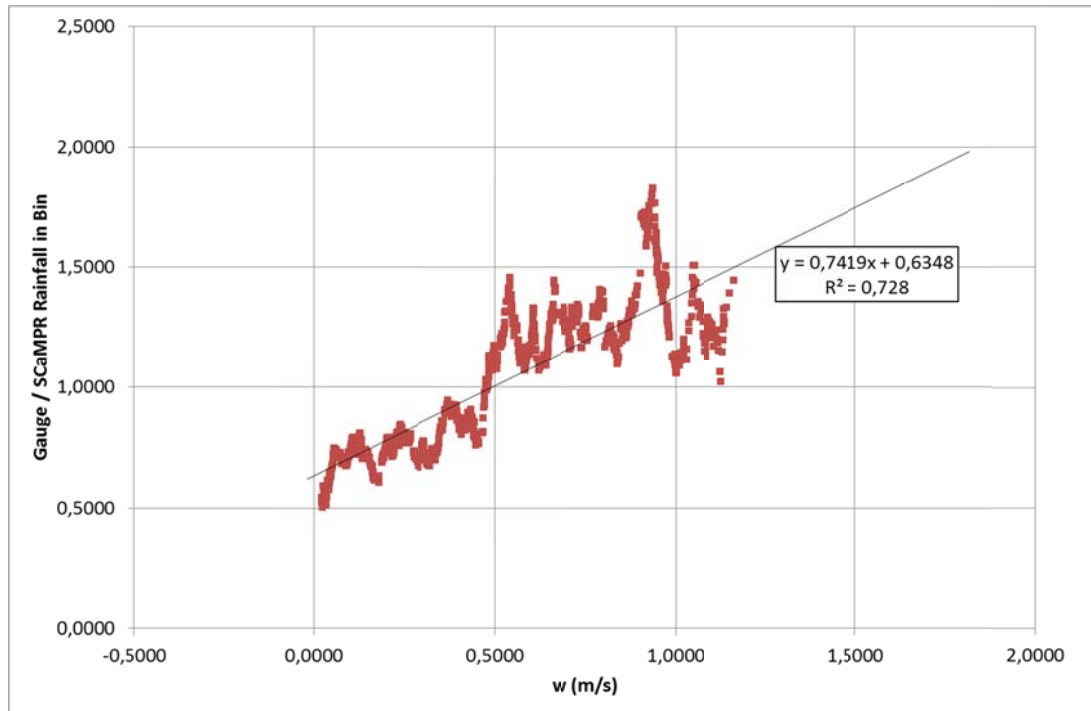


Figure 4.15: Total gauge / ScaMPR accumulations corresponding to vertical velocity bins using data from winter periods of 2002-2003 and 2003-2004. Threshold precipitation and estimation limits are 200 mm for 0.100 m/s updraft bin (a) and 475 mm for 0.500 m/s updraft bin (b). Fetch length is 15 km.

a)



b)

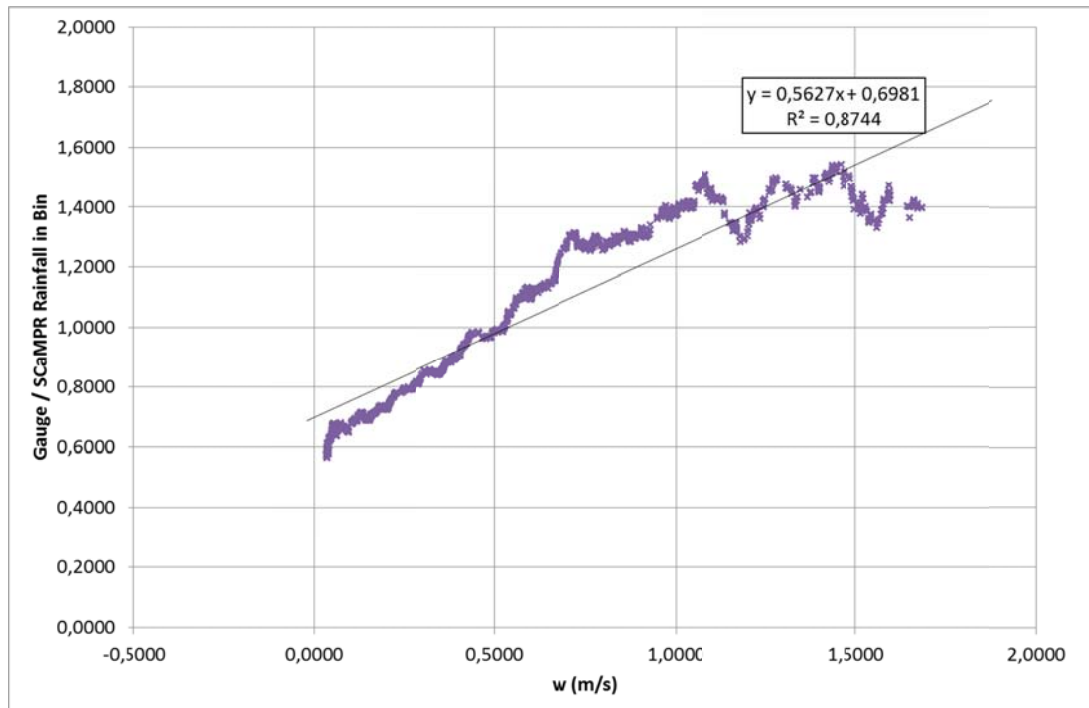
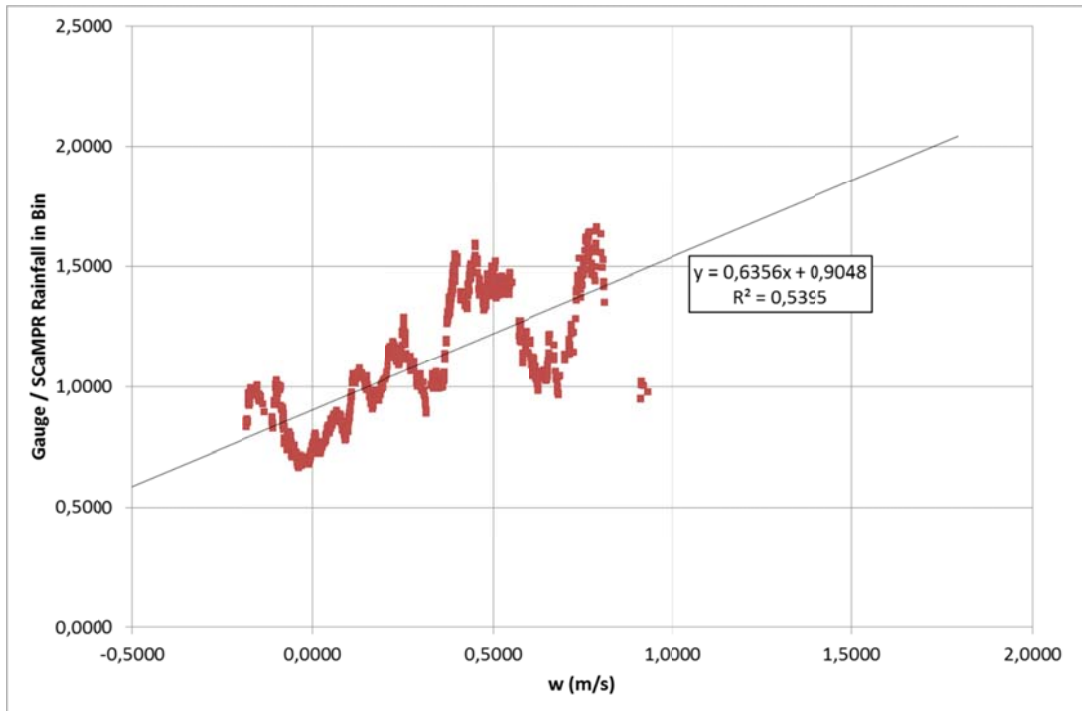


Figure 4.16: Total gauge / SCaMPR accumulations corresponding to vertical velocity bins using data from winter periods of 2002-2003 and 2003-2004. Threshold precipitation and estimation limits are 175 mm for 0.100 m/s updraft bin (a) and 450 mm for 0.500 m/s updraft bin (b). Fetch length is 20 km.

a)



b)

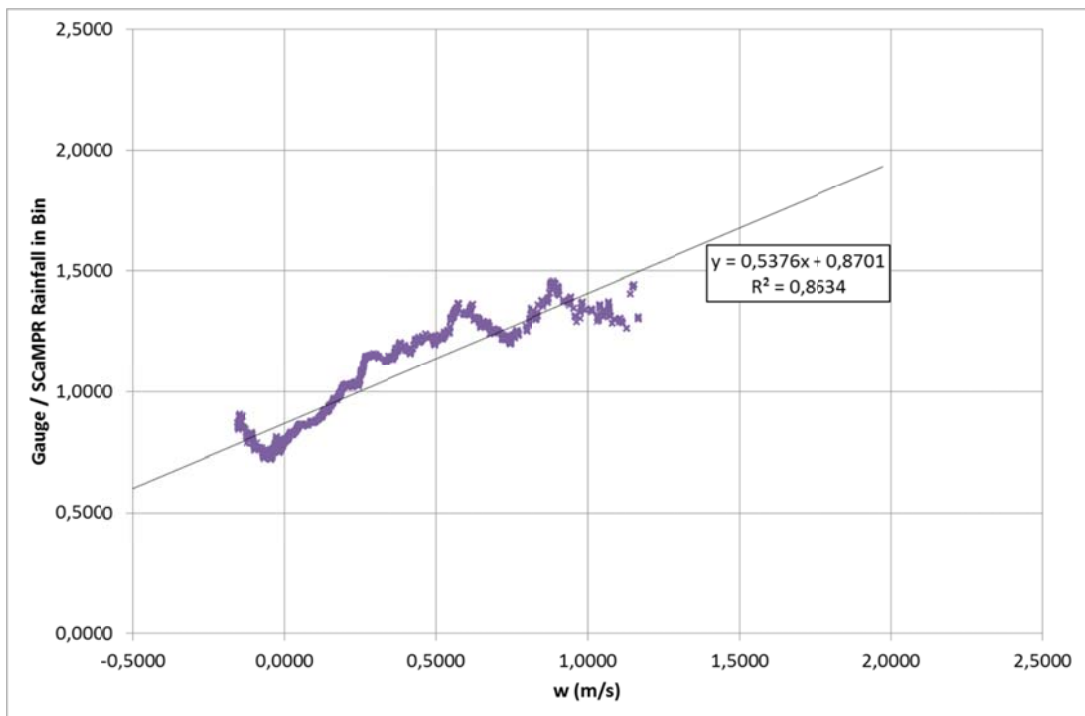
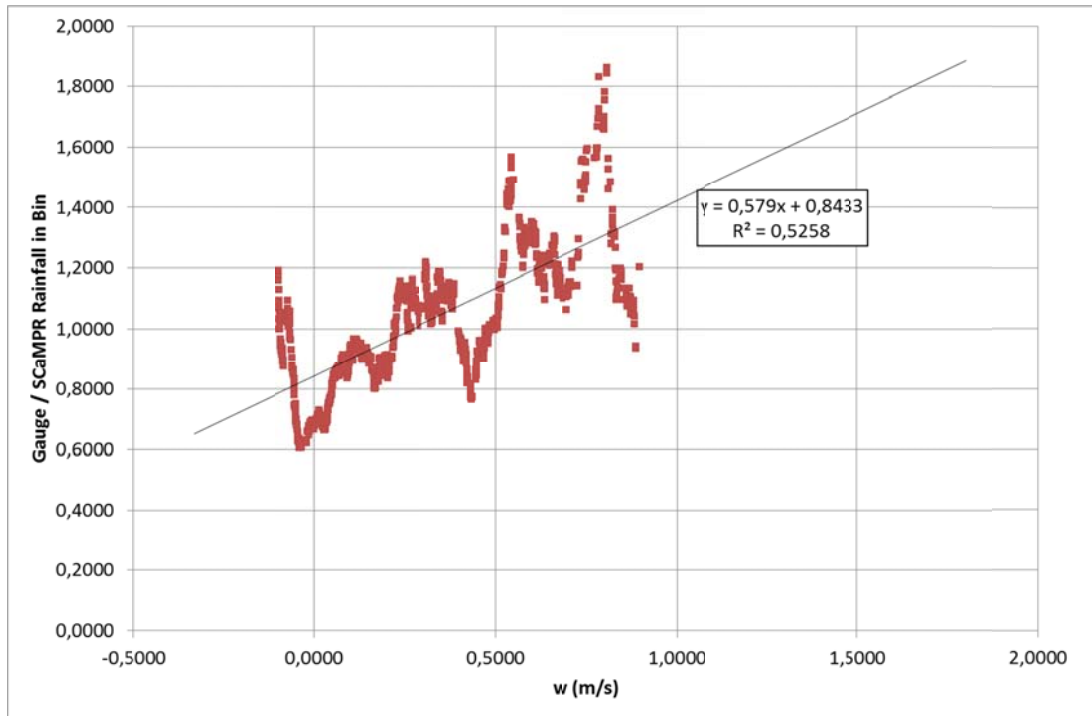


Figure 4.17: Total gauge / ScaMPR accumulations corresponding to vertical velocity bins using data from winter periods of 2002-2003 and 2003-2004. Threshold precipitation and estimation limits are 150 mm for 0.100 m/s updraft bin (a) and 400 mm for 0.500 m/s updraft bin (b). Fetch length is 7.5 minute wind duration.

a)



b)

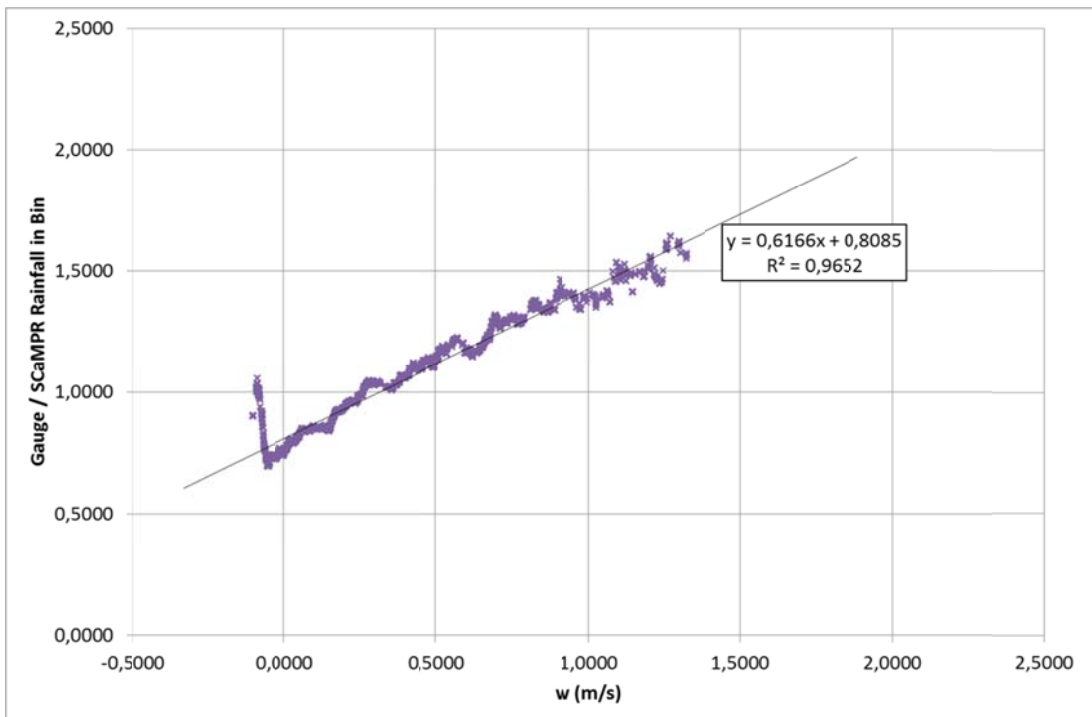
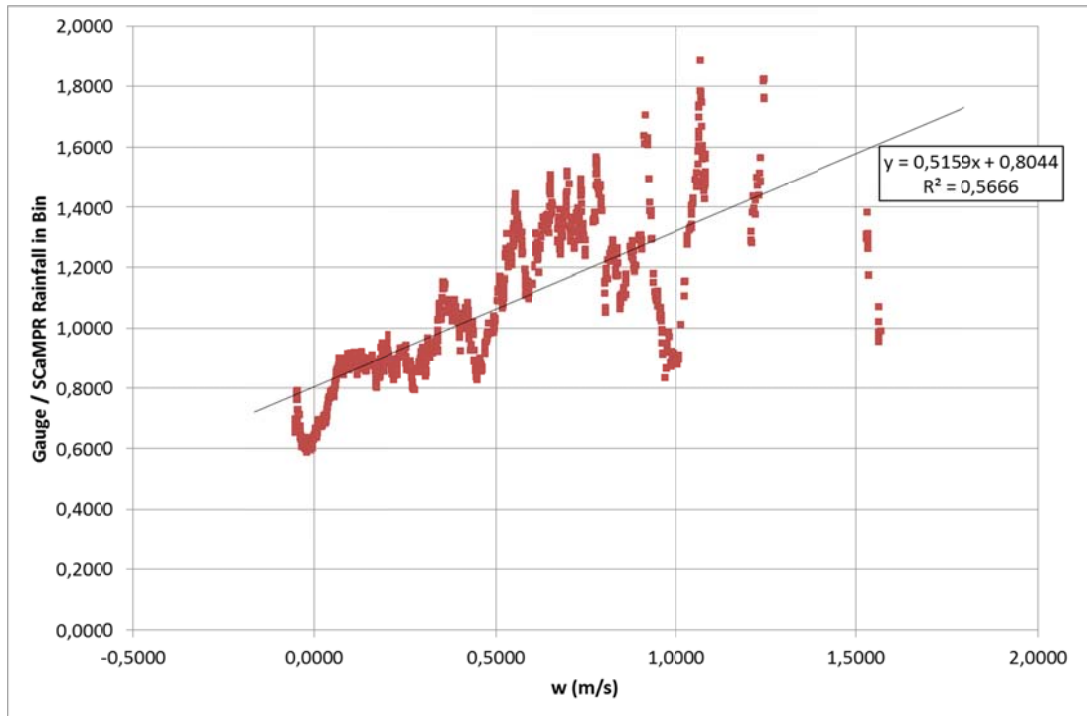


Figure 4.18: Total gauge / ScaMPR accumulations corresponding to vertical velocity bins using data from winter periods of 2002-2003 and 2003-2004. Threshold precipitation and estimation limits are 175 mm for 0.100 m/s updraft bin (a) and 400 mm for 0.500 m/s updraft bin (b). Fetch length is 10 minute wind duration.

a)



b)

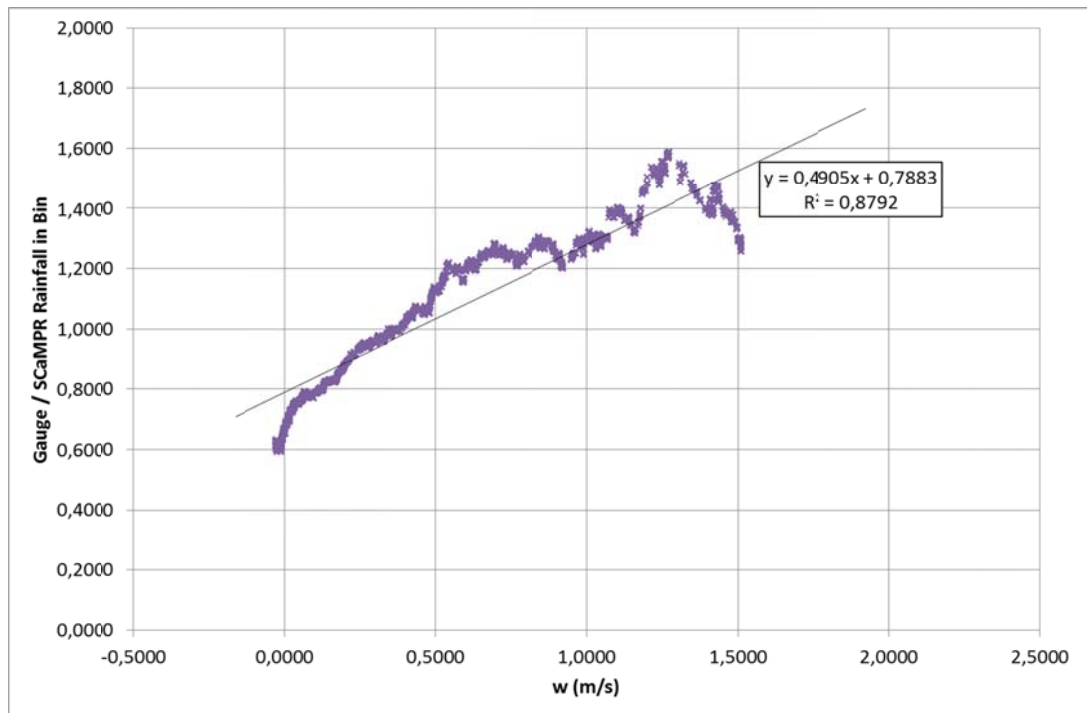
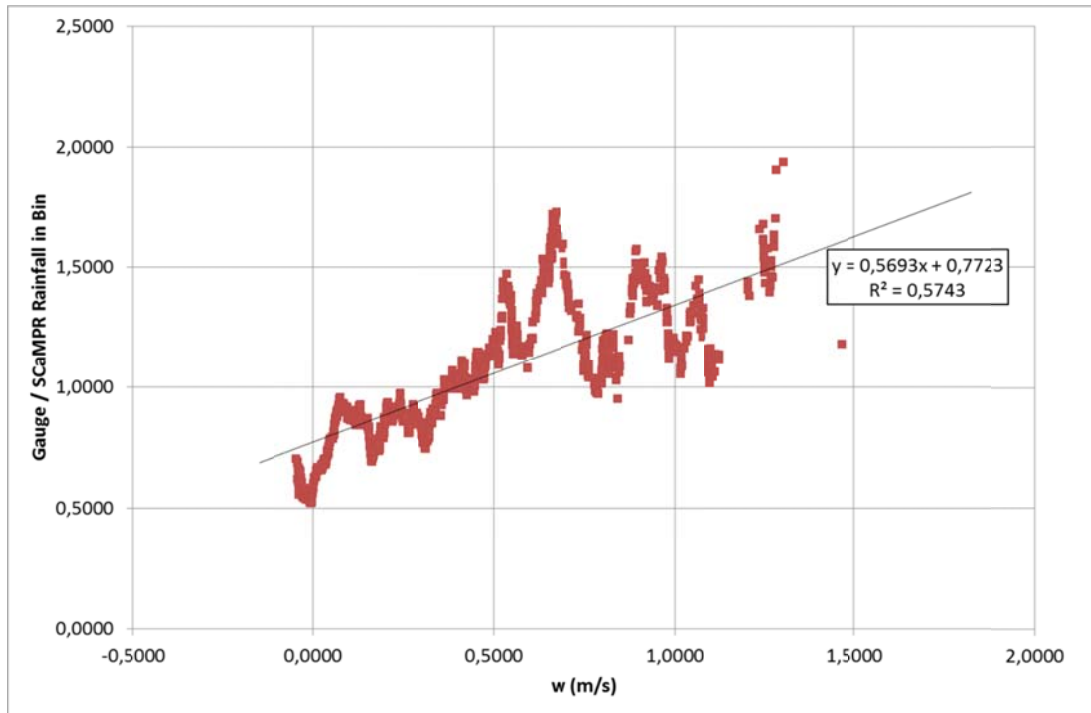


Figure 4.19: Total gauge / ScaMPR accumulations corresponding to vertical velocity bins using data from winter periods of 2002-2003 and 2003-2004. Threshold precipitation and estimation limits are 150 mm for 0.100 m/s updraft bin (a) and 450 mm for 0.500 m/s updraft bin (b). Fetch length is 14 minute wind duration.

a)



b)

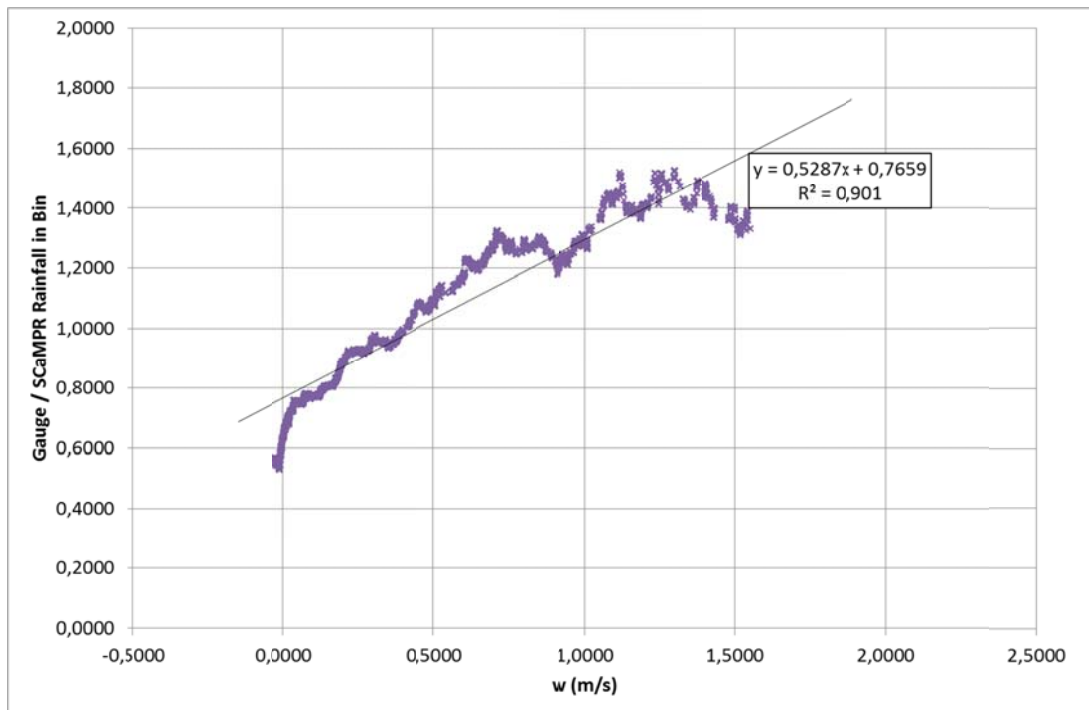
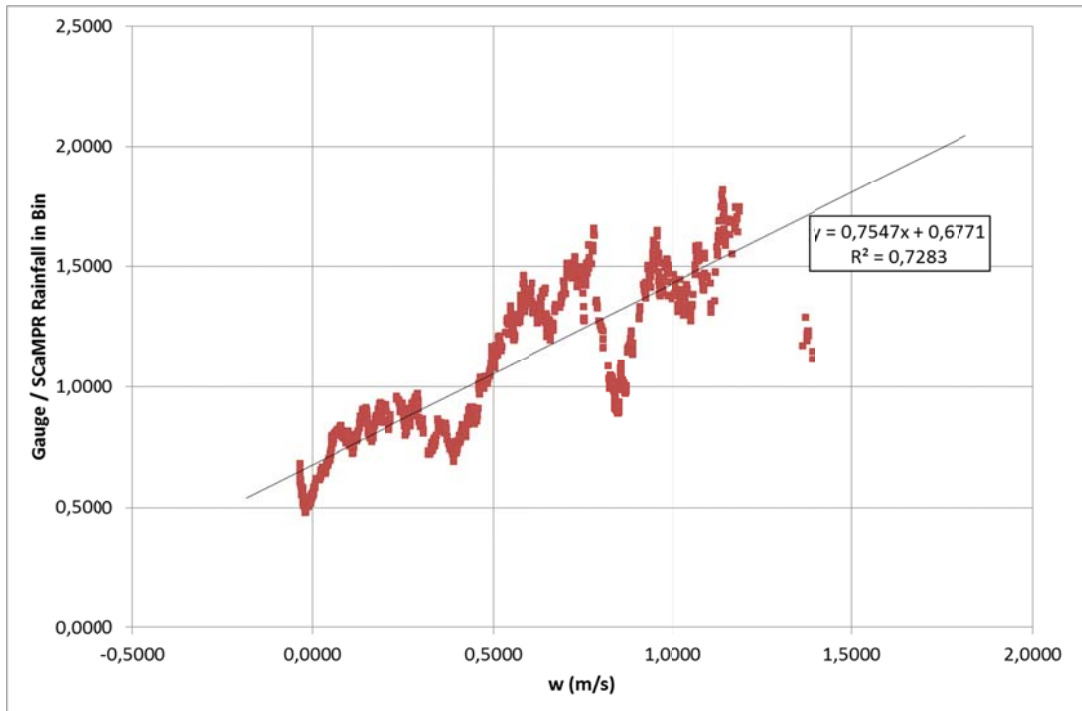


Figure 4.20: Total gauge / ScaMPR accumulations corresponding to vertical velocity bins using data from winter periods of 2002-2003 and 2003-2004. Threshold precipitation and estimation limits are 150 mm for 0.100 m/s updraft bin (a) and 450 mm for 0.500 m/s updraft bin (b). Fetch length is 15 minute wind duration.

a)



b)

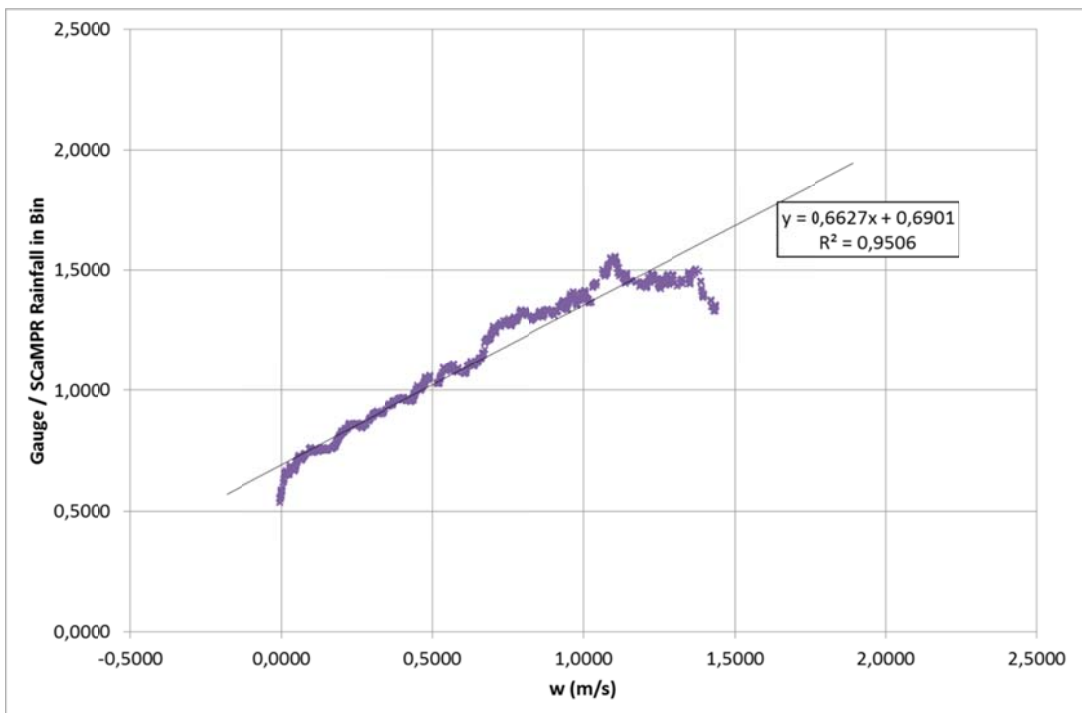


Figure 4.21: Total gauge / ScaMPR accumulations corresponding to vertical velocity bins using data from winter periods of 2002-2003 and 2003-2004. Threshold precipitation and estimation limits are 175 mm for 0.100 m/s updraft bin (a) and 600 mm for 0.500 m/s updraft bin (b). Fetch length is 20 minute wind duration.

Based on plots, all tested fetch values showed erroneous estimation by SCaMPR algorithm in presence of topographically driven vertical motion either upward or downward. Also all obtained trendline equations match the formation of multiplicative orographic adjustment formulation defined by Vicente et al. (2002). The main basis defined by the theoretical background for orographic adjustment is that if there is no topographically driven vertical movement on the air block of interest, then there will be no adjustment for orography. For multiplicative orographic formulation, this adjustment value will be unit, quantitatively 1.0 as multiplication of rain estimation with 1.0 will result with the original estimation. In order to achieve such correction formulation from the trendline equations, all trendline equations are normalized with respect to zero topographically driven vertical velocity point, so that the resultant equation will give not feature any adjustment at zero updraft location.

After orographic correction equations were obtained, a downwind value is defined as precipitation limit, below which no precipitation will be formed due to the strong downward motion of the air block, thus rainfall estimation at this point will be zeroed. As the correction equation is formed as a linear equation, orographic correction equation can assume negative value, which is not a meaningful physical value. Therefore the lowermost value, at which correction equation still assumes positive values, is defined as precipitation limit and all SCaMPR estimates with downwind values lower than precipitation limit is removed. The correction equations for each of the fetch lengths and associated precipitation limits are given in table 4.13.

Table 4.13: Trendline and resulting normalized correction equations with precipitation limit values for winter period measured for different fetch values

Fetch Duration / Length	Trendline Equation (ax + b)			Correction (ax + b) Equation		
	a	b	R ²	a	b	Precipitation Limit, w (m/s)
7.5 min	0.5376	0.8701	0.8634	0.6179	1.0000	-1.6185
10 min	0.6166	0.8085	0.9652	0.7626	1.0000	-1.3112
14 min	0.4905	0.7883	0.8792	0.6222	1.0000	-1.6071
15 min	0.5287	0.7659	0.9010	0.6903	1.0000	-1.4486
20 min	0.6627	0.6901	0.9506	0.9603	1.0000	-1.0413
10 km	0.6614	0.7621	0.9836	0.8679	1.0000	-1.1523
15 km	0.6195	0.7001	0.9613	0.8849	1.0000	-1.1301
20 km	0.5627	0.6981	0.8744	0.8060	1.0000	-1.2406

The achieved correction equations are plotted against vertical motion in Figure 4.22, and applied to the 1 hour winter data, and the statistics are presented for all data in the data series in Table 4.14 (a) and hit pixels on data series in Table 4.14 (b). When the obtained correction equations are analyzed, it can be seen that strongest orographic correction equation, that will enhance or degrade the precipitation estimate much higher based on the obtained vertical motion, is achieved with the application of 20 minute duration fetch length; while the smoothest correction equation is achieved via application of 7.5 minute duration fetch length.

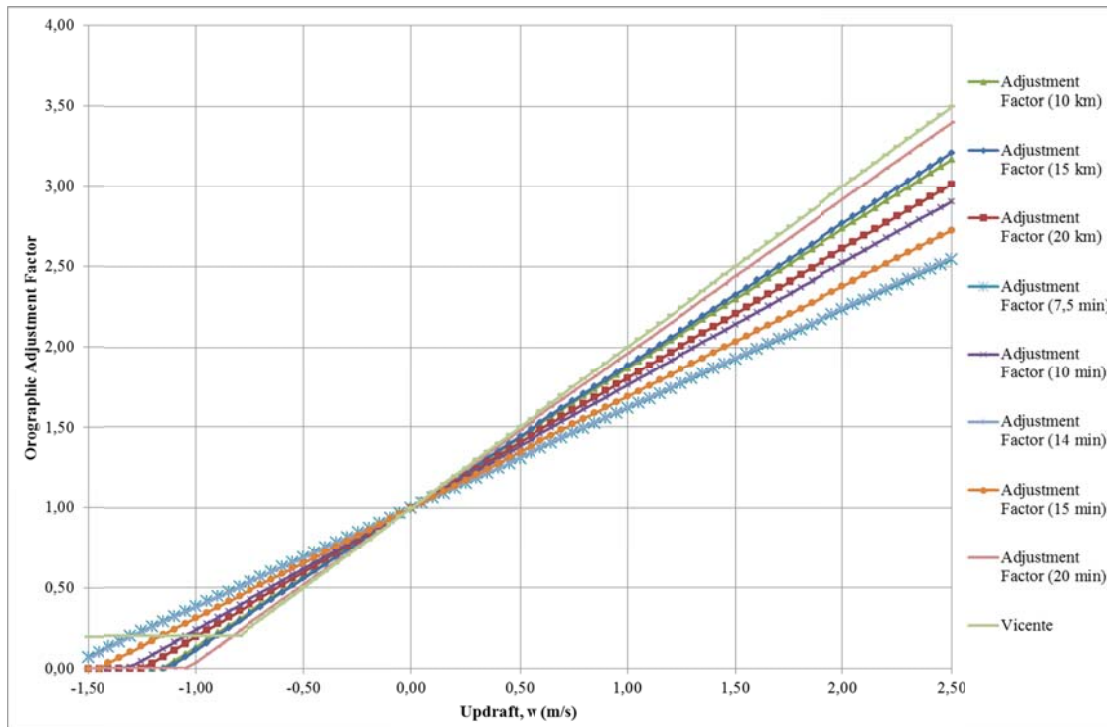


Figure 4.22: Correction equations achieved using winter data plotted against updraft

Table 4.14: Results of application of correction equations achieved using winter data, statistics of the all data series (a) and hit pixels (b) before and after orographic correction

a)	Applied correction (fetch length)	Real data length	Adjusted data length	Correlation	Bias	Bias (Ratio)	RMSE
	Before	292151	-	0.2807	-0.0010	0.9766	0.4524
	7.5 min	292151	292151	0.3042	0.0077	1.1786	0.4959
	10 min	292151	292151	0.3066	0.0115	1.2663	0.5186
	14 min	292151	292151	0.3062	0.0110	1.2538	0.5082
	15 min	292151	292151	0.3077	0.0126	1.2920	0.5179
	10 km	292151	292151	0.3064	0.0145	1.3365	0.5381
	15 km	292151	292151	0.3096	0.0179	1.4148	0.5505

b)	Applied correction (fetch length)	Hit pixels data length	Adjusted data length	Correlation	Bias	Bias (Ratio)	RMSE
	Before	3326	-	0.1075	-0.1437	0.9230	2.6576
	7.5 min	3350	3350	0.1654	0.2699	1.1445	2.9596
	10 min	3363	3363	0.1657	0.4339	1.2317	3.1366
	14 min	3363	3363	0.1574	0.4017	1.2149	3.0332
	15 min	3366	3366	0.1608	0.4776	1.2556	3.1047
	10 km	3368	3368	0.1685	0.5571	1.2979	3.2676
	15 km	3376	3376	0.1634	0.7041	1.3768	3.3529

As presented in the Table 4.14, correction made a positive impact on the correlation, with maximum increase with the application of 15 km fetch length as 10% and minimum increase with the application of 7.5 minute fetch length as 8%. Bias difference between SCaMPR estimates and gauge measurements are climb over zero, but stay at a reasonable level, between 0.0077 and 0.0179. RMSE values stays at the same levels, reflecting the low performance of the algorithm, with even an average increase of 11%. Although 15 km fetch length gives the highest correlation between SCaMPR estimates and gauge measurements, it also gives the lowest performance with highest bias and RMSE. Also, 7.5 minute fetch length gives the best performance after application with lowest bias and RMSE values, even though it features lowest correlation. The effects of orographic correction are much powerful on hit pixel values, with over 60% increase in correlation. But it should be noted that the statistical performance of the SCaMPR algorithm on hit pixels are much lower than statistical performance of the algorithm on all data. Also after application of orographic correction; bias and RMSE values of hit pixels climbs up to 0.26 to 0.70 values for bias difference and 2.95 to 3.35 values for RMSE.

4.4.2. Summer Period

For the summer period, the same methodology as in the winter period is followed. However, in summer analysis fetch lengths that are found to be effectively matching topography in the winter period analysis are used. Therefore 20 km and 20 minute duration fetch length are not analyzed in summer period as they come out to be too coarse to separate downwind data in the winter analysis. Also the analyses are done for only 0.500 m/s updraft bin, which reflect topographic effects much better. First total gauge / SCaMPR accumulations corresponding to 0.500 m/s vertical velocity bin calculated with 10 km fetch length are plotted in Figure 4.23.

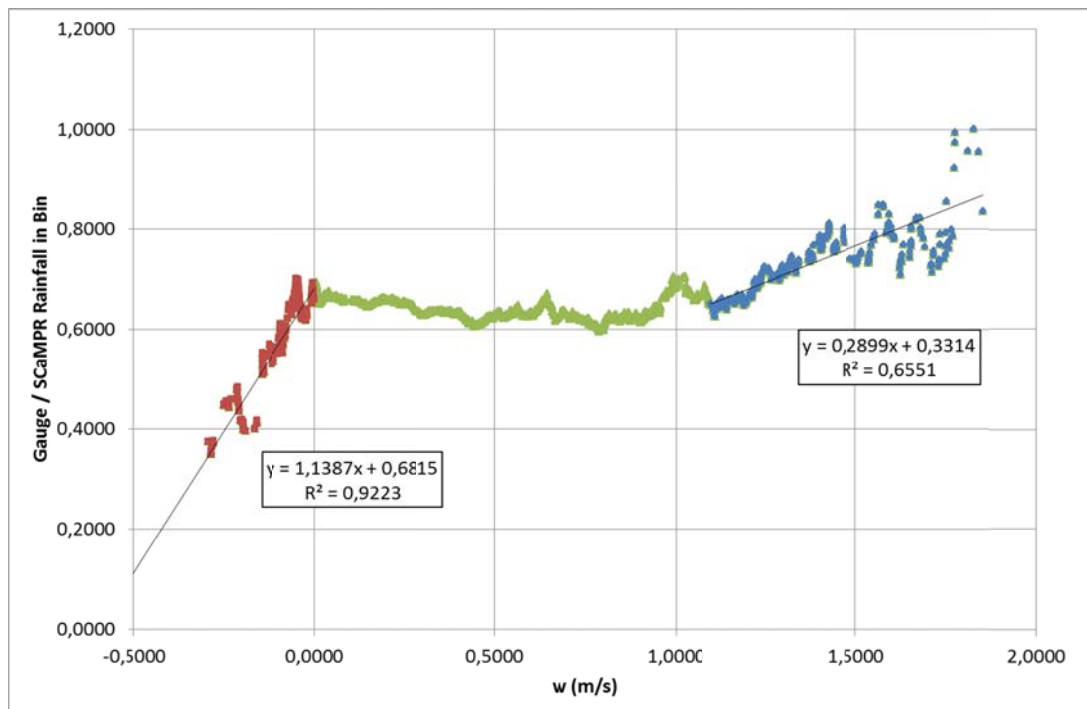


Figure 4.23: Total gauge / SCaMPR accumulations corresponding to 0.500 m/s vertical velocity bins using data from summer periods of 2002-2004. Threshold precipitation and estimation limits are 100 mm, fetch length is 10 km.

The distribution of total gauge / SCaMPR accumulations of summer data corresponding to orographically driven vertical velocity values come out to be completely different than winter data, also the distribution does not conform the theoretical orographic correction formulation defined by Vicente et al. (2002). The results show that between zero updraft value and 1 m/s updraft value, the

effect of increasing topographically driven upwind motion on gauge / SCaMPR values is almost non-observable. Over this level, multiplicative error value between gauge measurements and SCaMPR estimates stay between 0.6 and 0.7 level with a little fluctuation. Therefore for summer period, no orographic adjustment formulation is defined between zero and 1.0 m/s updraft values. The updraft portion that lay above 1 m/s upwind value and downward portion that lay below zero upwind value are defined by two separate equations in the summer period. The main reasoning on deciding two separate correction equations for upwind and downwind parts is that they feature different trendline equations, which need to be addressed with different adjustment coefficients. Also effects of orography on precipitation are not observed between zero and 1.0 m/s updraft values, and the observations does not conforms the theoretical background. Therefore upwind and downwind parts with a single adjustment equation may lead to erroneous estimates as a result of false correction.

The downwind adjustment equation is normalized with respect to zero topographically driven vertical velocity point, while updraft adjustment equation is normalized with respect to 1.0 upwind velocity as after this upwind value, the effects of orography can be observed.

The same analysis are performed for 10 minute duration (Figure 4.24), 14 minute duration (Figure 4.25), and 15 minute duration (Figure 4.26) fetch lengths and the results are plotted respectively.

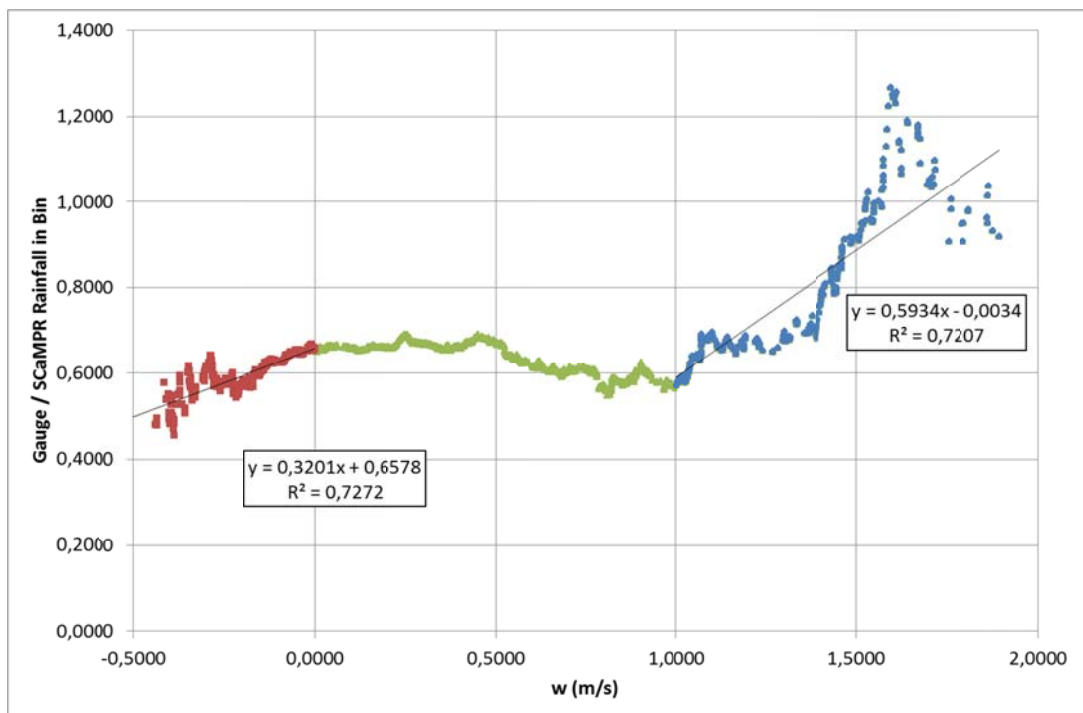


Figure 4.24: Total gauge / SCaMPR accumulations corresponding to 0.500 m/s vertical velocity bins using data from summer periods of 2002-2004. Threshold precipitation and estimation limits are 100 mm, fetch length is 10 minute wind duration.

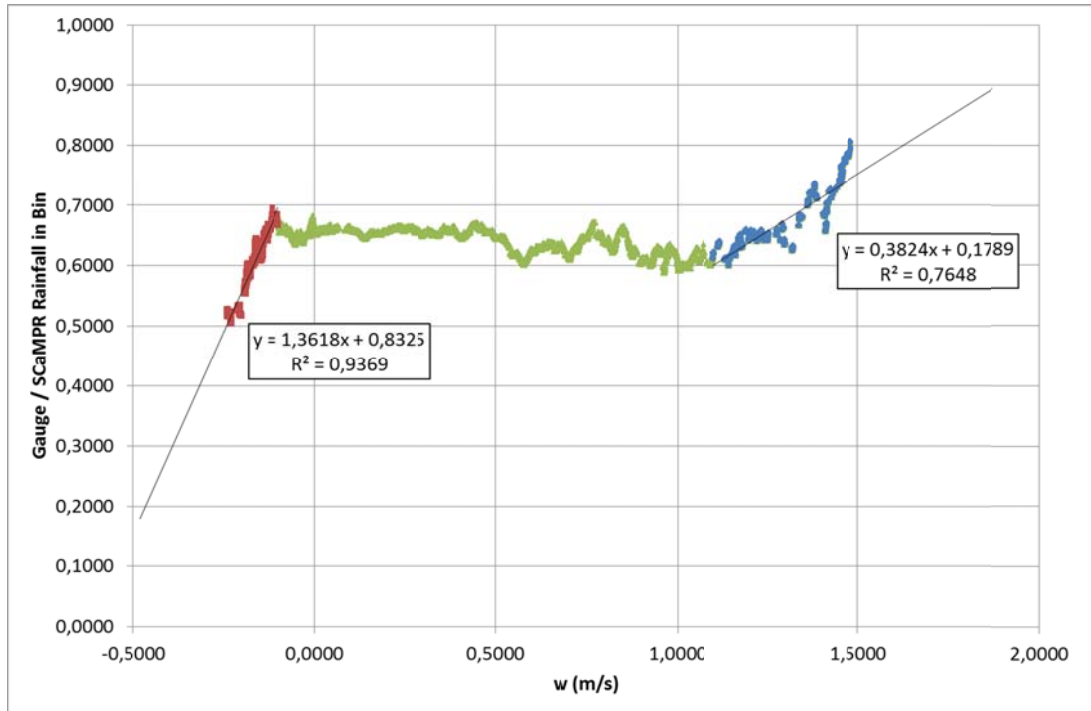


Figure 4.25: Total gauge / ScaMPR accumulations corresponding to 0.500 m/s vertical velocity bins using data from summer periods of 2002-2004. Threshold precipitation and estimation limits are 700 mm, fetch length is 14 minute wind duration.

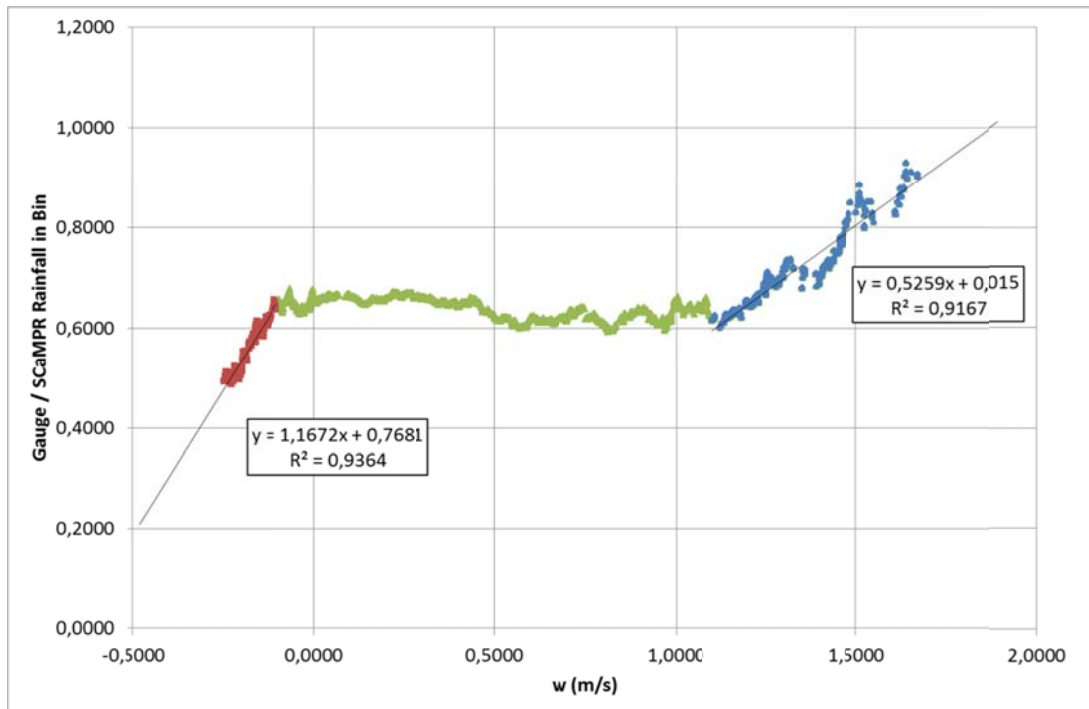


Figure 4.26: Total gauge / ScaMPR accumulations corresponding to 0.500 m/s vertical velocity bins using data from summer periods of 2002-2004. Threshold precipitation and estimation limits are 500 mm, fetch length is 15 minute wind duration.

Based on plots, all fetch values resulted with a high gap between zero updraft and approximately 1 m/s updraft where the orographic effects are not observable. On the other hand, the upward adjustment factor over 1 m/s updraft shows that in summer period SCaMPR algorithm underestimates rain rate in the presence of strong topographically upward motions, also overestimates the rain rate in the presence of topographically forced downward motion. As a result of this gap, two separate correction equations are defined for updraft and downdraft. The correction equations for each of the fetch lengths and associated precipitation limits for downdraft equations are given in Table 4.15.

Table 4.15: Trendline and resulting normalized correction equations for downwind (a) and upwind (b) values with precipitation limit values for winter period measured for different fetch values

a) Fetch Duration / Length	Trendline Equation (ax + b)			Start point	Correction (ax + b) Equation		
	a	b	R ²		a	b	Prec. Limit
10 km	1.1387	0.6815	0.9223	0.0000	1.6709	1.0000	-0.5985
10 min	0.3201	0.6578	0.7272	0.0000	0.4866	1.0000	-2.0550
14 min	1.3918	0.8325	0.9369	-0.1000	2.0074	1.2007	-0.5981
15 min	1.1672	0.7681	0.9364	-0.1000	1.7919	1.1792	-0.6581

b) Fetch Duration / Length	Trendline Equation (ax + b)			Start point	Correction (ax + b) Equation	
	a	b	R ²		a	b
10 km	0.2899	0.3314	0.6551	1.1000	0.4458	0.5096
10 min	0.5934	-0.0034	0.7207	1.0000	1.0058	-0.0058
14 min	0.3824	0.1789	0.7684	1.1000	0.6378	0.2984
15 min	0.4361	0.1336	0.9251	1.1000	0.7111	0.2178

The achieved correction equations are plotted against vertical motion in Figure 4.27, and applied to the 1 hour winter data, and the statistics are presented for all data in the data series in table 4.16 (a) and hit pixels on data series in 4.16 (b). It can be seen that, the achieved correction equations does not conform theoretical correction formulation defined by Vicente et al. (2002).

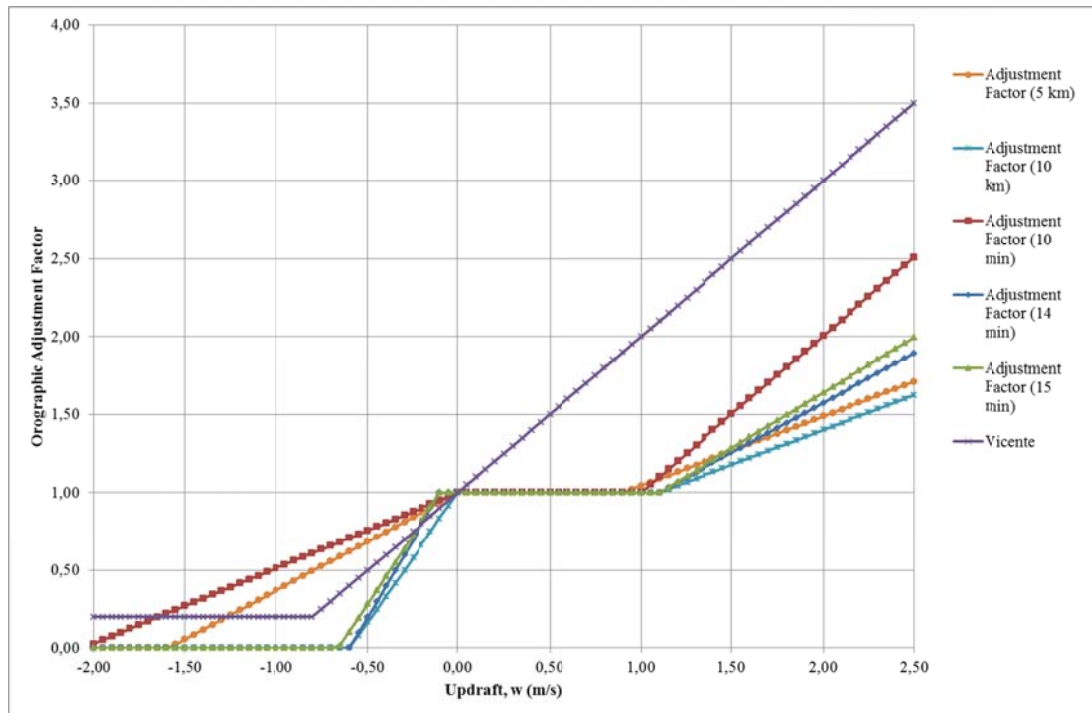


Figure 4.27: Correction equations achieved using summer data plotted against updraft

Table 4.16: Results of application of correction equations achieved using summer data, statistics of the all data series (a) and hit pixels (b) before and after orographic correction

a)	Applied correction (fetch length)	Real data length	Adjusted data length	Correlation	Bias	Bias (Ratio)	RMSE
	Before	391212	-	0.2772	0.1876	1.9491	1.7352
	10 km	391212	31530	0.2772	0.1873	1.9479	1.7345
	10 min	391212	107633	0.2778	0.1872	1.9472	1.7329
	14 min	391212	13202	0.2776	0.1874	1.9483	1.7339
	15 min	391212	12209	0.2773	0.1880	1.9514	1.7357

b)	Applied correction (fetch length)	Hit pixels data length	Adjusted data length	Correlation	Bias	Bias (Ratio)	RMSE
	Before	19763	-	0.1821	0.2415	1.0800	5.8409
	10 km	19727	1676	0.1830	0.2488	1.0824	5.8305
	10 min	19662	5475	0.1831	0.2606	1.0863	5.8335
	14 min	19756	927	0.1825	0.2469	1.0818	5.8327
	15 min	19757	843	0.1824	0.2515	1.0833	5.8332

As presented in the Table 4.16, correction made a small positive impact on correlation, with maximum increase with the application of 10 minute fetch length as 0.21%. Also with the application of 10 minute fetch length, bias difference between SCA-MPR estimates and gauge measurements are decreased with 0.21% which is not observed in application of orographic correction on winter data. Moreover, a little increase on the performance of algorithm is achieved with a 0.31% decrease in

RMSE value. Application of orographic correction to summer data leads to similar results on hit pixels also. On the other hand, these impacts are not very remarkable. Even after the adjustment, the bias and RMSE values are still at a high level, especially for hit pixel points.

When all the winter and summer data are analyzed together, 10 minute duration fetch length is selected as the ideal fetch length as it provides best distribution, especially in downwind side, and as its impact on the results are more remarkable.

After application of orographic correction to summer data, the statistical indices still show low performance of SCaMPR algorithm; for 1 hour temporal resolution, bias difference between gauge measurements and SCaMPR estimates comes out to be 0.1872 and RMSE value comes out to be 1.7329, while these values are 0.0115 and 0.5186 respectively for winter period. In order to further increase performance of the SCaMPR algorithm and define the cause of this phenomenon, effects of atmospheric variables are analyzed with respect to multiplicative error values between gauge measurements and SCaMPR estimates.

4.5. Stability Analysis for Correction Method

The distribution of total gauge/SCaMPR accumulations over topographically forced vertical motion looks different on summer and winter seasons. While winter distribution matches the orographic adjustment formulation defined by Vicente et al. (2002), summer distribution features a gap between zero updraft and 1 m/s updraft values where effect of orography is not observable. In order to define the cause of this phenomenon and further increase performance of SCaMPR algorithm, the stability of the air block over the station location is analyzed. The temperature, specific humidity, equivalent potential temperature and integrated moisture convergence variation over the station locations for summer and winter periods are compared and analyzed.

4.5.1. Temperature

Temperature of the air parcel at 700 hPa level is given in °K. The variation of 700 hPa temperature over summer and winter periods are analyzed by plotting the cumulative distribution of hit pixels vs. temperature on a logarithmic scale. (Figure 4.28)

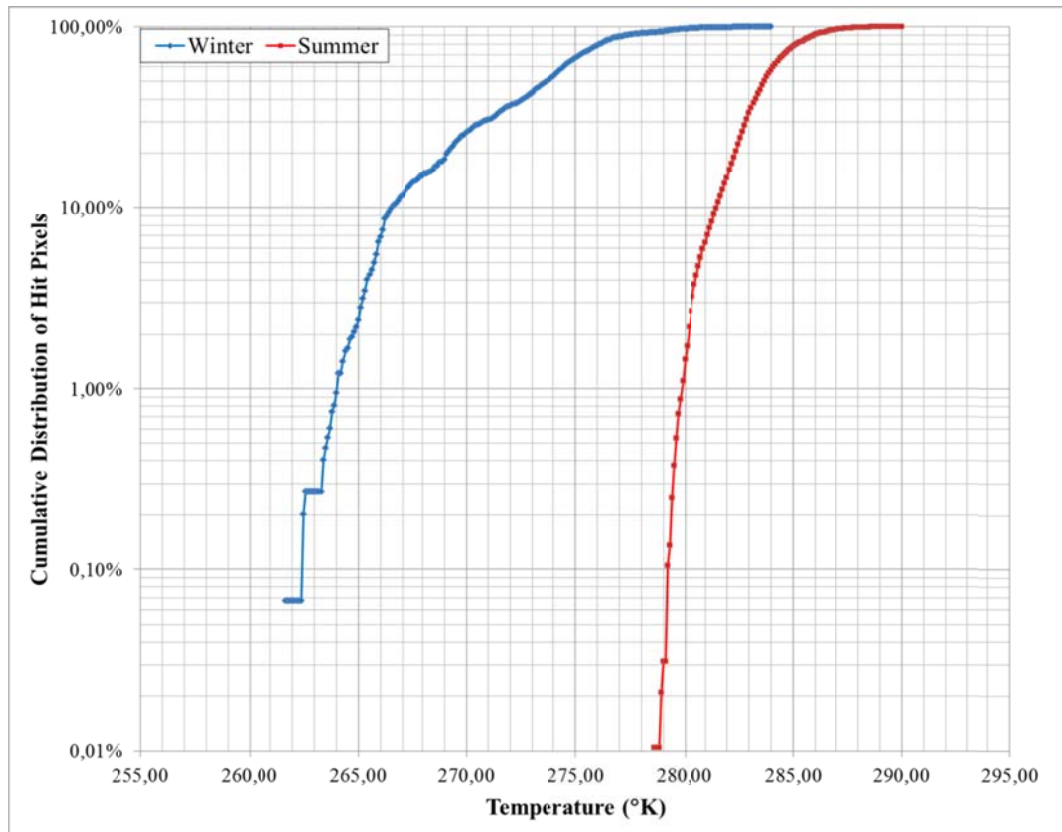
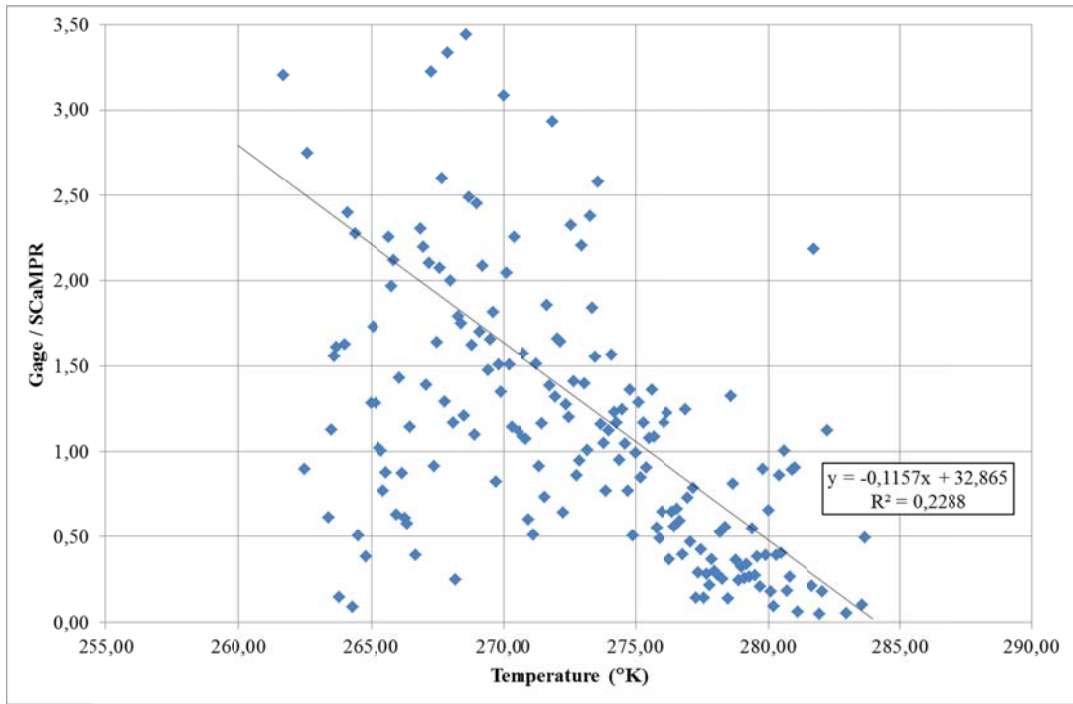


Figure 4.28: Variation of Temperature between summer and winter periods defined as the cumulative distribution of hit pixels vs. temperature

The variations of temperature between summer and winter periods are completely different, both in magnitude and in distribution. Temperature variation is limited to a narrow temperature strip in summer period, between 279 °K and 288 °K, whereas in winter period temperature variation is extended to a wider range, between 262 °K and 279 °K. Also the 50% of the winter data is located over 274 °K temperature value, while for summer period this amount of data is located over 284 °K temperature value, with an average of 10 °K temperature difference between summer and winter data.

To see the effect of temperature on winter period SCaMPR estimates are further investigated by plotting total gauge / SCaMPR accumulations vs. temperature values in Figure 4.29 (a). The plot gives a direct relation; as the temperature of the air block increases, SCaMPR algorithm overestimates rain rates. To show more isolated relation, gauge / SCaMPR accumulations are aggregated into 0.4 °K temperature bins in Figure 4.29 (b) to clarify the relation. It is clear that, over 275 °K, SCaMPR algorithm tends to overestimate precipitation, while tends to underestimate precipitation below this level.

a)



b)

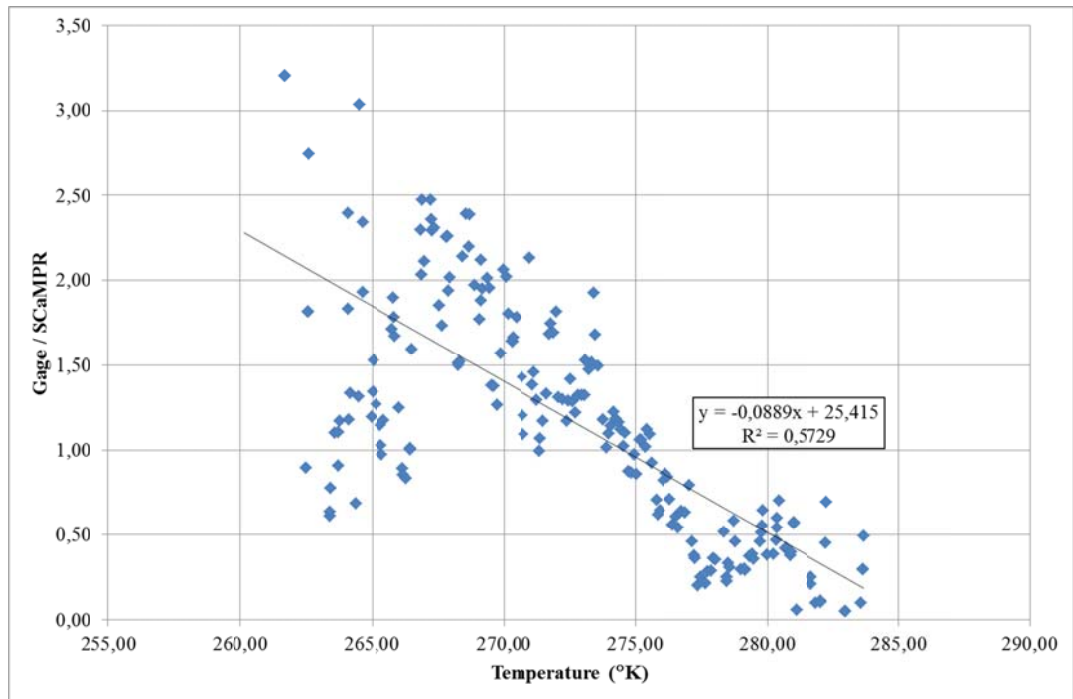


Figure 4.29: Total gauge / SCaMPR accumulations corresponding to point temperature values (a) and accumulations corresponding to 0.4 °K temperature bins (b) using data from winter periods of 2002-2003 and 2003-2004.

After temperature correction equation is obtained, a temperature value is defined as precipitation limit, above which no precipitation will be formed due to the high temperature value of the air block, which will prevent any formation of rain droplets by evaporating them, thus rainfall estimation at this point will be zeroed. As the correction equation is formed as a linear equation, temperature correction equation can assume negative value, which is not a meaningful physical value. Therefore the uppermost value, at which correction equation still assumes positive values, is defined as precipitation limit and all SCaMPR estimates with temperature values higher than precipitation limit is removed.

As the relation between temperature and gauge / SCaMPR aggregations is evident, for winter period a temperature adjustment formulation to eliminate overestimation of SCaMPR algorithm with the increasing temperature values is developed as follows:

$$\begin{aligned} RR_C &= RR_S \times (-0,0889T + 25,4150) \quad \text{for } T \leq 285,8830 \\ RR_C &= 0 \quad \text{for } T > 285,8830 \end{aligned} \quad (4.8)$$

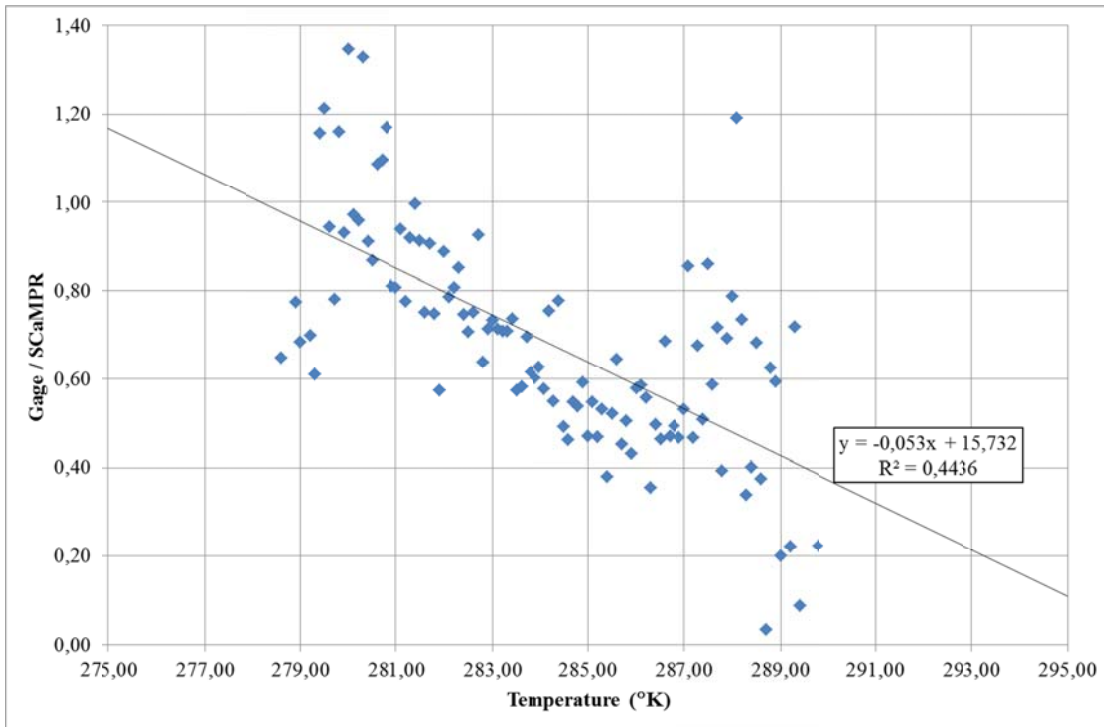
where RR_C is the corrected rain rate estimation, RR_S is the satellite rain rate estimation and T is the temperature in °K.

The same analysis is repeated for the summer period to develop a similar temperature adjustment equation. Total gauge / SCaMPR accumulations vs. temperature values are plotted in Figure 4.30 (a). The plot again gives a direct relation; as the temperature of the air parcel increases, SCaMPR algorithm overestimates rain rates. To show more isolated relation, gauge / SCaMPR accumulations are aggregated into 0.4 °K temperature bins in Figure 4.30 (b), which supports the relation. It is clear that, over 277.5 °K, SCaMPR algorithm tends to overestimate precipitation, while tends to underestimate precipitation below this level. When the data further analyzed, it can be seen from Figure 4.28 that, all of the data in summer period exists over this aforementioned temperature level, 277.5 °K. Therefore this may explain the bad performance of SCaMPR algorithm over summer seasons. Again temperature level is defined as precipitation limit, over which no precipitation will be formed.

For summer period a temperature adjustment formulation to eliminate overestimation of SCaMPR algorithm with the increasing temperature values is developed as follows:

$$\begin{aligned} RR_C &= RR_S \times (-0,0482T + 14,3720) \quad \text{for } T \leq 298,1743 \\ RR_C &= 0 \quad \text{for } T > 298,1743 \end{aligned} \quad (4.9)$$

a)



b)

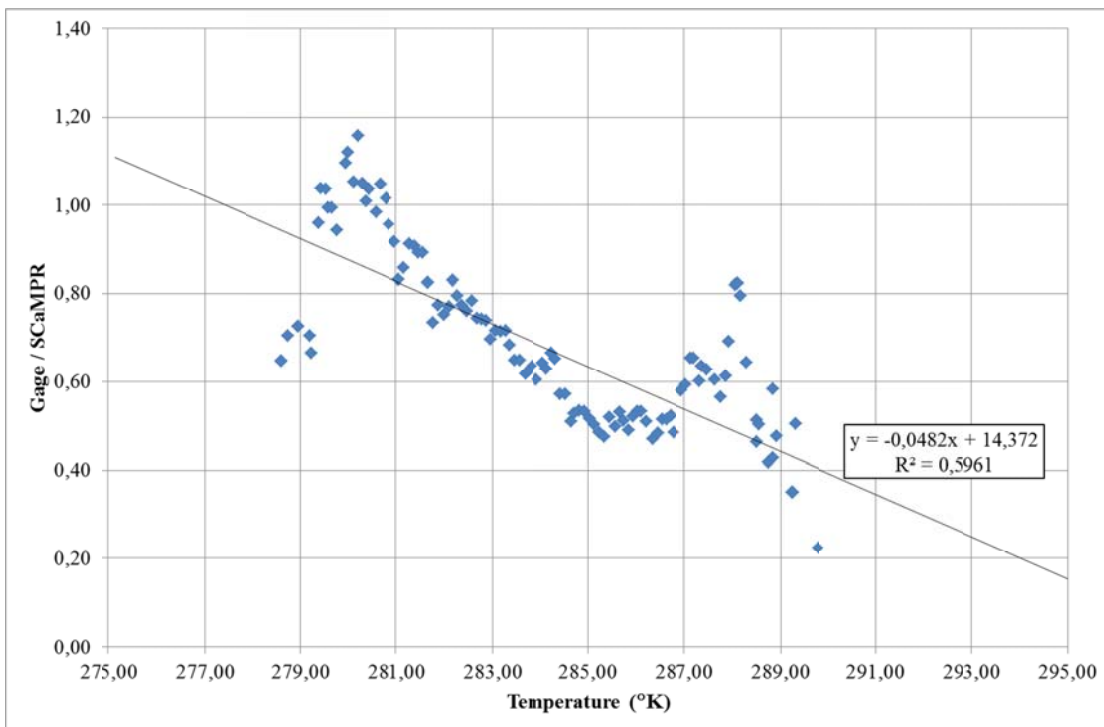


Figure 4.30: Total gauge / SCaMPR accumulations corresponding to point temperature values (a) and accumulations corresponding to 0.4 °K temperature bins (b) using data from summer periods of 2002-2004.

4.5.2. Specific Humidity

Specific humidity of the air parcel at 700 hPa level is given in kg/m^3 . The variation of 700 hPa specific humidity over summer and winter periods are analyzed by plotting the cumulative distribution of hit pixels vs. temperature on a logarithmic scale. (Figure 4.31)

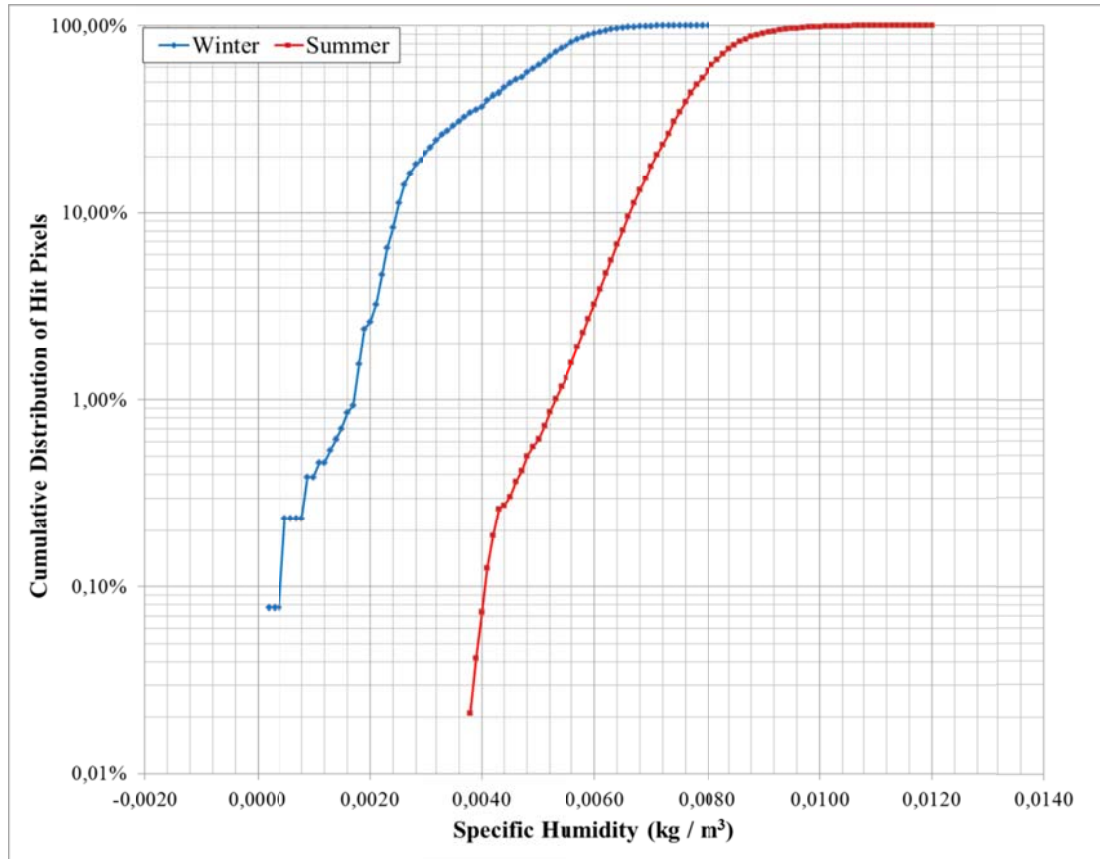
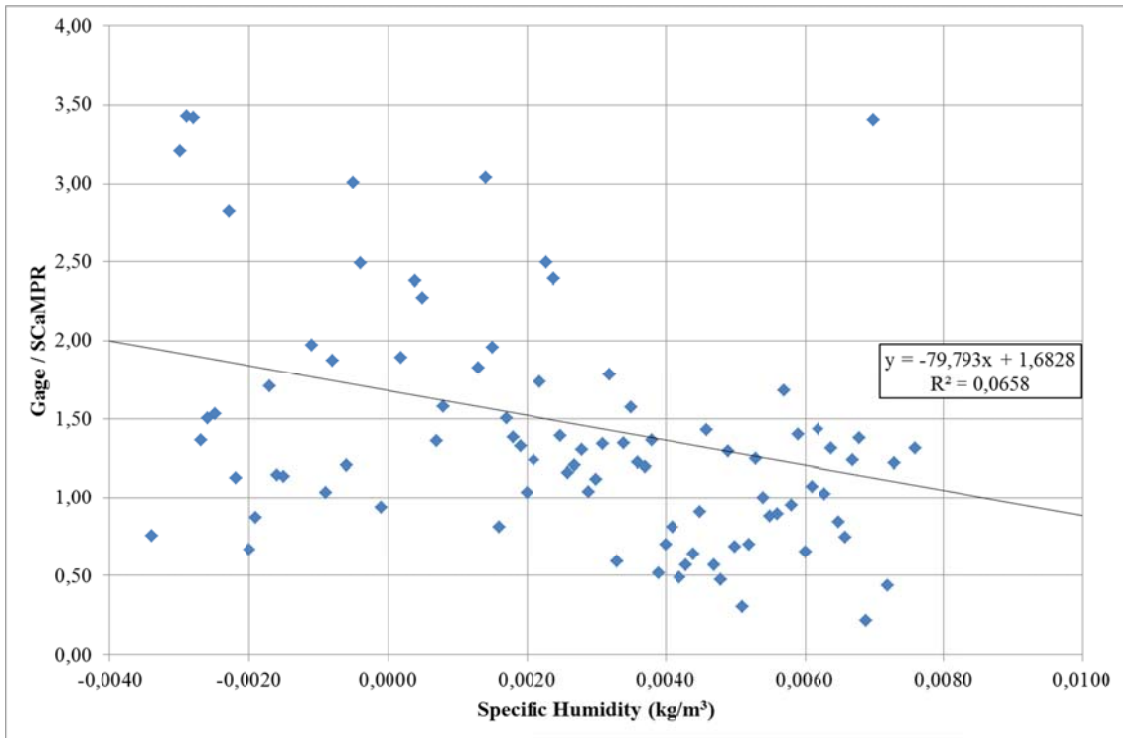


Figure 4.31: Variation of specific humidity between summer and winter periods defined as the cumulative distribution of hit pixels vs. specific humidity

Although the variations of specific humidity between summer and winter periods are similar in distribution, they are completely different in magnitude. Specific humidity variation is limited between $0.0040 \text{ kg}/\text{m}^3$ and $0.0100 \text{ kg}/\text{m}^3$ for summer period, whereas in winter period variation is extended between $0.0004 \text{ kg}/\text{m}^3$ and $0.0068 \text{ kg}/\text{m}^3$. The 50% of the winter data is located over $0.0044 \text{ kg}/\text{m}^3$ specific humidity level, while for summer period this amount of data is located over $0.0080 \text{ kg}/\text{m}^3$ level.

The effect of specific humidity on winter period SCA-MPR estimates is further investigated by plotting total gauge / SCA-MPR accumulations vs. specific humidity values in Figure 4.32 (a). Total gauge / SCA-MPR accumulations vs. specific humidity values for summer period are also plotted in Figure 4.32 (b). The two plots do not provide a direct and common relation between specific humidity and SCA-MPR estimates. Therefore a specific humidity adjustment formulation could not be developed.

a)



b)

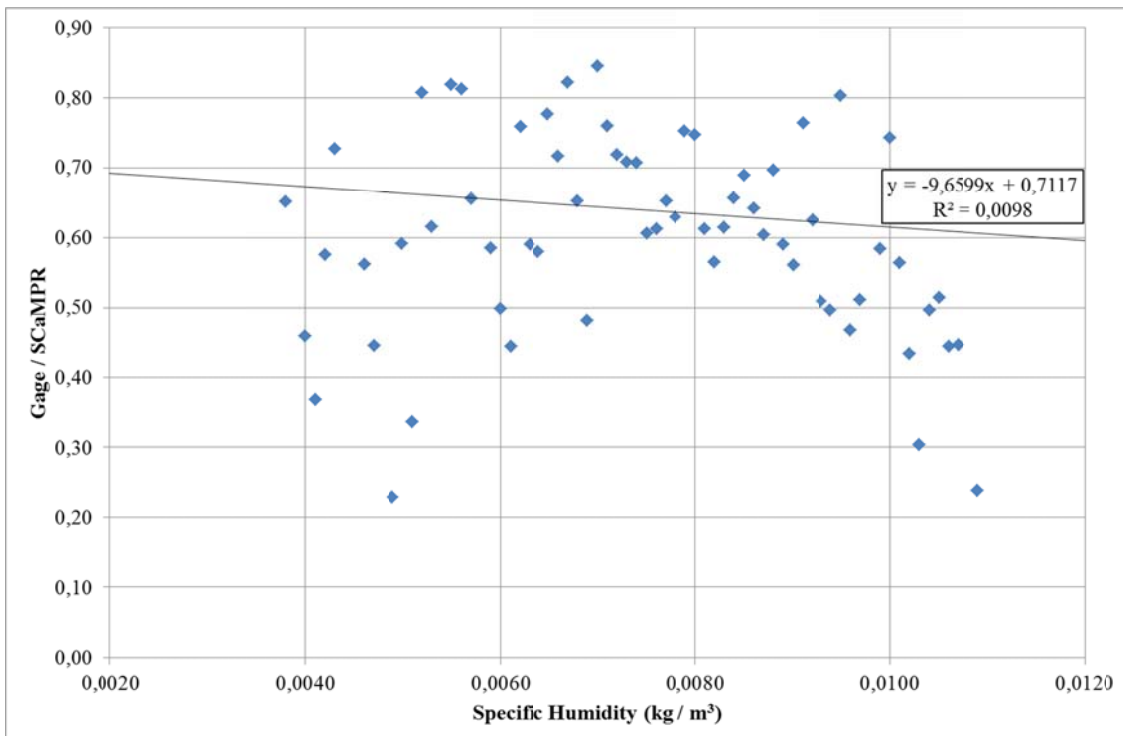


Figure 4.32: Total gauge / SCaMPR accumulations corresponding to point specific humidity values for winter periods of 2002-2003 and 2003-2004 (a) and summer periods of 2002-2004

4.5.3. Equivalent Potential Temperature, D_{the}

Equivalent potential temperature of the air block between 700 hPa and surface level is given in °K. The variation of equivalent potential temperature over summer and winter periods are analyzed by plotting the cumulative distribution of hit pixels vs. equivalent potential temperature on a logarithmic scale. (Figure 4.33)

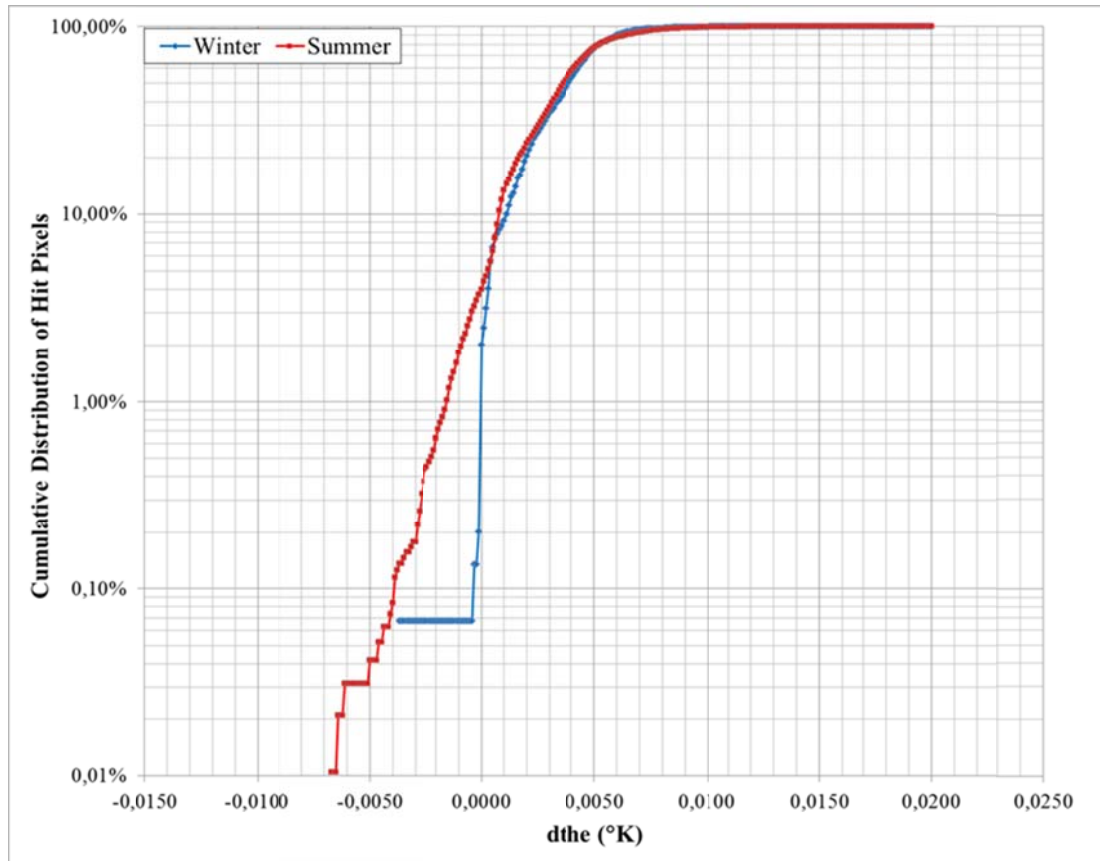
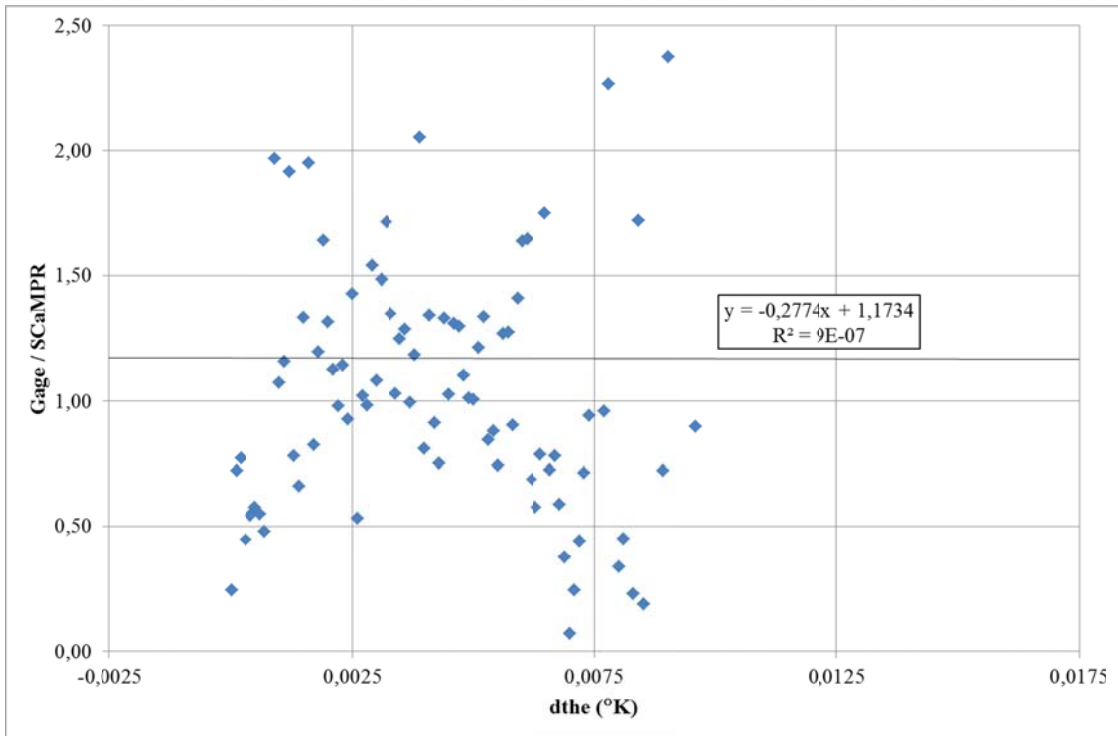


Figure 4.33: Variation of equivalent potential temperature between summer and winter periods defined as the cumulative distribution of hit pixels vs. d_{the}

The equivalent potential temperature distribution showed very similar distribution between summer and winter periods, with only 5% divergence at the lowest part.

The effect of equivalent potential temperature on winter period SCaMPR estimates is further investigated by plotting total gauge / SCaMPR accumulations vs. equivalent potential temperature values in Figure 4.34 (a). Total gauge / SCaMPR accumulations vs. equivalent potential temperature values for summer period are also plotted in Figure 4.34 (b). The two plots do not provide a direct and common relation between equivalent potential temperature and SCaMPR estimates. Therefore an equivalent potential temperature adjustment formulation could not be developed.

a)



b)

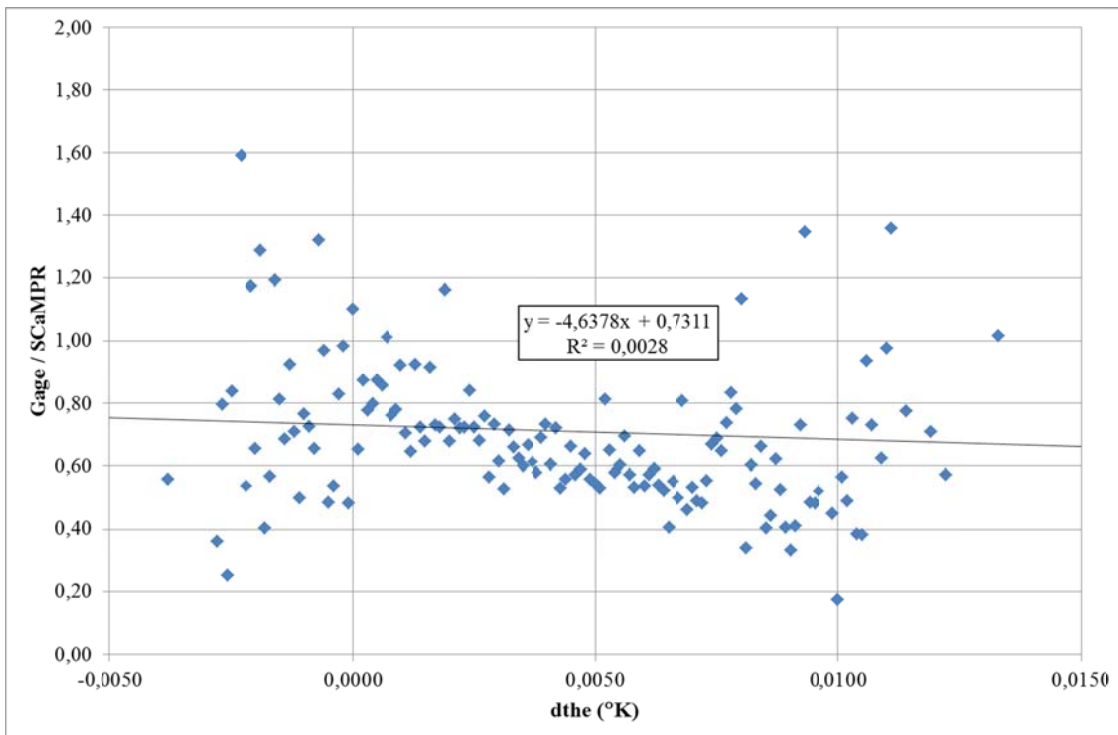


Figure 4.34: Total gauge / SCaMPR accumulations corresponding to point equivalent potential temperature values for winter periods of 2002-2003 and 2003-2004 (a) and summer periods of 2002-2004

4.2.4. Integrated Moisture Convergence, Iqcn

Integrated moisture convergence of the air block between 700 hPa and surface level is given in $\text{kg/m}^2/\text{s}$. The variation of integrated moisture convergence over summer and winter periods are analyzed by plotting the cumulative distribution of hit pixels vs. integrated moisture convergence on a logarithmic scale. (Figure 4.35)

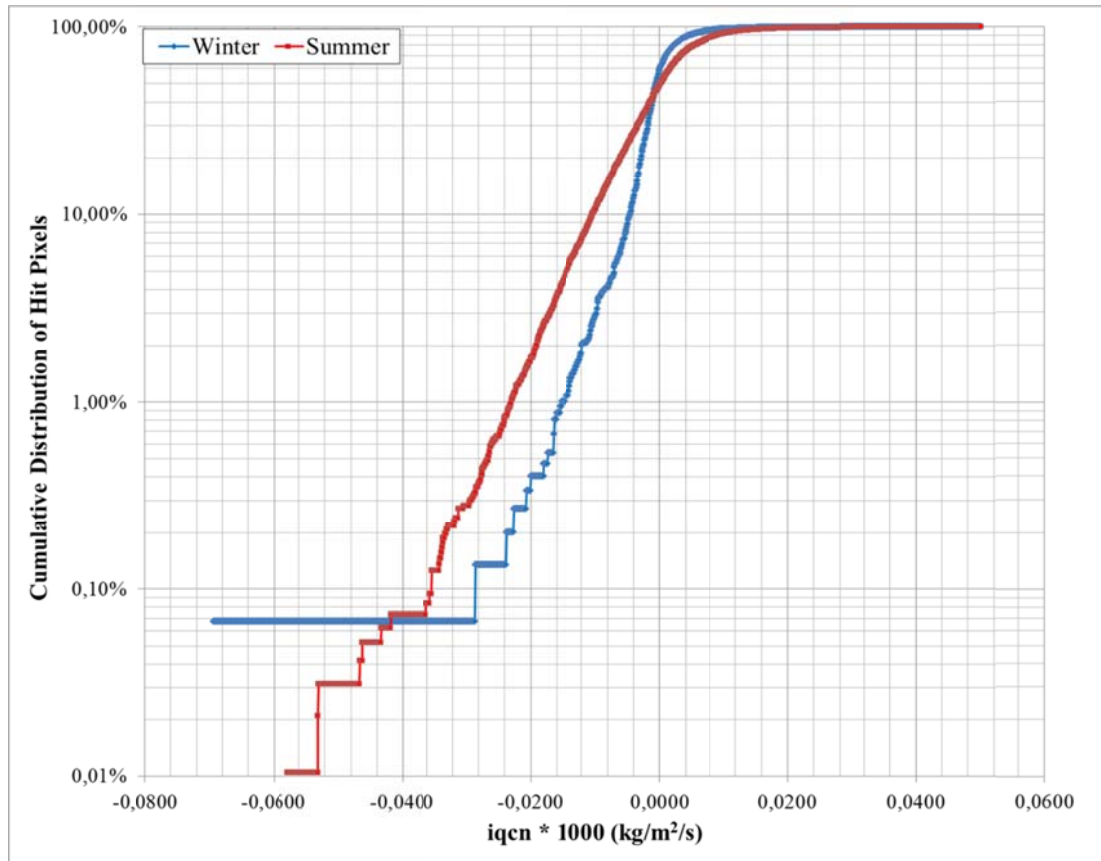
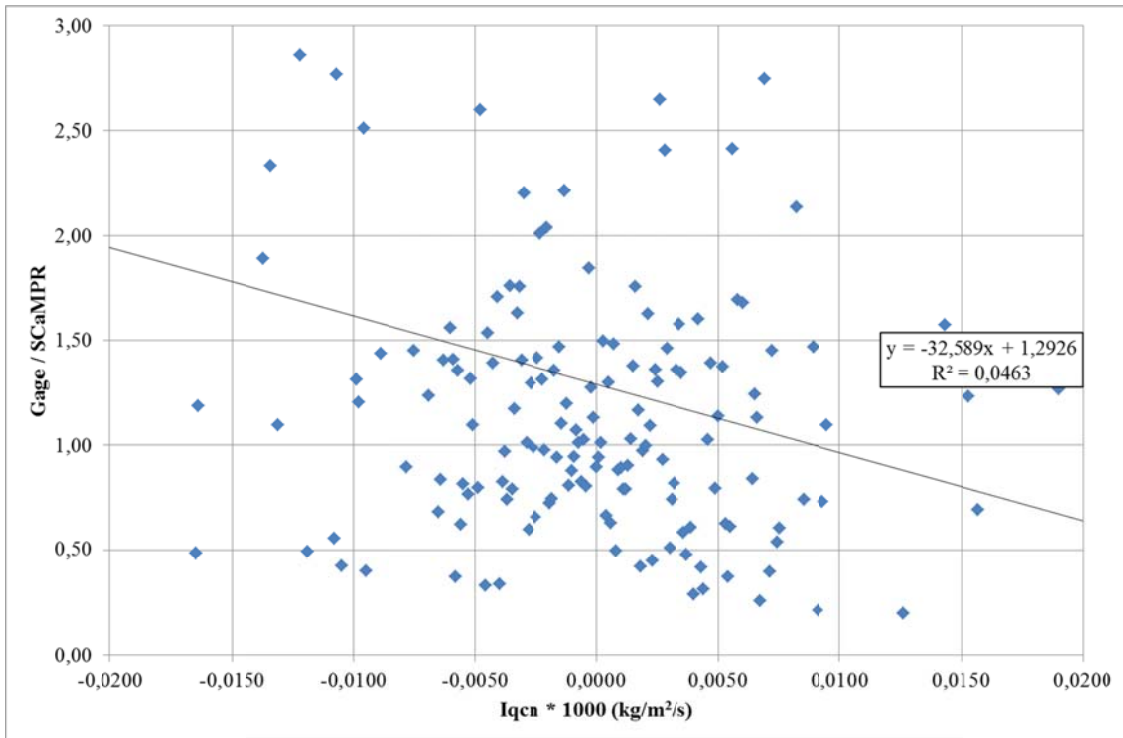


Figure 4.35: Variation of integrated moisture convergence between summer and winter periods defined as the cumulative distribution of hit pixels vs. iqcn

The integrated moisture convergence distribution showed very similar distribution between summer and winter periods, with small divergence.

The effect of integrated moisture convergence on winter period SCaMPR estimates is further investigated by plotting total gauge / SCaMPR accumulations vs. integrated moisture convergence values in Figure 4.36 (a). Total gauge / SCaMPR accumulations vs. integrated moisture convergence values for summer period are also plotted in Figure 4.36 (b). The two plots do not provide a direct and common relation between integrated moisture convergence and SCaMPR estimates. Therefore an integrated moisture convergence adjustment formulation could not be developed.

a)



b)

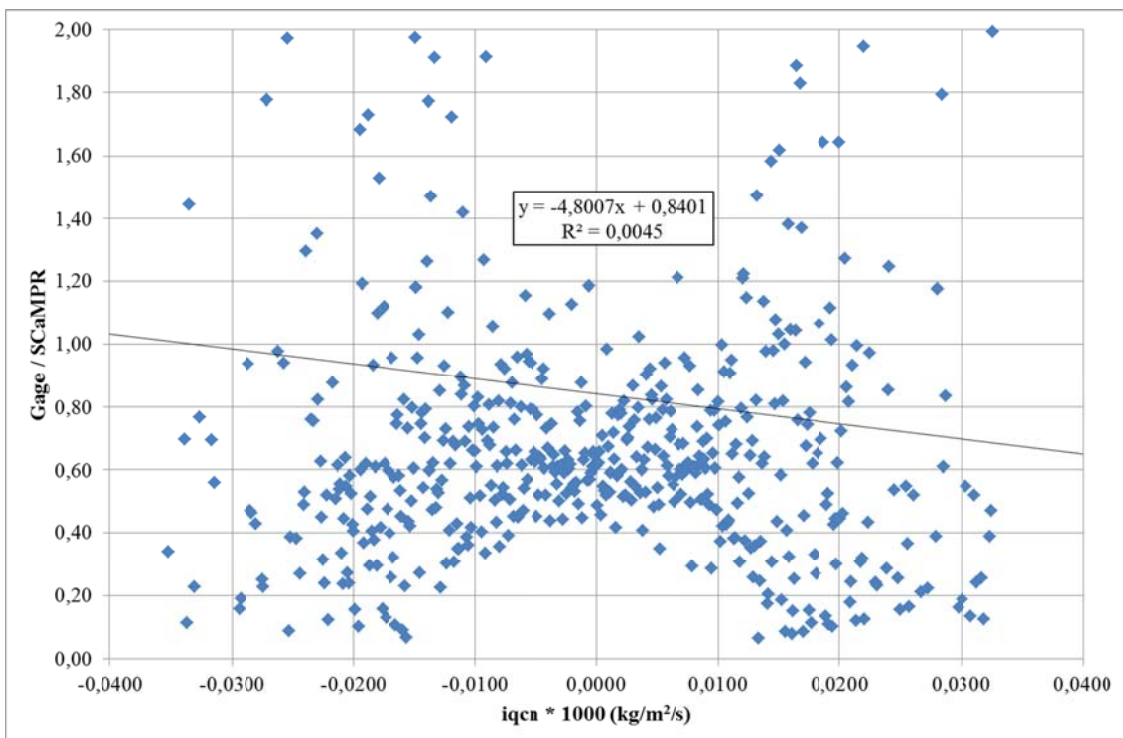


Figure 4.36: Total gauge / SCaMPR accumulations corresponding to point integrated moisture convergence values for winter periods of 2002-2003 and 2003-2004 (a) and summer periods of 2002-2004

4.6. Developing Final Correction Algorithm

4.6.1. Winter Period

The final orographic correction equation for winter period is defined as;

$$\begin{aligned} RR_C &= RR_S \times (0,7626w + 1,0000) \\ RR_C &= 0 \quad \text{for } w < -1,3112 \end{aligned} \quad (4.10)$$

The final temperature correction equation for winter period is defined as;

$$\begin{aligned} RR_C &= RR_S \times (-0,0889T + 25,4150) \\ RR_C &= 0 \quad \text{for } T > 285,8830 \end{aligned} \quad (4.11)$$

where RR_C is the corrected rain rate estimation, RR_S is the satellite rain rate estimation, w is the vertical air movement driven by topography in m/s and T is the temperature at 700 hPa level in °K.

4.6.2. Summer Period

The final orographic correction equation for summer period is defined as;

$$\begin{aligned} RR_C &= RR_S \times (0,4866w + 1,0000) \quad \text{for } w \leq 0,0000 \\ RR_C &= RR_S \times (1,0058w - 0,0058) \quad \text{for } w \geq 1,0000 \\ RR_C &= 0 \quad \text{for } w < -2,0550 \end{aligned} \quad (4.12)$$

The final temperature correction equation for summer period is defined as;

$$\begin{aligned} RR_C &= RR_S \times (-0,0482T + 14,3720) \\ RR_C &= 0 \quad \text{for } T > 298,1743 \end{aligned} \quad (4.13)$$

where RR_C is the corrected rain rate estimation, RR_S is the satellite rain rate estimation, w is the vertical air movement driven by topography in m/s and T is the temperature at 700 hPa level in °K.

CHAPTER 5

RESULTS

5.1. Winter Period

The corrected equations derived for orography and temperature are applied to 1 hour and 6 hour winter data separately. The results for 1 hour temporal resolution are shown for all data in Table 5.1 (a) and for hit pixels in Table 5.1 (b). The results for 6 hour temporal resolution are shown for all data in Table 5.2 (a) and for hit pixels in Table 5.2 (b).

Table 5.1: Results of application of correction factors to 1 hour temporal resolution for all data (a) and for hit pixels (b) in winter periods of 2002 – 2004 years

a)	Applied correction factor	Real data length	Adjusted data length	Correlation	Bias	Bias (Ratio)	RMSE
	No correction	292151	-	0.2807	-0.0010	0.9766	0.4524
	Orographic correction	292151	292151	0.3062	0.0110	1.2538	0.5082
	Temperature correction	291737	291737	0.2916	-0.0010	0.9779	0.4530

b)	Applied correction factor	Hit pixels data length	Adjusted data length	Correlation	Bias	Bias (Ratio)	RMSE
	No correction	3326	-	0.1075	-0.1437	0.9230	2.6576
	Orographic correction	3363	3363	0.1574	0.4017	1.2149	3.0332
	Temperature correction	3322	3322	0.1452	-0.0820	0.9559	2.5602

Table 5.2: Results of application of correction factors to 6 hour temporal resolution for all data (a) and for hit pixels (b) in winter periods of 2002 – 2004 years

a)	Applied correction factor	Real data length	Adjusted data length	Correlation	Bias	Bias (Ratio)	RMSE
	No correction	45151	-	0.4185	-0.0077	0.9708	1.7707
	Orographic correction	44741	44741	0.4519	0.0687	1.2591	2.0828
	Temperature correction	44741	44741	0.4553	-0.0047	0.9824	1.7115

b)	Applied correction factor	Hit pixels data length	Adjusted data length	Correlation	Bias	Bias (Ratio)	RMSE
	No correction	1497	-	0.2126	-0.0689	0.9870	7.8438
	Orographic correction	1497	1497	0.3025	1.5711	1.2974	9.1867
	Temperature correction	1487	1487	0.2706	0.1331	1.0251	7.3722

The findings suggest that application of both orographic and temperature correction equations yield to a performance increase in the SCaMPR algorithm, even though effect of temperature is not dominant in winter period. Application of orographic correction improved correlation between SCaMPR estimates and gauge measurements by 9% in 1 hour data and 8% in 6 hour data. On the other hand, Bias values between SCaMPR estimates and gauge measurements are increased with 0.0120 for 1 hour data and 0.0764 for 6 hour data. Also RMSE values are increased with 12% for 1 hour data and 17.6% for 6 hour data. The effects of orographic correction on hit pixels are much more intense as the performance of SCaMPR algorithm on hit pixels is lower. When these findings are compared with the operational HE orographic correction results, the proposed algorithm features much better results than operational HE orographic correction. Proposed orographic correction formulation for SCaMPR algorithm improves correlation between SCaMPR estimates and gauge measurements by 9% in 1 hour data and 8% in 6 hour data, while this improvement is limited to with 3.8% for 1 hour temporal resolution and 5.8% for 6 hour temporal resolution in operational HE algorithms. It should be noted that statistics for HE algorithm is available for only summer period.

5.2. Summer Period

The corrected equations derived for orography and temperature are applied to 1 hour and 6 hour summer data separately. The results for 1 hour temporal resolution are shown for all data in Table 5.3 (a) and for hit pixels in Table 5.3 (b). The results for 6 hour temporal resolution are shown for all data in Table 5.4 (a) and for hit pixels in Table 5.4 (b).

Table 5.3: Results of application of correction factors to 1 hour temporal resolution for all data (a) and for hit pixels (b) in summer periods of 2002 – 2004 years

a)	Applied correction factors	Real data length	Adjusted data length	Correlation	Bias	Bias (Ratio)	RMSE
	No correction	391211	-	0.2772	0.1876	1.9491	1.7352
	Orographic correction	391212	31530	0.2772	0.1873	1.9479	1.7345
	Temperature correction	386144	386144	0.2809	0.0652	1.3295	1.5500

b)	Applied correction factors	Hit pixels data length	Adjusted data length	Correlation	Bias	Bias (Ratio)	RMSE
	No correction	19763	-	0.1821	0.2415	1.0800	5.8409
	Orographic correction	19727	1676	0.1830	0.2488	1.0824	5.8305
	Temperature correction	18955	18955	0.1868	-0.7279	0.7608	5.7238

Table 5.4: Results of application of correction factors to 6 hour temporal resolution for all data (a) and for hit pixels (b) in summer periods of 2002 – 2004 years

a)	Applied correction factors	Real data length	Adjusted data length	Correlation	Bias	Bias (Ratio)	RMSE
	No correction	57621	-	0.4190	1.1994	1.9477	6.0695
	Orographic correction	57114	15512	0.4181	1.2062	1.9509	6.1033
	Temperature correction	56673	56673	0.4260	0.4324	1.3417	4.9085

b)	Applied correction factors	Hit pixels data length	Adjusted data length	Correlation	Bias	Bias (Ratio)	RMSE
	No correction	9708	-	0.2554	3.4740	1.5207	12.3073
	Orographic correction	9624	2608	0.2546	3.5192	1.5272	12.3821
	Temperature correction	9466	9466	0.2678	0.4031	1.0603	10.3558

The results suggest that orographic correction shows more influence in winter period than summer so that the improvements are more obvious with winter data. Even though bias and RMSE values are increased with orographic adjustment because of more enhanced rainfall with correction, correlation coefficient values are increased significantly in winter. Orographic correction seems to correct rainfall trend in winter. However, the effect of temperature correction is not distinct over the winter period, as performance of SCaMPR at low temperature levels is much powerful. Therefore temperature correction analysis shows better improvement in summer periods, where 700 hPa temperature levels stay at high levels, with 50% temperature level indicating 284 °K, with an average of 10 °K difference between winter data. This may explain the difference between summer and winter temperature correction.

Contrary to this, the impact of orographic correction is not significant in summer period. There are small improvements in bias and RMSE values in 1 hour data but no change in correlation coefficient values. However, temperature correction showed great improvement on SCaMPR rain during summer. Temperature adjustment resulted in lower bias, bias differences between SCaMPR estimations and gauge measurements decreased from 0.1876 to 0.0652 in 1 hour data and RMSE value decreased from 1.7352 to 1.5500 in 1 hour data.

When these findings are compared with the operational HE orographic correction results, the proposed algorithm features much better results than operational HE orographic correction in winter period, but in summer period the effects of the proposed correction formulation is not distinct over statistics. It should be noted that statistics for HE algorithm is available for only 2002 and 2003 summer periods while statistics for SCaMPR algorithm is available for 2002, 2003 and 2004 summer periods. In order to further define the effects of proposed orographic correction algorithm, scatter plots of 6 hour temporal resolution data are presented in Figure 5.1 (a) for summation of 2002 – 2004 winter periods and in Figure 5.1 (b) for summation of 2002 – 2004 summer periods.

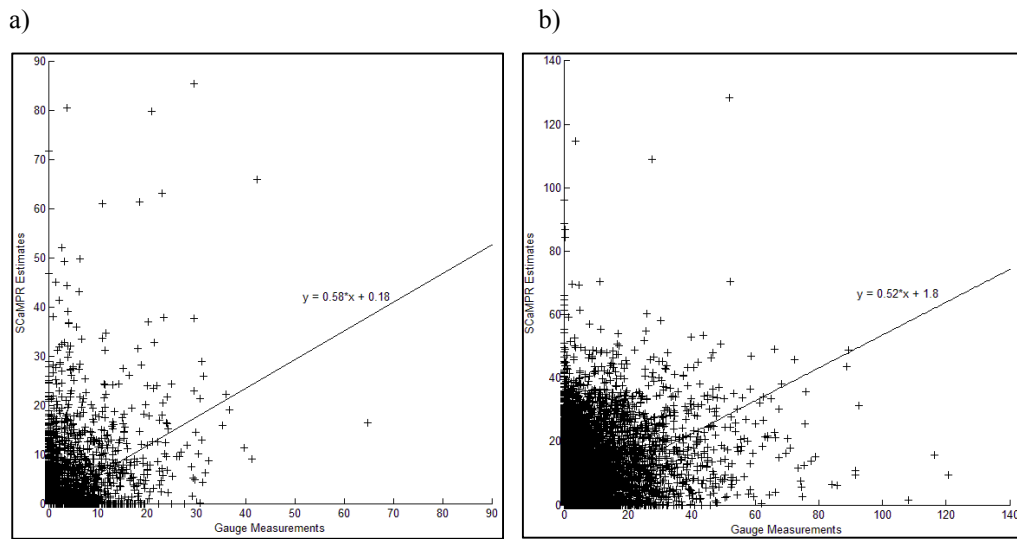


Figure 5.1: Scatter plots of gauge measurements vs. SCaMPR estimations for 6 hour temporal resolution in winter periods (a) and in summer periods (b) after application of orographic correction

The effect of orographic correction can be seen when Figure 5.1 is compared with the Figure 4.9 and Figure 4.10, where scatterplots of gauge measurements and SCaMPR estimates for winter and summer periods before application of orographic correction are shown. It is clear that, application of orographic correction cut down missing rains and underestimations, especially in winter period. This can be explained by the removal of elevation dependent bias structure that exists in the SCaMPR algorithm. But even after orographic correction, false alarms and missing rains still continue, which require further improvement of the algorithm.

CHAPTER 6

DISCUSSION AND CONCLUSIONS

Over mountainous regions, not every precipitation estimation and measurement techniques may be available. Radar is generally not in operation and rain gage data are very rare or non-existent. In order to overcome the problem, the satellite based rainfall estimates become an important alternative. Satellite rainfall algorithms provide a less accurate estimation of rainfall, but provide high spatial and temporal resolutions and complete coverage of the area. With the usage of satellite based estimates the correct distribution of rainfall over the whole topography may be achieved. Throughout this study, two of the current satellite based operational algorithms are investigated, and it has been shown that SCaMPR algorithm gives more reliable estimates than HE algorithm, even though when there is no orographic correction applied. With the application of correction factors, the continued improvement of the SCaMPR algorithm may be ensured.

Based on the work conducted these conclusions can be stated:

- It is shown that, satellite based precipitation estimates gives much reliable results in longer time steps, therefore usage of 6 hour or 24 hour aggregated rainfall estimation data will give much correct estimates than 1 hour rainfall estimation data.
- For orographic correction technique, a multiplicative approach is found out to be more reliable as it will protect the rain/no rain discrimination of the original algorithm. The other alternative of additive approach disturbs this rule.
- For orographic correction methodology, the formulation used by Vicente et al. (2002) is found out to be more reasonable than the formulation used by Kwon et al. (2008) as it reflects the topographic effects much better.
- It is shown that atmospheric indices are well represented by the NAM model, which enhances reliability of the algorithm.
- For an orographic enhancement, a fetch length based on 10 minute wind duration is found to reflect the topography in the optimum manner.
- The obtained correction equations match the formation of multiplicative orographic adjustment formulation defined by Vicente et al. (2002) for winter period, whereas in summer period the distribution is found to be completely different. Also during summer period, it is revealed that between zero updraft value and 1 m/s updraft value, orographic effects are not observed.
- The orographic correction suggested more improvement over winter period than summer period. The results of proposed orographic correction formulation are found out to show more improvement than operational HE orographic correction methodology. During summer period, orographic correction suggests little improvement but it removes elevation dependent bias structure.
- The effect of temperature correction is not distinct over the winter period; its performance is found to be much powerful over the summer period where 700 hPa temperature level stay at a high value. SCaMPR algorithm is found to be non-reliable at high temperature levels, where an application of a temperature correction is required.
- Orographic correction is more dominant during winter time while temperature correction is strong during summer time.
- For the further improvement of the SCaMPR algorithm, the effects of the precipitable water and relative humidity in the air block over the station location must be analyzed. Since precipitable water represents the quantity of moisture throughout entire atmospheric layer it may better help to establish correction relationship.
- These results recommend that orographic correction should be applied to operational SCaMPR algorithm during winter period for all topographically driven vertical movements, and during summer period for topographically driven vertical movements outside zero – 1m/s upwind zone.
- Rainfall estimates over a catchment area along with a surface runoff model may provide lacking flow data in hydrological and hydraulic models as well as estimate flash flood events.
- Reliability of a satellite based rainfall algorithm may be achieved only with the continued development and calibration of the algorithm.
- A rain gauge network which has the capability to sample the temporal and spatial patterns of rainfall across regional topographic gradients was not available in Türkiye, as a result this study could

not be conducted for Türkiye. Such a rain gage network with the same capability is needed to be installed in order to study and implement satellite based rainfall algorithms in Türkiye.

REFERENCES

- Bell, R. S. (1978) "The forecasting of orographically enhanced rainfall accumulations using 10-level model data." *Meteor. Mag.*, 107, 113–124.
- Bergeron, T. (1961). "Preliminary results of 'Project Pluvius'". Royal University of Uppsala, Uppsala, Sweden.
- Carruthers, D. J., and Choularton T. W (1983). "A model of the feeder - seeder mechanism of orographic rain including stratification and wind-drift effects" *Quart. J. R. Met. Soc.*, 109, 575 - 588.
- Collier, C. G. (1975) "A representation of the effects of topography on surface rainfall within moving baroclinic disturbances." *Quart. J. Roy. Meteor. Soc.*, 101, 407–422.
- Gochis, D.J., Jimenez, A., Watts, C. J., Garatuza-Payan, J., and Shuttleworth, W. J. (2003) "Analysis of 2002 and 2003 Warm-Season Precipitation from the North American Monsoon Experiment Event Rain Gauge Network", *Monthly Weather Review*, 132, 2938 - 2953.
- Gochis, D.J., Leal J., Shuttleworth, W. J., Watts, C. J., and Garatuza-Payan, J. (2004) "Notes and Correspondence: Preliminary Diagnostics from a New Event-Based Precipitation Monitoring System in Support of the North American Monsoon Experiment", *Journal of Hydrometeorology*, 4, 974 - 981.
- Gochis, D.J., Watts, C. J., Garatuza-Payan, J. and Cesar-Rodriguez, J. (2007) "Spatial and Temporal Patterns of Precipitation Intensity as Observed by the NAME Event Rain Gauge Network from 2002 to 2004", *Journal of Climate*, 20, 1734 - 1750.
- Korleski, C., and Strickland, T. (2009). "Biological and Water Quality Study of Grand River Basin", State of Ohio Environmental Protection Agency, EPA Technical Report EAS/2009-6-5.
- Kuligowski, R. J. (2002). "A self-calibrating real-time GOES rainfall algorithm for short-term rainfall estimates", *J. Hydrometeor.*, 3, 112-130.
- Kwon E., Sohn B., Chang D., Ahn M., and Yang S. (2008). "Use of Numerical Forecasts for Improving TMI Rain Retrievals over the Mountainous Area in Korea". *American Meteorology Society*, 2008 July, 1995-2004.
- Misumi, R., V. A. Bell, and R. J. Moore, (2001) "River flow forecasting using a rainfall disaggregation model incorporating small-scale topographic effects." *Meteor. Appl.*, 8, 297–305.
- NAM model webpage. <http://www.emc.ncep.noaa.gov/index.php?branch=NAM>. Last visited 15/01/2013.
- MAME webpage. http://www.cpc.ncep.noaa.gov/products/Global_Monsoons/American_Monsoons/NAME/index.shtml. Last visited 15/01/2013.
- Roe, Gerald H. (2005). "Orographic Precipitation". *Annu. Rev. Earth Planet. Science*. 2005.33, 645–671.
- Scofield, R. A., and Kuligowski, R. J., (2003). "Status and Outlook of Operational Satellite Precipitation algorithms for Extreme-Precipitation Events", *Weather Forecasting*, 18, 1037-1051.
- Servicio Meteorológico Nacional webpage. <http://smn.cna.gob.mx/climatologia/Normales8110/NORMAL25100.TXT>. Last visited 15/01/2013.
- Sinclair, M. R. (1994) "A diagnostic model for estimating orographic precipitation." *J. Appl. Meteor.*, 33, 1163–1175.
- Smith, R. (1979) "The influence of mountains on the atmosphere." *Advances in Geophysics*, Vol. 21, Academic Press, 87–230.
- Smith R. (2003) "A linear upslope-time-delay model for orographic precipitation." *J. Hydrol.*, 282, 2–9.
- Smith R. and I. Barstad (2004) "A linear theory of orographic precipitation." *J. Atmos. Sci.*, 61, 1377–1391.
- Smith R. (2006) "Progress on the theory of orographic precipitation." *Tectonics, Climate, and Landscape Evolution*, S. D. Willett et al., Eds., Geological Society of America, 1–16.

STAR/NESDIS webpage. <http://www.star.nesdis.noaa.gov/smcd/emb/ff/index.php>. Last visited on 15/01/2003.

University of Wyoming webpage. <http://www.weather.uwyo.edu/upperair/sounding.html>. Last visited 15/01/2003.

Urbanski, P. D. (1982). "Use of Satellite Imagery to Estimate Convective Precipitation over Complex Terrain in Western United States". MSc Thesis. Department of Meteorology, The University of Utah.

Vicent G. A., Davenport J. C., and Scofield R. A. (2002). "The Role of Orographic and Parallax Corrections on Real Time High Resolution Satellite Rainfall Rate Distribution". *Int. Journal of Remote Sensing*, Vol. 23, No. 2, 221-230.

Yucel, İ., Kuligowski, R. J., and Gochis D. J. (2009). "Evaluating the hydro-estimator satellite rainfall algorithm over a mountainous region". *International Journal of Remote Sensing*, iFirst, 2011, 1-28.